On physical oceanography of the Santos Estuary

by

Belisa T. Speranzini

in partial fulfillment of the requirements for the degree of

Master of Science

in Hydraulic Engineering

at Delft University of Technology,

to be defended publicly on June 16, 2017 at 13:00.

Supervisor:	Prof. dr. ir. S.G.J. Aarninkhof,	TU Delft
Thesis committee:	Dr. ir. G.J. de Boer,	Van Oord
	Prof. dr. ir. J.C. Winterwerp,	TU Delft & Deltares
	Dr. D.S. van Maren,	TU Delft & Deltares
	Prof. dr. ir. S.B. Vinzon,	UFRJ (Brazil)

An electronic version of this thesis is available at
`http://repository.tudelft.nl/`.

Van Oord
Marine ingenuity

TU Delft
Delft University of Technology

Abstract

This thesis investigates the origins of large sedimentation volumes in the Port of Santos, São Paulo - Brazil. The port is located in the Santos - São Vicente estuarine system, delimited by scarps and subject to intense rainfall. The terminals are placed inside the estuary and their access is provided by a 24 km long channel with mean depths of 15 m DHN, subject to annual maintenance dredging with volumes in the order of 4 Mm^3 [CODESP, 2016a].

A literature-based sediment mass balance is formulated for the system. Sediment sources and sinks are assessed based on data of the period 2005 to 2012 and expert judgment. The largest sediment input is given by winter storms (65%) followed by river sediment loads (25%). Up-estuary import of fine sediment is found as a third source, computed from the deficit between sources and sinks (trapping in the mudflats and maintenance dredging).

An explorative process based model is set to evaluate the hypothetical sediment balance and expand the understanding of the system behavior. A period of six months is simulated to capture the expected seasonal variability in salinity gradients. Conditions for fluid mud formation are found in the entire channel. A rerun with salinity switched off promotes an expressive reduction (70%) in the cumulative fine sediment import. Up-estuary sediment transport is found as a result of salinity-induced residual currents, which increase in strength with deeper channels [van Maren et al., 2015].

Fine sediment deposits in the final stretches of the channel that probably have been accounted in previous studies as from river discharges, according to this study are provided from marine sources. Model results suggest an annual import of 1.1 Mton of sediment, six times larger than the literature-based estimate. Additionally, results indicate that little quantity of riverine sediment reaches the channel. The literature mass-balance is therefore modified to incorporate these findings: river contribution is set to 15%, up-estuary transport to 30%, and winter storms to 55%.

Summary

This thesis investigates the origins of large sedimentation volumes in the Port of Santos, São Paulo - Brazil. The port is located in the Santos - São Vicente estuarine system, delimited by scarps and subject to intense peak rainfall. The terminals are placed inside the estuary and their access is provided by a 24 km long channel with mean depths of 15 m DHN, subject to annual maintenance dredging with volumes in the order of 4 Mm^3 [CODESP, 2016a].

A literature-based sediment mass balance is formulated for the system. Sediment sources and sinks are assessed based on data of the period 2005 to 2012 and expert judgment. The largest sediment input is given by winter storms (65%) followed by river sediment loads (25%). Up-estuary import of fine sediment is found as a third source, computed from the deficit between sources and sinks (trapping in the mudflats and maintenance dredging).

An explorative process based model is set to evaluate the hypothetical sediment balance and expand the understanding of the system behavior. A period of six months is simulated to capture the expected seasonal variability in salinity gradients. Conditions for fluid mud formation are found in the entire channel. A rerun with salinity switched off results in an expressive reduction (70%) of cumulative fine sediment transport into the estuary. Up-estuary sediment transport is found as a result of salinity-induced residual currents, which increases in strength with deeper channels [van Maren et al., 2015].

Fine sediment deposits in the final stretches of the channel that probably have been accounted in previous studies as from river discharges, according to this study are provided from marine sources. Model results suggest an annual import of 1.1 Mton of sediment, six times larger than the literature-based estimate. Additionally, results indicate that little quantity of riverine sediment reaches the channel. The literature mass-balance is therefore modified to incorporate these findings: river contribution is set to 15%, up-estuary transport to 30%, and winter storms to 55%. To accommodate uncertainties in the sources and sinks, the sediment mass-balance is presented in terms of a best estimate with lower and upper bands, as per Figure 1.

From a dredging perspective, the findings of this research suggest that sedimentation in the channel might considerable reduced by the removal of fine sediment available in the bed of Santos bay - assuming the existence of this source. Overdredging is likely to increase sedimentation volumes, considering that it typically leads to a deeper

penetration of the salt wedge into the estuary and stronger residual currents, promoting a larger up-estuary sediment transport. Water injection dredging might work as a short-term solution, given that model results indicate a strong capacity of importing fine material discarded in the bay.

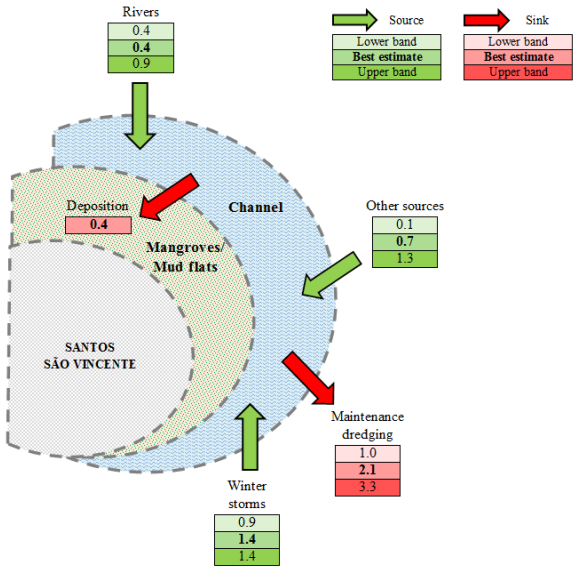

Figure 1: Sediment mass balance [Mton/year] of the Santos Estuary, averaged over the period of 2005 to 2012. Dredging ranges are attributed to different densities of the dredged material.

Resumo

Este trabalho investiga as origens da sedimentação do Porto de Santos, São Paulo - Brasil. O porto está situado no Sistema Estuarino de Santos-São Vicente, delimitado pela Serra do Mar e sujeito a intensos eventos de precipitação. O acesso aos terminais é dado por um canal de navegação de 24 km de comprimento com profundidades de até 15 m DHN. Anualmente, o canal e terminais são dragados para manter o calado mínimo, resultando em volumes de dragagem da ordem de 4 4 Mm^3 [CODESP, 2016a].

Um balanço de masssa de sedimento é formulado para o sistema. Fontes e sumidouros são levantados com base em dados do período de 2005 a 2012 e no parecer de especialistas. A maior fonte de sedimentos é dada pelos eventos de ressaca (65%), seguido pela descarga de sedimentos fluviais (25%). A importação de sedimentos estuário acima é definida como uma terceira fonte e computada a partir do déficit entre fontes e sumidouros (retenção de sedimentos nas planícies de marés e dragagem de manutenção).

Em Delft3D um modelo explorativo é preparado para avaliar este balanço de massa e expandir o conhecimento sobre o comportamento do estuário de Santos. Um período de seis meses é simulado com o intuito de capturar a esperada variabilidade sazonal nos gradientes de salinidade. Condições para formação de lama fluida são encotradas em toda extensão do canal. Uma segunda simulação sem incluir salinidade resulta em redução expressiva (70%) na importação de sedimentos. Resultados indicam que o transporte de sedimentos estuário acima é decorrente de circulações residuais, as quais são ampliadas com o aprofundamento de canais [van Maren et al., 2015].

Depósitos de sedimentos finos encontrados nos segmentos finais do canal de navegação são, de acordo com este estudo, oriundos da baía de Santos, e não da descarga de rios no estuário, conforme proposto em outros estudos. Resultados do modelo sugerem que o estuário importa 1,1 Mton de sedimento ao ano, seis vezes mais que o estimado com base na literatura. Ainda, resultados indicam que uma pequena fração do sedimento de origem fluvial atinge o canal. Desta forma, o balanço de massa de sedimento é modificado para incorporar estas proposições: a contribuição dos rios passa a ser 15%, o transporte estuário acima 30% e os eventos de ressaca 55%. Para acomodar as incertezas, o balanço é apresentado em termos de uma melhor estimativa com bandas, conforme Figura 2.

Do ponto de vista da dragagem, os resultados desta tese sugerem que a sedimentação de finos no canal pode ser significativamente reduzida através da remoção dos finos

presentes no fundo da baía de Santos - uma vez confirmada a existência desta fonte. Sobredragagem não se mostra como alternativa promissora dado que canais mais profundos podem fortalecer as circulações residuais e aumentar a importação de sedimentos. Dragagem de agitação (*Water injection dredging*) pode funcionar como uma medida de curto prazo, visto que o sistema parece importar sedimentos finos presentes na baía com relativa facilidade.

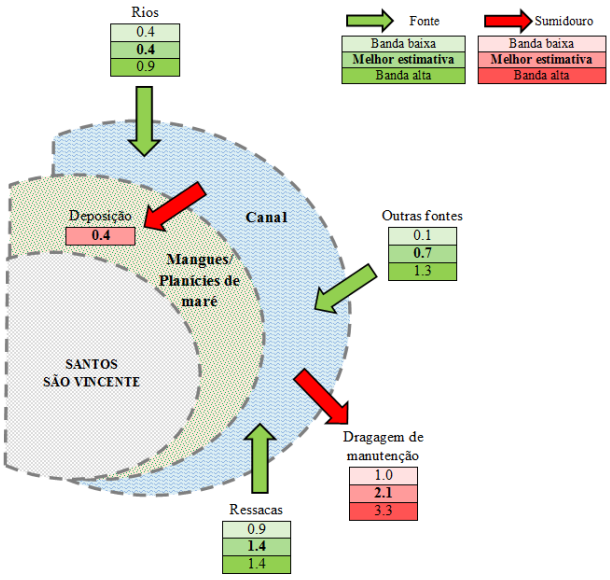

Figure 2: Balanço de massa de sedimentos para o período de 2005 a 2012 [Mton/ano]. Variações na dragagem são dadas pelas diferentes combinações de densidades de materiais.

Preface

A few years ago I started working with hydraulic engineering in a stimulating environment in Brazil. Soon I joined a project in the port of Santos and little did I know that later I would be modeling this estuary.

The topic of this research was proposed to me by Van Oord and I immediately decided to take up the challenge. In the past nine months I was engaged collecting data, setting up a model, and interpreting results. I am pleased to share the outcome in this report.

I would like to thank Gerben for the opportunity to conduct this thesis at Van Oord and for his unwavering support. Gerben was always available for questions and enthusiastic with the project. I also wish to thank the committee members: Stefan for his practical insights, Bas for his help with the sediment balance, model set-up, and writing, Han for his critical view, and Susana for the support on data collection and understanding of the system.

To my friends from Brazil and from TU Delft, thank you for keeping me motivated. My parents deserve a particular note of thanks: your wise words and encouragement, as always, served me well.

Belisa T. Speranzini

Rotterdam, June 08, 2017.

x

Contents

List of Figures

List of Tables

Nomenclature

Abbreviations

CODESP	Companhia Docas do Estado de São Paulo / Port of Santos Authority
DAEE-SP	Departamento de Águas e Energia Elétrica - São Paulo
DHI	Engineering consultant DHI
DHN	Diretoria de Hidrografia e Navegação reference level
EIA	Environmental Impact Asssessment
ETM	Estuarine Turbidity Maximum
F1	Fluvial(riverine) sediment fraction 1
HW	High water
INPH	Instituto Nacional de Pesquisas Hidroviárias
LW	Low water
M1	Marine sediment fraction 1
M2	Marine sediment fraction 2
MSc	Masters of Science
PoS	Port of Santos
RMSE	Root mean square error
S1	Section 1
S2	Section 2
S3	Section 3
S4	Section 4
SE	Santos Estuarine System
SLR	Sea level rise
TSHD	Trailing suction hopper dredger

TUD	Delft University of Technology
WID	Water injection dredging

Other Symbols

A	Area of mudflats and mangroves [km^2]
D	Deposited mass of sediment[ton/year]
V	Deposited volume of sediment [m^3/year]

Symbols

$\gamma_{mix,bulk}$	Dry bulk density of fine and coarse sediment mixture (1:1 ratio) [kg/m^3]
$\gamma_{mud,bulk}$	Dry bulk density of mud [kg/m^3]
$\gamma_{sand,bulk}$	Dry bulk density of sand [kg/m^3]

1

Introduction

The Port of Santos (PoS), located in the estuary of Santos (Figure 1.1), south-east Brazil, is the largest port in the country in terms of total shipping tonnage and one of the busiest ports in Latin America. This port has been central to the Brazilian economy since its founding in 1892, especially for exporting dry bulk and general cargo and playing an important role in coastwise shipping. In 2016, the throughput of PoS was nearly 114 Mt, corresponding to 10% of the total throughput of Brazil [CODESP, 2016b].

Figure 1.1: Area of study: Santos estuary - SP, Brazil.

Around 5,000 vessels call on the PoS every year, on average one vessel every 1.5 hour. The access to the terminals is given by a two-way channel, divided in four sections, as presented in Figure 1.2 and Table 1.1. At the end of the Santos navigation channel begins the Piaçaguera channel, owned by a private entity.

Table 1.1: Main characteristics of the PoS navigation channel [CODESP, 2016b] [CODESP, 2016a].

Section	Coordinates Start		End		Length [m]	Width [m]	Draft [m]
S1	361,974.6 E	7,339,067.4 S	368,734.4 E	7,346,710.4 S	11,560	220	13.2
S2	368,734.4 E	7,346,710.4 S	366,953.5 E	7,350,374.6 S	4,340	220	13.2
S3	366,953.5 E	7,350,374.6 S	365,392.2 E	7,353,010,0 S	3,440	220	12,7
S4	365,392.2 E	7,353,010,0 S	360,518.1 E	7,354,640.4 S	5,260	220	11.2

Figure 1.2: Harbor approach channel, Port of Santos (Google Earth®).

1.1 Dredging activities

The navigation channel of PoS has an extensive record of dredging activities. The graph of Figure 1.3 presents dredging volumes[1] from 1938 to 2016. The peaks refer to channel expansions and it can be seen that after the 1990s there has been a significant increase in the maintenance volumes. This fact is explained not only by the larger areas to be dredged but also by an increased up-estuary sediment transport, and therefore, higher sedimentation rates.

[1] From 1932 to 2005 dredging volumes were measured in the hopper. From 2006 to 2016, in situ volume measurements.

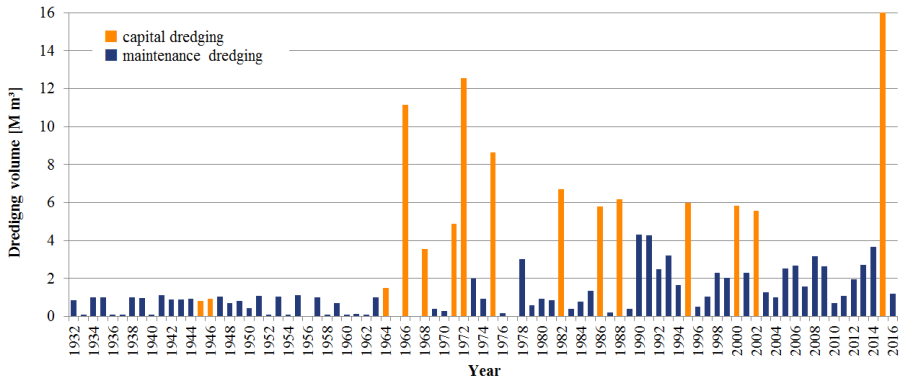

Figure 1.3: Annual dredging volumes period 1938 to 2016 [FRF, 2008] [CODESP, 2016a].

In general, deepening of channels and reclamation of intertidal areas leads to a combination of tidal amplification, increased estuarine circulation, and strenghtening of residual currents. As consequence, a larger up-estuary sediment transport is expected [van Maren et al., 2015].

Alfredini and Lavieri [2013] discussed these higher sedimentation rates when estimating accretion volumes for a design depth of - 15 m DHN [2]. The authors attributed the infilling of S2, S3, and S4 to rivers that discharge in the estuary bringing considerable amounts of sediment along with residual circulation induced by tidal currents.

The morphological equilibrium depth of Santos estuary is estimated to be 10 m in the entrance of estuary and 8 m DHN by the end of S4 [Alfredini and Lavieri, 2013]. With deeper channels and fewer intertidal flats, the system tends to import sediment in order to re-establish its equilibrium depths, resulting in larger sedimentation volumes [van Maren et al., 2015]. More information on estuarine dynamics will follow in Section 1.2.

Maintenance dredging contract

Recent information from the port authority provides that the annual sedimentation in the channel is of approximately 3,8 Mm^3 in S1 and a total of 2,2 Mm^3 in the stretch from S2 to S4 [CODESP, 2016c]. CODESP requires the execution of the dredging works by trailing suction hopper dredgers (TSHD) with disposal of the material in an offshore area 8 nautical miles distant from the entrance of the estuary.

Dredging experience in the Port of Santos indicates the existence of hot-spots where material accumulates after heavy rainfall and/or storm surges [Van Ooord, 2016]. These events raise the costs of the annual maintenance of the channel as a result of larger volumes to be dredged in addition to the (probable) necessity of re-mobilizing dredging

[2] All the vertical levels in this thesis are referenced to the 0 DHN datum. For simplicity, DHN will be omitted in the following level indications.

equipment to the area after these episodes. Moreover, sedimentation hot-spots may also cause down-time and temporarily reduce the maximum draft of the channel.

For the period of 2016-17 maintenance volumes were assessed in 1,0 Mm^3 for S1 and 3,3 Mm^3 for S2 to S4, with estimated costs of BRL 120M (EUR 36M) [CODESP, 2016a]. Dredging works in PoS are carried out by qualified contractors selected on tendering processes with a lowest price criteria.

A global understanding of the system behavior of Santos estuary is, therefore, a valuable asset for both CODESP and dredging contractors. Efforts have been made in understanding the hydrodynamics and morphodynamics of the Santos estuary (see Alfredini and Lavieri [2013], Coelho [2008], Ferreira [2013], Lopes [2015]), yet there is space to connect and evolve the existent knowledge. In this regard, the present study, proposed by Van Oord is developed in collaboration with Delft University of Technology (DUT) and Deltares.

1.2 Estuarine dynamics

The area object of study is an estuarine system. A brief description of estuarine dynamics is provided in the following paragraphs in order to establish the approach of taken in this project.

Estuaries are, in the traditional sense, regions of transition from river to ocean. They are characterized by tidal motions from the sea and salinity and density gradients associated with progressive admixture of fresh and salt water. The basic non-tidal circulation associated with maintaining the salinity distribution in estuaries consists of a seaward flow of fresh water and density driven currents [Hansen and Rattray, 1966a] [Hansen and Rattray, 1966b].

Complex 3D structures of residual circulation can be found in the inner basin of estuaries as a cause of interaction between tidal motion and bottom morphology, and may also occur due to river flow and compensation for Stoke‘s drift. Besides, these residual currents play an active role in the morphological evolution of channels and tidal flats [Bosboom and Stive, 2015]. Tidal distortion can strengthen or weaken the magnitude of the maximum flood flow compared to the maximum flow. It can also lead to asymmetry in the duration of the associated slack periods. These asymmetries have a great influence in the net movement of sediment, thus, in the development of the morphology of the basin in time.

A basic scheme of estuarine circulation is presented in Figure 1.4. In the presence of considerable suspended loads of fine sediment, an estuarine turbidity maximum (ETM) is formed in the null zone. The null zone corresponds to the region where the residual, near-bottom, up-estuary current reverses and flows in the seaward direction due to river inflow [Schoellhamer and Burau, 2007].

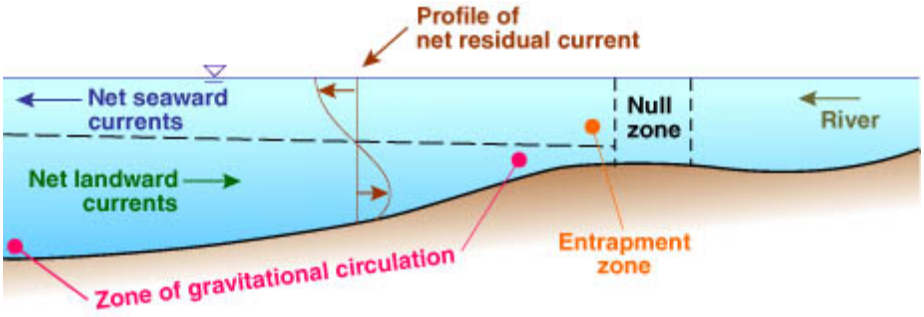

Figure 1.4: Conceptual model of entrapment and null zones [Schoellhamer and Burau, 2007].

The ETM region is characterized by locally-elevated suspended matter concentration, where particle trapping occurs by asymmetrical tidal transport of a pool of resuspended particles with a limited range of settling velocities [MacCready and Keister, 2011]. Flocculation and disaggregation can be active processes, depending on the characteristics of the material and estuarine circulation patterns. The null zone location, therefore ETM location, varies within the tidal cycle, being dependent on the strength of the tide, spring-neap tidal cycles, river discharges, and seasonality.

Medium to coarse net sediment transport is determined by residual flow velocity, amplitude of M2 tidal component, and the relative amplitude phases of M4 and M6 components to the M2 component [Bosboom and Stive, 2015].

For fine sediment, time lags of settling and resuspension must be taken into account. Asymmetries in slack water periods imply asymmetries in the sediment concentration. In flood dominated estuaries, strong sedimentation occurs around flow reversal from flood to ebb. That is due to larger sediment concentration combined to a long period for the sediment to settle. In low water slack sedimentation is also present, but it is less pronounced. After a complete tidal period, a net up-estuary sediment transport is expected [Bosboom and Stive, 2015].

The dynamics of suspended sediment in estuarine environments are rather complex to quantify. Considering salinity on top of the mentioned mechanisms imply that density driven currents are up-estuary directed near the bottom. These currents combined with larger sediment concentrations near the bottom generate landward sediment transport. Moreover, spatial variations may extend settling lag due to up-estuary decreasing flow velocities or depth, contributing to up-estuary sediment transport [van Maren et al., 2015].

1.3 Objective and approach

The aim of this research is to better understand sediment transport processes within the Santos estuary, including sediment sources. The methodology applied is in correspondence with the subsequent chapters of this document:

- Chapter 2: the initial approach is to perform a literature review in the system and gather available data of the dominant variables in estuary dynamics: tides, fresh water flow, and geomorphology;
- Chapter 3: a sediment mass balance is constructed based on the findings of Chapter 2, assuming that the estuary of Santos is a closed cell;
- Chapter 4: a explorative process based numerical model is built with Delft 3D in order to evaluate the hypothetical sediment balance and to explore the system hydrodynamics and morphodynamics;
- Chapter 5: model results are evaluated together with the sediment balance, providing expanded insights in the system behavior; and
- Chapter 6: results are evaluated from the dredging perspective. Recommendations on maintenance dredging strategies and further investigation are presented.

The methodologies carried out on each of the phases of this project are described along the chapters. Beforehand, sedimentation patterns in the Santos estuary can be divided in two systems. The first comprehends S1 and is dominated by long shore transport of coarse sediment during winter storms. The second, comprehends the middle and upper areas of the estuary (S2 to S4) and is dominated by fine sediment transport [Alfredini and Lavieri, 2013]. Focus will be given to the latter.

2

Santos system

The Santos Estuarine System comprises three main channels for the exchange of fresh and salt water: São Vincente (west side), Port of Santos (east side), and Bertioga (north-east side). This system is illustrated in Figure 2.1. The present MSc thesis focuses on the first two channels and for simplicity, the system will be addressed as Santos estuary (SE).

A description of the SE is given in the following sections. In summary, the estuary drains considerably large volumes of rainfall, on average 60 m^3/s [FRF, 2008], carrying coarse to fine sediment which is partially retained by mangroves and mudflats and partially deposited in the channels.

Current velocities are up to 0.5 m/s, driven, at most, by tidal forcing. The tidal character is semi-diurnal with daily inequalities and average amplitudes of 1.43 m. The estuary is partially mixed to stratified, and the salt transport within the estuary is due to the up-estuary propagation of the salt wedge and eddy diffusion [Miranda et al., 2012].

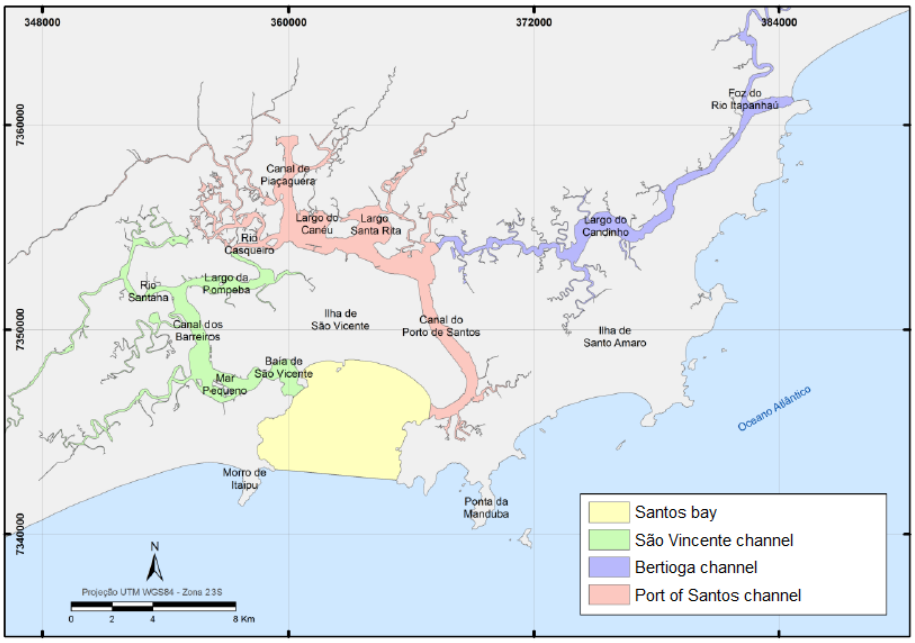

Figure 2.1: Santos Estuarine System. Adapted from Roversi [2012].

2.1 Metocean conditions

A metocean study is fundamental for the understanding of the physical oceanography of the area. In the first stage of this research, a metocean study is undertaken based on literature. The most relevant aspects for the SE are presented in the following subsections.

2.1.1 Mixed semi-diurnal tidal regime

The mean spring tidal range in the estuary is 1.34 m, measured in station 3. Santos Port (2.2) and presented in Table 2.1. In Appendix A the astronomical components measured in four other stations along the SE and in the Santos bay are presented. The largest tidal components are M_2, S_2, M_3, O_1, K_2, and K_1. In general, all the components are amplified as they propagate into the estuary. The M_2 and S_2 component amplify the most when reaching the end of Piaçaguera channel: 30.6% and 21.9%, respectively [Lopes, 2015].

Pond and Pickard [1978] introduced the tidal form factor $F=(K_1+O_1)/(M_2+S_2)$ to evaluate the dominance of diurnal and semidiurnal components. In the area of study, the computed F equals 0.3, denoting a mixed, mainly semi-diurnal tidal regime. A characteristic of a semi-diurnal regime is the generation of the M_4 tidal component, resulting in an asymmetry that can be computed in terms of phase (ϕ) differences between the tidal components M_2 and M_4. If the phase relation of the water levels $90^o \leq (2\phi_{M2}$

Table 2.1: Tidal astronomic components - station Santos (Porto).

Station:	Santos (Porto) - SP		FEMAR #237		
Location	Torre Grande 2.2		Organization:	INPH/CODESP/DHN	
Latitute	23º 57,3' S		Longitude	46º 18,6' W	
Period of analysis:	01/01/1956 to 23/12/56		MSL [m]	0.77	
MHHW [m]*	1.41		MHLW [m]*	0.29	
MLHW [m]*	1.30		MLLW [m]*	0.07	
Selected astronomic components					
Component	Amplitude [m]	Phase [deg]	Component	Amplitude [m]	Phase [deg]
M_2	0.364	88	MU_2	0.021	122
S_2	0.225	91	$2N_2$	0.02	149
O_1	0.115	81	Mf	0.017	141
Sa	0.102	25	L_2	0.016	37
K_2	0.074	82	Msf	0.015	121
K_1	0.063	143	MN_4	0.013	318
N_2	0.054	149	M_1	0.008	95
Ssa	0.05	180	J1	0.008	192
M_3	0.049	234	T_2	0.008	20
Mm	0.042	289	MO_3	0.007	96
M_4	0.026	355	SN_4	0.006	61
Q_1	0.025	58	NU_2	0.004	139
MK_3	0.025	117	OO_1	0.002	133
P_1	0.023	136	MNS_2	0.002	189
MS_4	0.022	143	MTM	0	0

*above MSL

Figure 2.2: Location of station Torre Grande - FEMAR 237 (Google Earth®).

- ϕ_{M4}) <270° holds, high water slack duration is larger than low water slack, therefore, landward transport prevails [van Maren and Winterwerp, 2013]. This property is specially important for fine sediment, as tides with a longer high water slack when compared to low water slack provide a longer time for sediments to settle after flood [Friedrichs, 2012]. Evaluating the phases of these tidal components at Santos station, an asymmetry of 181° is found, indicating a net import of sediment due to this process.

A second criteria on the phase relation ($2\phi_{M2}$ - ϕ_{M4}) for water levels is positive asymmetry (flood dominance) if this phase relation is between 180° and 360°, and negative asymmetry (ebb dominance) for the remaining [Friedrichs and Aubrey, 1988]. An analysis on the M_2 and M_4 tidal components of the four stations provides a negative asymmetry for the upper area of the estuary (stations 4 and 5) and a positive asymmetry in stations 1 to 3. Therefore, at at some point between stations 3 and 4, the tidal character is reversed.

One should note that the water level measurements carried by FEMAR and presented in these tables refer from periods before the expansion of the navigation channel and land reclamation for terminals. Lopes [2015] investigated the impact of deepening the Santos navigation channel on tidal asymmetries and found a reduction of up to 20% in the ebb peak velocities during spring tide along the Santos estuary, related to the modification of relative phase of M_2 and M_4 in tidal currents. Moreover, an increase in diurnal inequalities of the ebb velocities, related to the periodical distortions produced by the terdiurnal tidal constituents was observed.

M_3 component

The M_3 terdiurnal tidal component (period of 8.28 hours) related to the asymmetries in the tidal currents observed in the SE. Distortions are found in every two tidal cycles, providing an indication that the M_3 component is related to the daily inequalities in the tidal amplitudes [Lopes, 2015]. In Figure 2.3 it is possible to see the influence of the terdiurnal component on the tidal signal. Numbers 1 and 3 present changes in the water levels, while numbers 2 and 4 present the distortion in the rise and fall periods of the water levels.

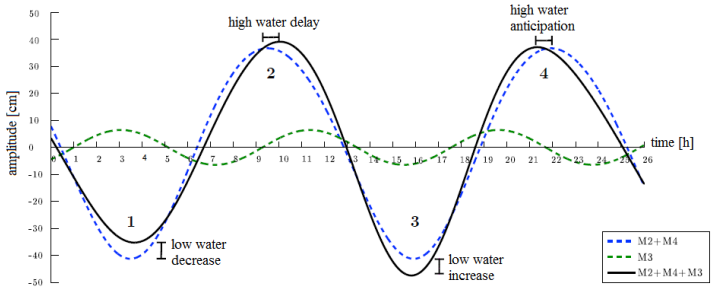

Figure 2.3: Superposition of M_2, M_3, and M_4 tidal components, showing the influence of the M_3 in the tidal distortion. Adapted from Lopes [2015].

2.1.2 Winter storms

Apart from the astronomical tide, storm surges also provide significant changes in the water levels of the region. The larger water level variations are induced by low pressure systems over the ocean. In south Brazil, these events are followed by south and south-east storms that arise mostly during autumn and winter periods. Considering the Coriolis effect on the ocean currents and the orientation of the coastline in Santos, south winds pile up the water against the coast (set-up), while north winds have the opposite effect (set-sown). Transverse winds are of minor influence in the water levels of the area [Truccolo, 1998].

Campos et al. [2010] analysed the occurence of extreme sea level events in Santos over the period of 1951 to 1990. The results show a seasonal variability, with positive extreme events taking place mostly during autumn (40.2%) and winter (30.8%). Positive events are characterized by surge elevations larger than 0.38 m.

An annual average of 12 positive events took place in the analysed period, associated with wind velocities above 8 m/s over the ocean, close to the coast. These events are considerably energetic in the estuary of Santos and are related to coastal erosion and flooding in adjacent areas [Campos et al., 2010] [FAPESP, 2015] [Lopes, 2015].

2.1.3 Easterly winds

The Subtropical High Pressure center of the South Atlantic and its interations with the Sub Polar pressure govern the atmospheric circulation in Baixada Santista [Harari et al., 2008]. Additionally, the complex configuration of the topography strongly influences the wind regime of the SE.

For typical conditions, the most frequent winds in all seasons blow from East, with average velocities of 1.5 m/s. When strong western winds occur in the limit of the sub tropical and sub polar regions, cold fronts modify the atmospheric conditions in the SE. They force eastern winds to rotate to north and west - phenomena that take a few hours, with wind velocities of up to 10 m/s. This rotation is followed by winds blowing from south for 1 to 3 days, with velocities between 5 and 10 m/s. As the air temperature drops and the atmospheric pressure rises, winds turn back to east until temperature and pressure come again to normal values.

Figure 2.4 illustrates the described wind motions for summer and winter periods, with measurements taken from a station 140 km SSE distant from the estuary. The instabilities are more recurrent and pronounced in winter, with 3 to 6 events per month [Castro, 1985].

2.1.4 Easterly waves

Wave measurements were taken from two stations close to Baixada Santista for the periods 1968 to 1969 and 1982 to 1985 and analysed by M.G. Tessler [2006]. Results give that the most frequent waves for mild and storm conditions come from SE-E and

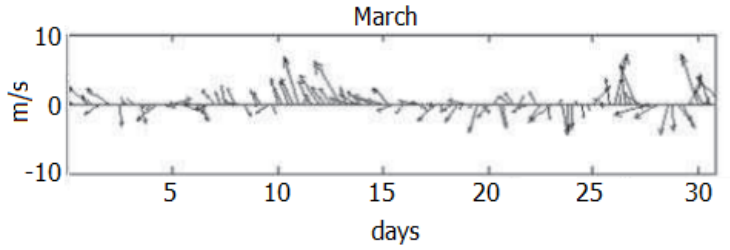

(a) Summer conditions.

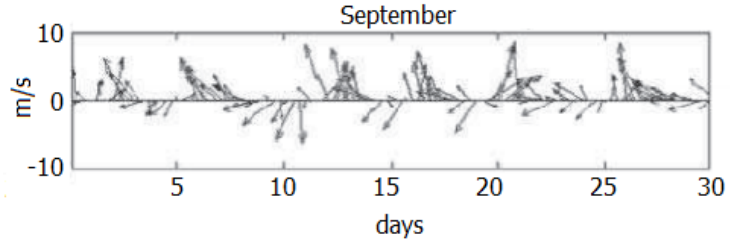

(b) Winter conditions.

Figure 2.4: Wind conditions averaged over the years of 1980 to 2004 at the position 22°30'S 45°W [Harari et al., 2008].

SE-E respectively. Wave periods are on average between 6 and 20 s, with larger occurrence of periods of 9 to 11 s. Wave heights are between 0.5 and 2.0 m during 90% of the time, being 50% in the interval of 1.0 to 1.5 m.

For the SE, little information can be found regarding wave conditions. A measurement campaign carried in São Vincente bay by INPH between November 1972 and November 1973 and analysed by Alfredini [2003] apud Farinnaccio et al. [2009] provides waves with average periods of 9 to 11 s and average heights of 1.0 to 2.0 m.

Alfredini and Lavieri [2013] limit the influence of waves in sediment transport to Section 1. According to the author, Sections 2 to 4 are sheltered from waves . Existing modelling studies in the estuary also neglected wave agitation inside the SE [Bundgaard, 2008] [Elfrink et al., 2008] [INPH, 2013] [Roversi, 2012].

2.2 Partially mixed to stratified estuary

The SE comprehends the central region of the Baixada Santista basin (Figure 2.5), with a catchment area of 920 km^2 [FRF, 2008]. This basin is delimited on the land-side by a scarp, Serra do Mar. From there, dozens of rivers spring and flow downstream shaping plains, draining mangroves, and discharging in the estuarine channels [CBH, 2000].

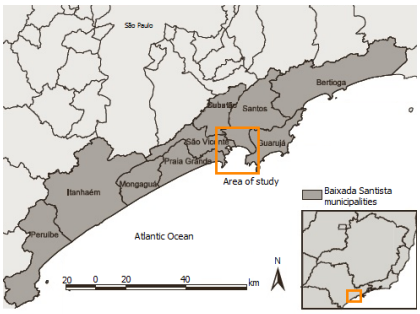

(a) Location [IBGE, 2017].

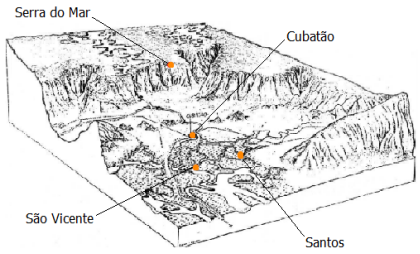

(b) Scheme of the topography in the estuary [Titarelli, 1986].

Figure 2.5: Baixada Santista and the topography of the Santos estuary.

2.2.1 Currents

Water circulation in SE is given by tidal flood currents floating close to the bottom, in layers below 2 m depth, and ebb currents floating mainly through the upper layers of the water body [Gianesella, 1978]. Average current velocities are given in Table 2.2 and Figure 2.6.

Current patterns in SE do not present significant differences between winter and summer periods as they are driven mostly by the tidal forcing [Harari et al., 2008]. Maximum current velocities are of 0.5 m/s and, during flooding, sea-to-estuary currents are found in the entire estuary. According to Harari et al. [2008], tidal waves coming from Santos and São Vicente channel meet west of Casqueiro island, between sections 4 and 6 of Figure 2.6.

Table 2.2: Typical current velocities in the SE for measurments taken near COSIPA, in the Piaçaguera channel (23°54.0'S 46°22.6W') [Harari et al., 2008].

	Spring tide		Neap tide	
Location	Ebb [m/s]	Flood [m/s]	Ebb [m/s]	Flood [m/s]
Surface	-0.45	0.35	-0.27	0.32
5 m depth	-0.35	0.3	-0.22	0.26
10 m depth	-0.26	0.25	-0.15	0.25

2.2.2 Salinity

Temperature and salinity conditions were assessed in September 2005 and March 2006 during spring flood-tidal conditions. Three stations of Figure 2.6a were measured: 1 (entrance of Santos port), 5 (mid Piaçaguera channel), and 8 (entrance São Vincente channel). The isohalines and isopyncals presented in Figure 2.7 indicate that the salinity is the dominant contributor to the density of the water that flows in the system [Harari et al., 2008].

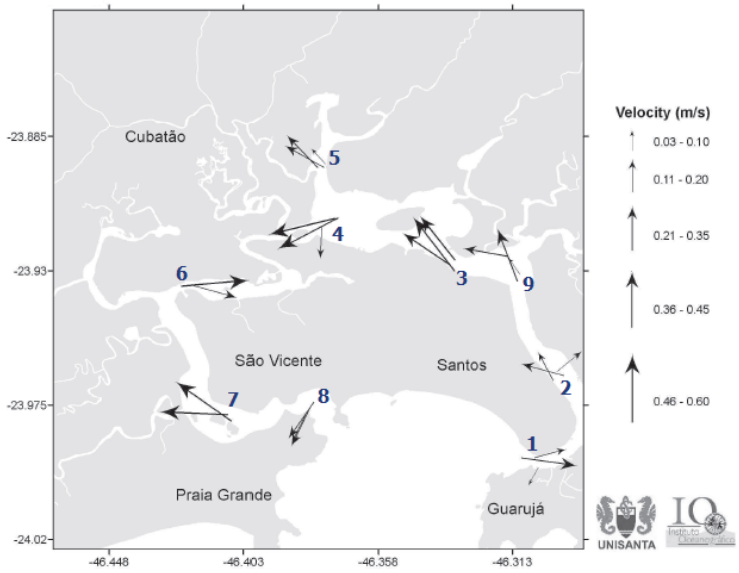

(a) Surface.

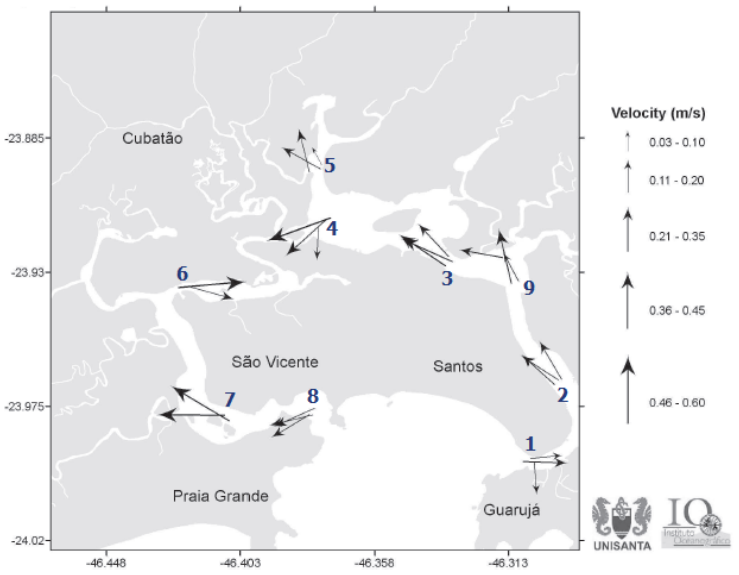

(b) Mean average over multiple measured depths.

Figure 2.6: Time-averaged currents measured in September 2005 (adapted from Harari et al. [2008]). Measurements were taken for nine stations during flood- spring-tide conditions. Light grey corresponds to land, white to water.

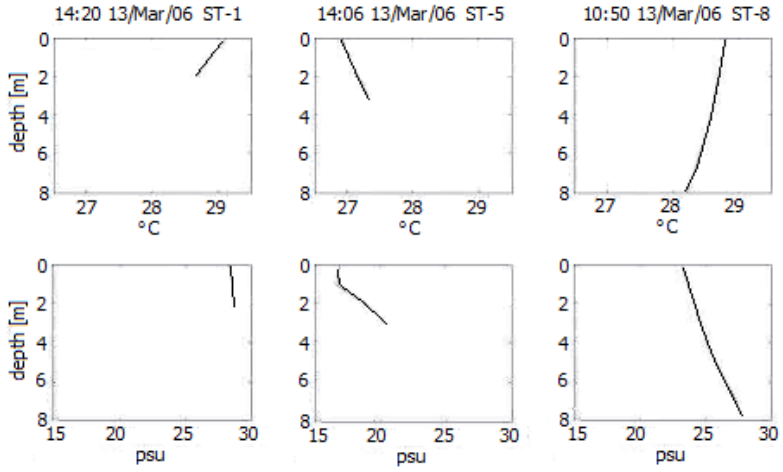

(a) Summer conditions.

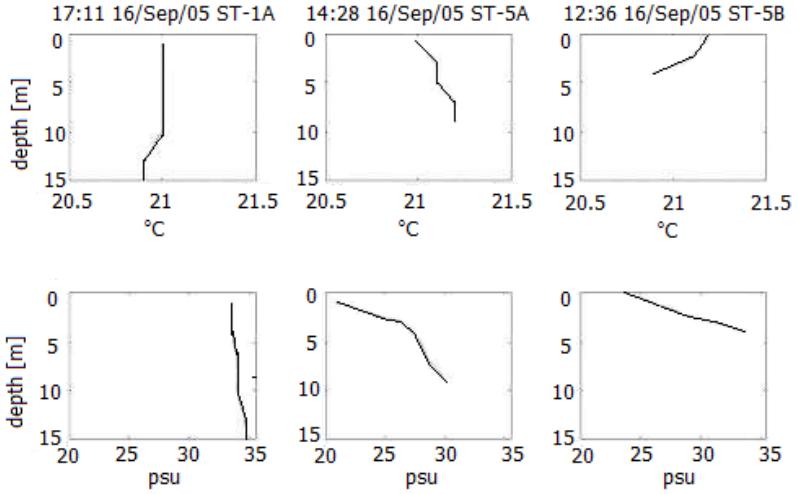

(b) Winter conditions.

Figure 2.7: Vertical profiles for temperature and salinity (adapted from Harari et al. [2008]). Measurements were taken for stations 1, 5, and 8 during flood- spring-tide conditions. Salinity stratification are found inside the estuary, whilst in the entrance it is negligible. This holds for both summer and winter conditions.

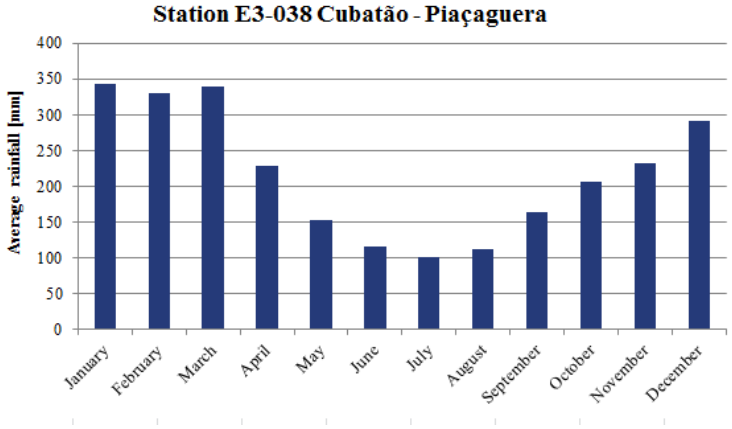

Figure 2.8: Average monthly rainfall recorded in Cubatão (SP), station E3-038 averaged over the period between 1936 and 2000 [DAEE, 2016].

2.2.3 Summer peak rainfall and river discharges

Baixada Santista region is subject to one of the largest rainfall rates in Brazil, with annual totals of up to 4,400 mm. From Figure 2.8 it can be seen that the wet season ranges from December to March. A rich and complex system of small rivers drain into the SE.

Discharge volumes and river flows were estimated during the preparation of the Environmental Impact Asssessment (EIA) of the expansion of Santos channel in 2008 [FRF, 2008]. The methodology applied was proposed by Departamento de Águas e Energia Elétrica - São Paulo (DAEE-SP) and considers parameters as annual rainfall, catchment areas, average slopes, and length of the rivers. Considering the catchment area of 9.2 km^2 and a rainfall of 4,400 mm/year, the average river discharges of 60 m^3/s, outflow corresponds to 46%, and evaporation and percolation to 54%.

Figure 2.9 presents a diagram of these rivers while Table 2.3 presents their resultant average discharges in the SE. It can be seen that most of the rivers discharge in the middle and upper areas of the estuary, where the largest areas of mudflats and mangroves are present. Rivers Itatinga, Itapanhaú, Cubatão, Boturaca, and Quilombo give the largest contribution, both in typical as in peak rainfall conditions.

Erosive processes

The most recent geological evolution resulted in unconsolidated layers in the lower areas of the scarp [CBH, 2000]. The intensity and frequency of erosive processes in the scarps have a direct impact on the deposition of sediment in the lower areas of the basin. Large rainfall rates are associated with steep slopes, promoting the formation of thick layers of unconsolidated material [FRF, 2008].

In the event of peak rainfalls, part of these vegetated layers slide and deposit in drainage

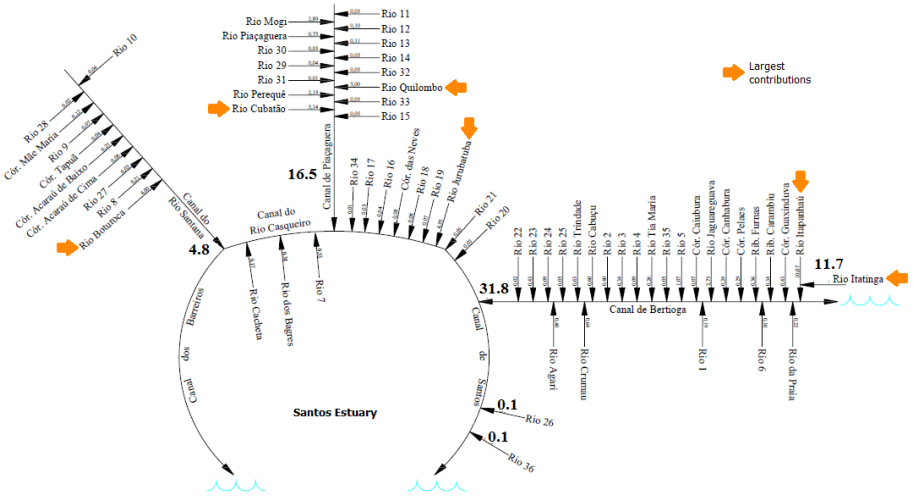

Figure 2.9: Single line diagram of the tributary rivers in the SE. Values indicate average discharges [m^3/s.], see Table 2.3. Adapted from [FRF, 2008].

Table 2.3: River discharges in the SE, see Figure 2.9. Adapted from FRF [2008].

	Discharge [m^3/s]		
	Min	Average	Max
Itatinga	3	12	187
Itapanhau	2	10	114
Cubatão	1	5	214
Quilombo	1	5	117
Boturoca	1	4	105
Jurubatuba	1	4	90
Others	5	19	1,300

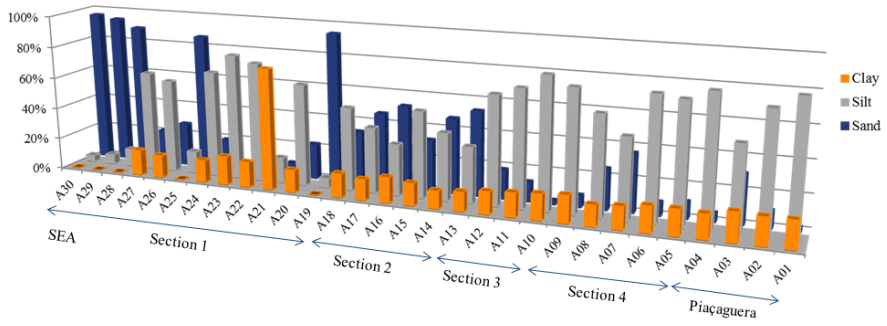

Figure 2.10: Superficial bed composition based on 30 samples taken along the channel in February 2006 and sieved in laboratory [FRF, 2008].

channels, resulting in a positive feedback of erosive processes. In the steep scarps, one can find blocks of displaced material transported in the occurrence of these events, resulting in large fluxes of mud traveling downstream and accumulating in the lower plains of the system.

Erosive processes in the basin have been enhanced by human activities in the last decades. Urban sprawl, construction of roads, and placement of pipelines are mentioned as the causes of increased volumes of sediment transported downstream by the rivers [FRF, 2008].

Large volumes of marine and mixed sediments can be found in the SE, which are subject to marine, riverine, and/or wind action. These deposits of sandy to clayey material with high contents of organic matter form layers of up to 50 m thick in gentle slopes ($<2\%$) [CBH, 2000]. Mangroves are associated to most of the river mouths in the basin.

2.2.4 Sandy to clayey sediment

Figure 2.10 presents the bottom composition along the Santos channel. Coarser sediment can be found in Sections 1 and 2, both subject to marine action. These sections also present a considerable fraction of fine sediment - up to 80% in entrance of the port. Sections 3 and 4, and the Piaçaguera channel are composed mainly by silty material.

Sedimentation patterns in the SE indicate sediment sources as: river inflows, erosion of banks and holocene trangressive deposits, and crosshore and longshore transports [FRF, 2008]. Mangroves in the lower areas of Baixada Santista retain the larger fraction of sediment carried downstream by the rivers. In the tidal plain, residual riverine fluxes transport silty to clayey material in the direction of Santos bay, adding to the marine sediment [Fúlfaro and Poçano, 1976].

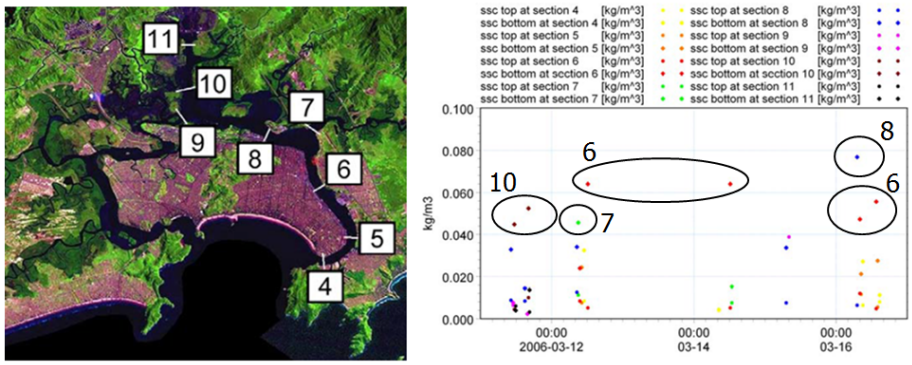

Figure 2.11: Suspended sediment concentration [Elfrink et al., 2008]. Samples were taken from 1 m below water level and 1 m above the bottom, in the middle of the indicated sections.

Sediment concentration

Concentration of solids in suspension were measured in March 2006 by Instituto Nacional de Pesquisas Hidroviárias (INPH) and the engineering consultant DHI. Samples were taken from eight points along the estuary, in the surface and bottom of the water column. The results, presented in Figure 2.11, show that the highest concentrations occur close to the mouths of rivers Cubatão and Quilombo and also in the Section 2 of the channel, possibly due to up-estuary transport of fines by tidal waves [Tommasi, 2008]. No information regarding ETM location and concentration was available during the execution of this thesis.

Fluid mud

Ferreira [2013] studied the presence and behavior of fluid mud in Sections 3 and 4 of Santos channel. According to the author, resuspension of material in these areas occurs during peak flows and is limited by the stratification in the water column. The resuspended matter stays a few meters above the bottom and the resultant net transport is close to zero.

Hence, fluid mud sediment remains in its original location and the fluid mud behaves as an almost stationary layer with thickness governed by the intensity of the currents in the tidal cycles.

3

Sediment balance

A sediment mass balance of the Santos estuary is built to estimate the relevant sinks and sources in the SE. The underlying assumption is that the estuary is a closed cell, i.e., there is no natural sediment export.

The results are presented in Table 3.1 and illustrated in Figure 3.1. The largest contributor to the sedimentation in the channel are winter storms, providing fine and coarse material to the navigation channel. Due to uncertainties in the data collected, quantification is presented in terms of a best estimate, with lower and upper bands. The following sections depict the methodologies and data applied to assess the sediment sinks and sources.

Table 3.1: Sediment balance results.

Source(+) / Sink(-)	Lower band [Mton/year]	Best estimate [Mton/year]	Upper band [Mton/year]
River input	0.4	0.9	1.9
Retained mud flats	-0.4	-0.4	-0.4
Winter storms	0.9	1.4	1.4
Maintenance dredging	-1.0	-2.1	-3.3
Other sources	0.1	0.2	0.4

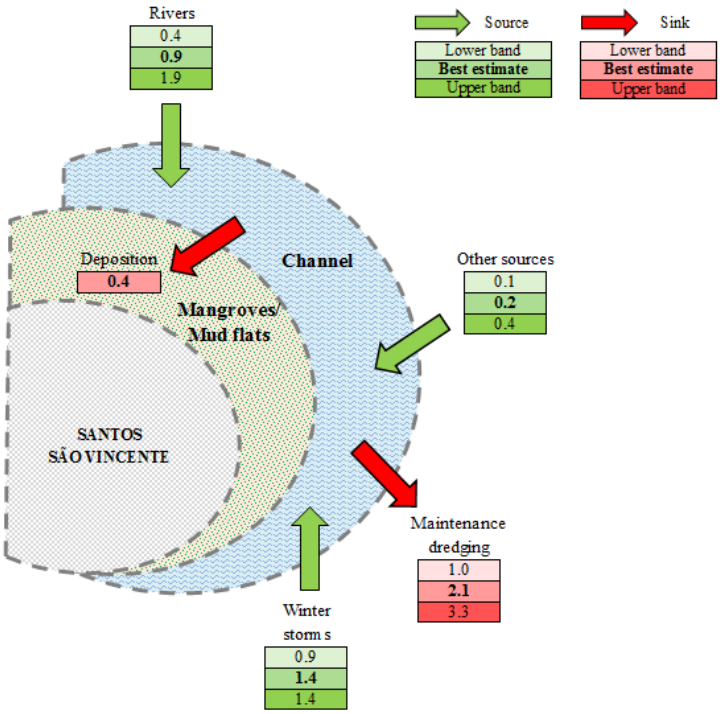

Figure 3.1: Mass sediment balance period 2005 to 2012 [Mton/year]

3.1 River input

According to Section 2.2.3, more than thirty rivers discharge in the SE bringing fresh water with coarse to fine sediment. Measured data regarding bed and suspended sediment load of these rivers are unavailable. Moreover, due to the episodic erosion patterns, these loads vary greatly during the year and among the years, turning it problematic to quantify these loads. Therefore, to evaluate the river sediment input, an average sediment concentration is associated to the river discharges. Sediment concentration is selected by expert judgment based on vegetation, geomorphology, human activities in the basin, and run-off rates.

The yearly discharge volumes for the studied period are obtained by correcting the average estimated in the EIA (2008) with the recorded rainfall for these years, obtained from DAEE. This method is illustrated in Figure 3.2 and the resultant annual average sediment input is presented in Table3.2.

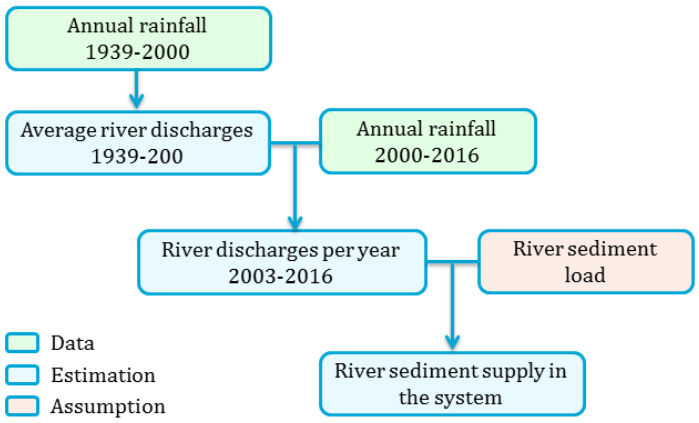

Figure 3.2: Methodology for estimation of annual river sediment supply in Santos estuary.

Table 3.2: Estimated sediment input by the rivers.

Average river discharge (EIA 2008)		60	m³/s
Sediment concentration	Lower band	0.2	kg/m³
	Best estimate	0.5	kg/m³
	Upper band	1	kg/m³

Year	Annual rainfall / average	Sediment input [Mton]		
		Lower band	Best estimate	Upper band
2005	1.1	0.4	1.0	2.0
2006	0.9	0.4	0.9	1.8
2007	0.8	0.3	0.7	1.5
2008	0.9	0.3	0.8	1.7
2009	0.8	0.3	0.8	1.6
2010	1.3	0.5	1.2	2.4
2011	1.2	0.4	1.1	2.2
2012	0.9	0.3	0.8	1.7
Annual average	1.0	0.4	0.9	1.9

3.2 Deposition

A fraction of the sediment supplied by the rivers to the system is retained by the mangroves and mudflats that occupy a considerable area of the estuary [Alfredini and Lavieri, 2013], correspondent to the green area highlighted in Figure 3.3. To estimate the amount retained by the mangroves, it is assumed that these mangrove areas are rising at the same rate as the absolute sea level rise (SLR).This assumption is sustained by the fact that the sediment supply is sufficient and that the SLR pace provides sufficient accommodation time to the species. Environmental monitoring in the mangroves around Cubatão and Barnabé shows that these areas have been growing in the past years [CODESP, 2016b].

This sink of sediment is estimated by Equation 3.1:

$$D = SLR * A * \gamma_{mud} \tag{3.1}$$

With:

- D the deposited mass of sediment [ton/year];
- SLR the annual rate of sea level rise [m/year];
- A the area of mud flats and mangroves [m^2]; and
- $\gamma_{mud,bulk}$ the average bulk density of the deposited material [ton/m^3].

According to a study carried out by the University of São Paulo together with other institutes, the absolute mean sea level rise in Santos between 1993 and 2013 was 3 mm/year [FAPESP, 2015]. The area of mud flats and mangroves in the estuary is retrieved from satellite imagery of Google Earth®and is approximately 109 km^2 (highlighted green areas of Figure 3.3). These areas are considered to be composed by con-

Figure 3.3: Estimate of mangrove area (green) retrieved from Google Earth ®.

solidated deposits of mud, which present an average dry bulk density of 1,000 kg/m^3 [Dyer, 1998].

Applying this values to equation 3.1, the resultant best estimate of retained sediment is 0.4 Mton/year. No lower or upper bands are applicable given the provided data.

3.3 Winter storms

Winter storms in Santos bay provide another source of sediment to the estuary. Alfredini and Lavieri [2013] attribute wave agitation to the infilling of S1 with sandy and silty material, especially in episodic events as winter storms . This is corroborated by the bed composition presented in Figure 2.10 that provides a predominance of sandy material in the first three kilometers of the channel in the estuary.

Based on dredging records from 1997 to 2013, Alfredini and Lavieri [2013] estimate sedimentation volumes of 0.9 Mm^3 for a 1-way, 13.7 m deep channel. To convert this information from volume to mass, different bulk densities are assigned for different compositions of dredged material and their respective mass was computed by Equation 3.2:

$$D = \gamma_{material} * V \tag{3.2}$$

Provided that:

- D the deposited mass of sediment [ton/year];
- $\gamma_{material}$ the average bulk density of the deposited material [ton/m^3]; and
- V the deposited volume of sediment [m^3/year].

A mixture of fine and coarse sediment is considered for the lower band, provided the fine material present in the bay, with dry $\gamma_{mix,bulk}$ of 1,050 kg/m^3. For the best estimate, it is considered 100% of sand, with dry bulk density $\gamma_{sand,bulk}$ of 1,600 kg/m^3.

Applying the described bulk densities to the estimated volume of sediment deposited by winter storms, a best estimate of 1.4 Mton/year is found, with a lower band of 0.9 Mton/year. A upper estimate is not applicable for the present case.

3.4 Maintenance dredging

Maintenance dredging is the most relevant sink of sediment. As previously stated, every year relatively large amounts of sediment are dredged in the Port of Santos. The information available regarding dredging records are the ones from CODESP. These volumes were measured in situ and are presented in Table 3.3.

The mass of dredged sediment are computed with Equation 3.2. As information on the composition of the dredged material is unavailable, the lower and upper bands and the best estimate were computed by considering three compositions of deposited sediment. A best estimate is given by fresh deposits of mixed sediment (coarse and fine) with low consolidation and average dry $\gamma_{mix,bulk}$ of 1,050 kg/m^3. The lower band consists of fresh deposits of fine sediment only, with average dry $\gamma_{freshmud,bulk}$ of 500 kg/m^3. The upper band consists of deposits of sand with dry $\gamma_{sand,bulk}$ of 1,600 kg/m^3. Results of these computations and the estimated annual averages are shown in Table 3.3.

It must be noted that the dredging records:

- May not correspond to the complete maintenance of the channel;
- May also cover dredging of berths and turning basins;
- May also cover dredging tolerances of up to 0.7 m in Section 1 and 0.3 m in sections 2, 3 and 4.

The observations above provide uncertainties on top of the accounted variations in composition of the dredged material. These volumes uncertainties are hardly possible to assess with the available data. For this reason, the dredged volumes is taken as absolute, i.e., without error bands.

Table 3.3: Maintenance dredging records in Santos Port and respective mass estimates.

Material bulk density	Lower band	500	kg/m³
	Best estimate	1,050	kg/m³
	Upper band	1,600	kg/m³

Year	Dredged volume [Mm³]	Dredged mass [Mton] Lower band	Best estimate	Upper band
2005	2.5	1.3	2.6	4.0
2006	2.7	1.3	2.8	4.3
2007	1.6	0.8	1.7	2.5
2008	3.2	1.6	3.3	5.1
2009	2.6	1.3	2.8	4.2
2010	0.7	0.4	0.7	1.1
2011	1.1	0.6	1.2	1.8
2012	1.9	1.0	2.0	3.1
Annual average	2.0	1.0	2.1	3.3

3.5 Other sources

Given the assumption that the estuary is a closed cell, the results of Sections 3.1 to 3.4 indicate that a third source of sediment possibly exists, represented by the deficit in Table 3.4 [1]. This is in agreement with the yet not estimated import of sediment due to the referred estuarine circulation introduced in Section 1.2.

A strong source candidate is the fine sediment available at the entrance of the estuary which becomes mobile by the action of wind and tidal waves and is then transported up-estuary by gravity flows.

Yet, the mentioned uncertainties in the sources and sinks of previous sections influence in the estimation of this source. Nonetheless, the resultant sediment balance provides a proper overview of the sediment agents in the system and their relative importance to the net input of sediment in the SE.

[1] When lower and/or upper bands were not provided, the correspondent best estimate result is applied in the balance.

Table 3.4: Sediment balance results.

Source(+) / Sink(-)	Lower band [Mton/year]	Best estimate [Mton/year]	Upper band [Mton/year]
River input	0.4	0.9	1.9
Retained mud flats	-0.4	-0.4	-0.4
Winter storms	0.9	1.4	1.4
Maintenance dredging	-1.0	-2.1	-3.3
Deficit	0.1	0.2	0.4

4

Explorative Delft3D model

An explorative process-based model is set in Delft3D-FLOW to expand the knowledge in the system and also evaluate the proposed sediment balance. Model results suggest that the sediment transport of fines is mostly given by baroclinic currents and that conditions for the formation of fluid mud exist. Details on the model set-up, calibration, and results are described in the following sections.

4.1 Delft3D-FLOW

Delft3D is a modeling suite applied to investigate flows, waves, water quality, sediment transport, morphological developments, and ecology in coastal, fluvial, and estuarine environments. The FLOW module is a 2D or 3D hydrodynamic and transport simulation software that computes non-steady flow and transport phenomena resultant from tidal and meteorological forcing on a boundary fitted grid [Deltares, 2016].

In this research, Delft3D is chosen for its capability in simulating the most relevant physical processes in the SE, such as tidal filling and emptying, density-driven vertical circulation, and fine sediment transport. Given the size of the area to be modeled, a Cartesian coordinate system is set with twelve σ-layers in the vertical direction, resulting in a 3D model. The latter is necessary to account for the significant variations in the water column, as salt intrusion and suspended sediment.

4.2 Model set-up

Data is collected from different sources and refer to different periods in time. The most suitable data set is formed for years 2004 to 2006, for which a combination of bathymetries of the estuary is available, together with water level measurements, salinity, and sediment concentration information. For the referred period, the design depth of Santos channel varied from 12 m to 13 m.

The model is discretized with a curvilinear grid of 278 x 199 cells, covering part of Santos bay, Santos and São Vicente channels, mudflats, and mangroves. The computational grid is presented in Appendix B. It is more refined in the area of interest - the

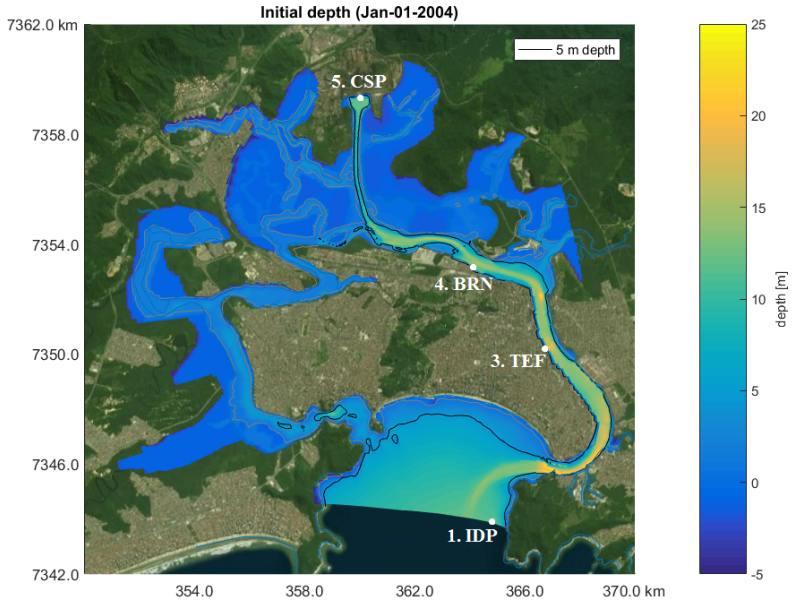

Figure 4.1: Initial bathymetry.

Santos channel, with grid cells of up to 100 m x 70 m. The set of bathymetries of year 2004 is interpolated in the referred grid and presented in Figure 4.1.

4.2.1 Parameters

The parameters applied in the sediment transport model are presented in Table B.1 of Appendix B. In reality, waves continuously re-suspend sediment in the bay, which is subsequently transported into the estuary. Setting up a detailed wave model is beyond the scope of the present study, therefore, the effect of waves on the fine sediment is parametrized by switching off deposition in the bay, i.e., setting the critical bed shear stress for sedimentation to 1E-03 N/m^2.

Critical bed shear stress for erosion depends on factors as the median diameter of the bed forming flocks, the time that the time-varying bed shear stress exceeds the cohesive forces within the bed, cohesion due to interparticle forces, and mean bed shear stress and its variance. Critical bed shear stress for erosion ($\tau_{cr,er}$) can vary from 0.1 N/m^2 to 5 N/m^2. For freshly deposited mud it ranges between 0.1 N/m^2 and 0.5 N/m^2 [Winterwerp and van Kersteren, 2004] [Winterwerp, 1989].

In the present study, three sediment fractions were assigned: marine 1 (M1), marine 2 (M2)[1] and fluvial (F1). The fractions M1 and F1 have the exact same properties, but

[1]Marine fraction refers to sediment put into the estuary through the sea boundary. This sediment is, in

are added to the system via different sources. Their $\tau_{cr,er}$ is 0.1 N/m^2. Fraction M2 differs from the other fractions only by the $_{cr,er}$, which is 0.3 N/m^2. Distinct critical bed shear stress for erosion of the sediment are applied as a simplification to account for the possible different characteristics of the sediment present in reality, as this property is unknown in the present study.

4.2.2 Boundary conditions

The seaward boundary indicated in red in Figure B.1 (Appendix B is the only open boundary in the model. The remaining boundaries are defined as closed boundaries. At open boundaries, flow and transport boundary conditions are required. For the flow condition, two time-series of water levels are employed for separate purposes:

- Measured hourly time series at Ilha das Palmas for the period of April-21 to May-07, 2004. Applied for model calibration; and
- Hourly time series obtained with aid of t_tide[2]. Input: astronomical components published in FEMAR table 236, Ilha das Palmas [FEMAR, 2017]. Applied in the six-month simulations.

Transport boundary conditions for salinity vary between 29 ppt and 33 ppt during wet and dry seasons, respectively, and remained constant for sediment: 0.025 kg/m^3 for each of the two marine fractions and zero for the fluvial fraction. These conditions are set constant along the open boundary.

At the close boundaries, fresh water discharges are assigned. These discharges represent the river input in the SE and are grouped in six locations along the middle and upper areas of the estuary, as shown in Figure 4.2. As data for river discharges in 2004 in the SE is unavailable, approximate values are obtained by correcting the monthly discharge estimates given in the EIA (2008) with the monthly precipitation records at station Caeté in 2004. This methodology is similar to the one applied in Section 3.1 for the annual discharge averages. The resultant estimates of monthly average river discharges in 2004 are presented in Table 4.1.

Sediment loads carried by the river are likewise unknown, therefore a concentration of 0.5 kg/m^3 is selected based on expert judgment. This load is the best estimate provided in the sediment mass balance of Section 3 and is set constant along the year, representing an estimated average between extreme rainfall and normal conditions.

4.2.3 Initial conditions

The initial conditions are:

- 2004 bathymetry set, courtesy of Lopes [2015];

reality, terrigenous sediments, i.e., derived from land and deposited in the sea floor.

[2] t_tide is a tidal analysis toolbox that uses harmonic analysis to estimate tidal constituents and their uncertainties in scalar and vector time series in a MATLAB environment [R. Pawlowicz and Lentzb, 2002]

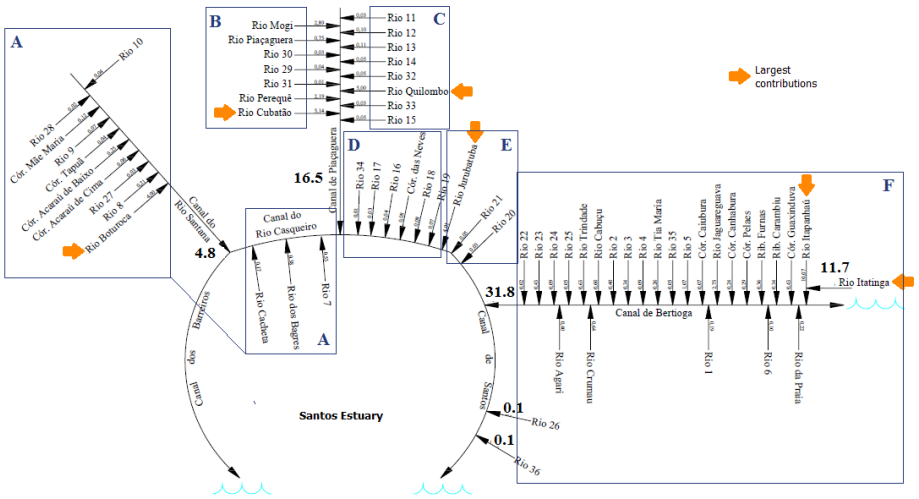

Figure 4.2: Grouping of rivers for fresh water discharge input. Respective discharges are given in Table 4.1. Adapted from FRF [2008].

Table 4.1: Estimated average monthly river discharges for year 2004. Groups indicated in Figure 4.2.

	Average river discharges [m^3/s]											
Group	Jan-04	Feb-04	Mar-04	Apr-04	May-04	Jun-04	Jul-04	Aug-04	Sep-04	Oct-04	Nov-04	Dec-04
A	8	11	6	7	3	2	7	3	5	5	6	8
B	11	16	9	10	4	3	10	4	7	7	8	10
C	4	6	3	4	1	1	3	2	2	2	3	4
D	7	10	6	7	2	2	7	3	5	5	5	7
E	6	8	5	6	2	1	5	2	4	4	4	6
F	43	61	34	40	14	10	38	17	27	27	31	40

- Salinity map based on the results of an 1-year 2D simulation with tidal forcing and fresh water discharges. The system is considered in dynamic equilibrium in respect to this physical quantity at the start of the morphodynamic simulation; and
- No sediment available in the bottom nor in suspension. This was chosen in order to investigate the behavior of the system concerning the fine sediment sources assessed in the mass sediment balance.

4.2.4 Calibration

Figures 4.3 to 4.5 present the calibration results for water levels of the monitoring stations of Figure 4.1. Model calibration for water levels presented satisfactory root mean square errors (RMSE), below 0.08 m. The errors increased in the up-estuary direction (stations 3 and 4), which was expected due to scarce of bathymetry data in the upper region of SE.

The RMSE of the tidal components were also evaluated. The tidal components where extracted from the measured and modeled water levels with aid of t_tide and then the

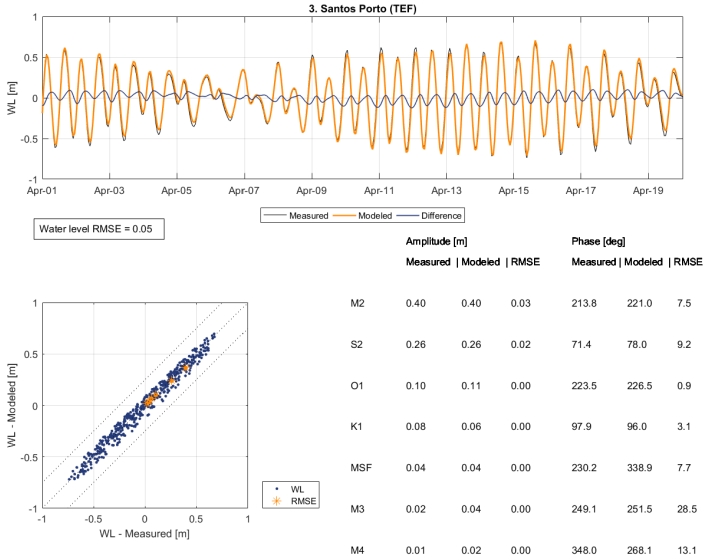

	Amplitude [m]			Phase [deg]		
	Measured	Modeled	RMSE	Measured	Modeled	RMSE
M2	0.40	0.40	0.03	213.8	221.0	7.5
S2	0.26	0.26	0.02	71.4	78.0	9.2
O1	0.10	0.11	0.00	223.5	226.5	0.9
K1	0.08	0.06	0.00	97.9	96.0	3.1
MSF	0.04	0.04	0.00	230.2	338.9	7.7
M3	0.02	0.04	0.00	249.1	251.5	28.5
M4	0.01	0.02	0.00	348.0	268.1	13.1

Figure 4.3: Calibration results for water level at 3. Santos Port (TEF).

RMSE was computed for each of the components. The main tidal components of the SE are also well predicted for amplitudes, with the largest RMSE = 0.11 for the M_2 component. Phase errors were pronounced for the tidal components M_3, MSF, and M_4. However, these components also present a small amplitude when compared to the main tidal components of the system M_2 and S_3, therefore, these errors do not influence significantly in the overall RMSE of the system. A

Several roughness compositions are applied in the accepted range for sandy-clayey bottom and the composition that presents the lowest RMSE for water levels is selected. That corresponds to a Chézy value of 8 $m^{1/3}/s$ for the mudflats and mangroves and 80 $m^{1/3}/s$ for the channels and remaining areas of the estuary. With respect to wind forcing, in typical conditions wind velocities are rather low and, therefore, neglected in the scope of this study.

Currents are not assessed in detail given that current measurement time-series are not available for this research. Modeled depth average current velocities present magnitudes of up to 0.5 m/s, as it can be seen in Figure 4.6. These values are in correspondence to the averages found in literature, as per Section 2.2.1, Figure 2.6b. In the Piaçaguera channel, however, this currents were underestimated by the model. This is very likely a result of the poor bathymetry data for the area, including the adjacent mud flats, where water might spread and reduce current velocities. Deviations in current velocities imply, among others, in a quadratic error in the estimation of bed shear stresses. Sedimentation is possibly overestimated in the Piaçaguera channel.

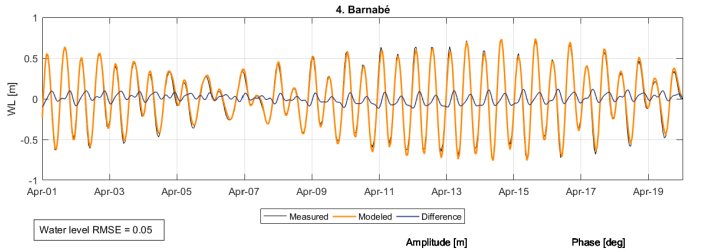

	Amplitude [m]			Phase [deg]		
	Measured	Modeled	RMSE	Measured	Modeled	RMSE
M2	0.41	0.42	0.06	216.3	223.2	9.8
S2	0.27	0.28	0.04	74.5	80.9	12.1
O1	0.10	0.11	0.01	228.7	227.0	1.3
K1	0.08	0.07	0.00	91.4	96.9	4.0
M3	0.04	0.04	0.01	227.6	258.2	73.1
MSF	0.02	0.03	0.00	228.8	344.3	121.3
M4	0.02	0.02	0.01	309.1	266.9	11.9

Figure 4.4: Calibration results for water level at 4. Barnabé (BRN).

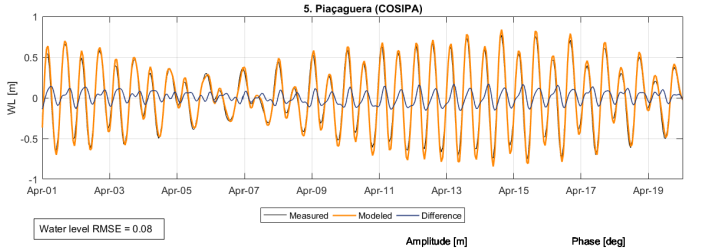

	Amplitude [m]			Phase [deg]		
	Measured	Modeled	RMSE	Measured	Modeled	RMSE
M2	0.42	0.47	0.10	222.1	231.0	17.6
S2	0.27	0.31	0.07	82.0	89.9	21.1
O1	0.12	0.11	0.01	228.0	228.4	2.7
K1	0.08	0.07	0.00	90.9	99.5	6.6
M3	0.04	0.05	0.02	242.3	277.0	54.3
M4	0.03	0.04	0.00	222.8	284.7	61.8
MSF	0.01	0.03	0.01	271.4	317.0	62.0

Figure 4.5: Calibration results for water level at 4. Piaçaguera (CSP).

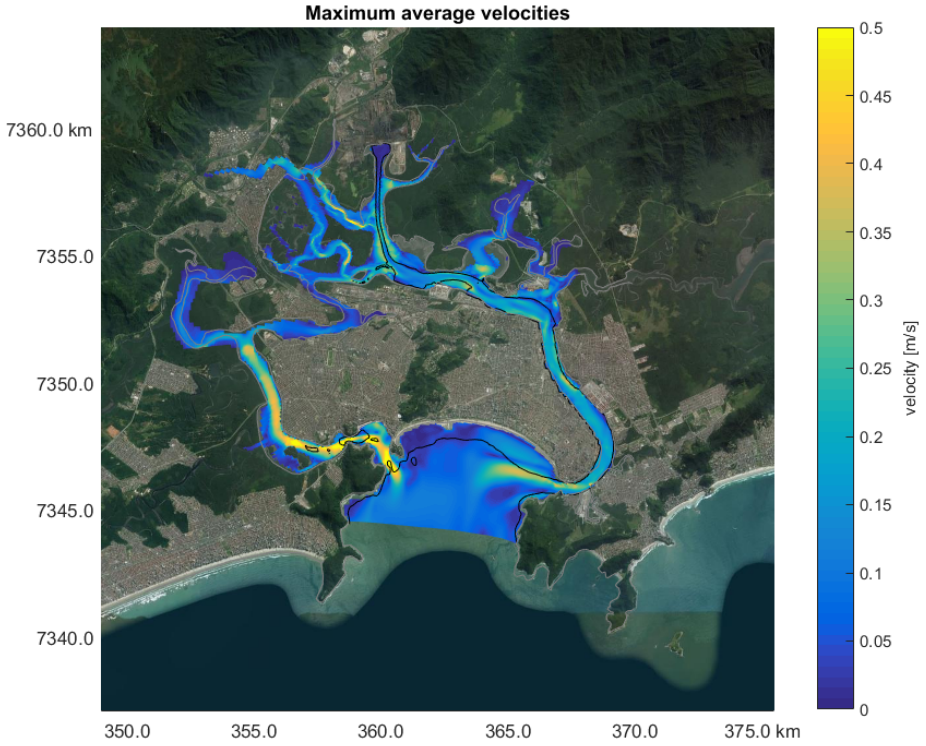

Figure 4.6: Maximum depth averaged flow velocities.

4.3 Results

The aim of the hydro- and morphodynamic model is to assess sedimentation patterns in the SE. From literature research and the sediment balance, seasonality is expected. Therefore, once the model is calibrated a six-month period is simulated (January 01 to July 01, 2004) with the initial and boundary conditions presented in the previous items. The results are evaluated in four categories:

- Summer and winter condition, i.e., high and low river discharges;
- Spring and neap tides;
- Flood and ebb conditions;
- High water (HW) and low water(LW).

	Summer		Winter	
Spring tide	Flood	HW	Flood	HW
	Ebb	LW	Ebb	LW
Neap tide	Flood	HW	Flood	HW
	Ebb	LW	Ebb	LW

Figure 4.7: Scenarios for the evaluation of results.

Appendices C andD contain a set of cross-sectional and map plots representing each of the sixteen scenarios above. The cross-sectional plot contains results of flow velocity magnitude and direction, salinity, sediment concentration, and salinity differences. It corresponds to a cross-section along the center of the Santos navigation channel and the Piaçaguera channel.

4.3.1 Currents

Maximum average velocities of 0.8 m/s were found in the Santos channel. In order to investigate transport patterns, aim of this research project, residual flows are computed from the mean velocities found in the simulation. Results are shown in Figure 4.8. In the entire channel, a residual flow in flood direction is visible with depth average velocities with mean of up to 0.04 m/s and standard deviation of up to 0.1 m/s. The maximum depth averaged mean velocities found in the estuary correspond to approximately 10% of the maximum depth averaged velocities.

Depth averaged residual currents for summer and winter periods, during spring and neap tide are presented in the Appendix D.2. Stronger depth averaged residual currents are found during summer spring tide. That is due to larger fresh water discharge during this season when compared to winter, promoting a stronger residual circulation. In spring tide condition the residuals are more pronounced as a result of the periods with relatively low water levels and larger influence of fresh water input in the circulation. One can see that the standard deviation of the depth averaged currents in spring tide reaches up to 100% the mean depth averaged currents, representing the large variance

between high and low water conditions. In neap tide the water level differences between high and low water are approximately five times smaller, thus the variance of the depth averaged residual currents is reduced when compared to spring tide conditions. This pattern is also found during winter, however with lower mean depth averaged residual currents, result of the already mentioned reduction of fresh water input in the system.

An indication of flood or ebb dominance is given by comparing the maximums depth averaged velocities during ebb with the maximums during flood. Figure 4.9 presents the ratio of these maximum velocities. S1, S2, and S3 of the channel present a flood dominance, with some ebb dominance alongside the channel, in the port terminal basins. S4 presents both ebb and flood dominant characters. The Piaçaguera channel presents a flood character, oppositely of what is found in literature. Once again, this is probably a result of changes in the bathymetry, and/or scarce information on the actual bathymetry of the channel and surrounding areas.

From the sixteen scenarios presented in Appendix C.1, the following observations are obtained with respect to flow velocities and direction:

- During ebb and flood, the velocity magnitudes clearly vary between spring and neap tides as a result of the spring tide amplitudes being approximately twice the neap tide amplitudes. Velocity directions during flood are similar during summer and winter, spring and neap tides;
- A complicated pattern is found for summer neap tide during ebb. This might be a result of the relative larger influence of fresh water discharges over the tidal forcing in this condition;
- Around LW, a seasonal variance can be found during neap tide. During summer neap tide a current in the surface is found between stations 2. Praticagem and 3. Santos (TEF). This is very likely a result of the higher fresh water discharge during summer, which can be seen when tidal forcing is less pronounced. A variation in direction is also found during neap tide; and
- Around HW no clear seasonal variation is found.

4.3.2 Salinity

The entire estuary contains salt water during all the conditions of Figure 4.7. In the water column, salinity varies up to 10 ppt between bottom and surface layers and the system presents characteristics of a stratified estuary. Salinity varies seasonally (Figure 4.10), attributed to the variance of fresh water discharge in the estuary, which is up to three times larger during summer. This seasonal variance in salinity is not experienced in the bay, which can be a model result due to the location of the open boundary (in the bay) and/or can be explained by the relatively low volume of fresh water discharge in comparison to the extent of the bay.

From the sixteen scenarios presented in Appendix C.1, the following observations are derived:

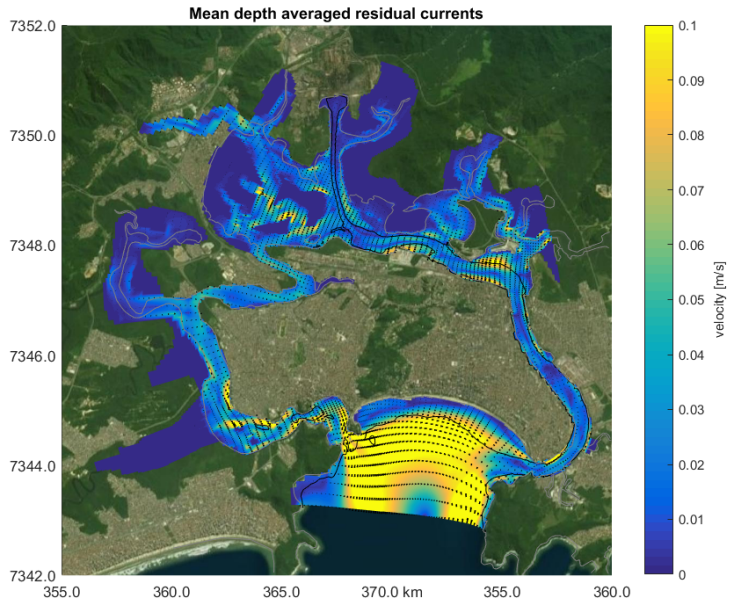

(a) Mean depth averaged residual currents.

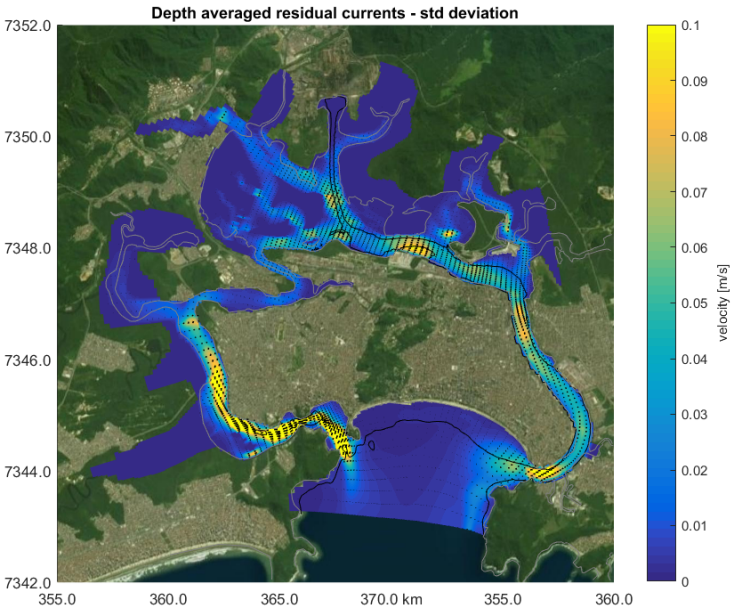

(b) Standard deviation of maximum depth averaged residual currents.

Figure 4.8: Depth averaged residual currents in the estuary.

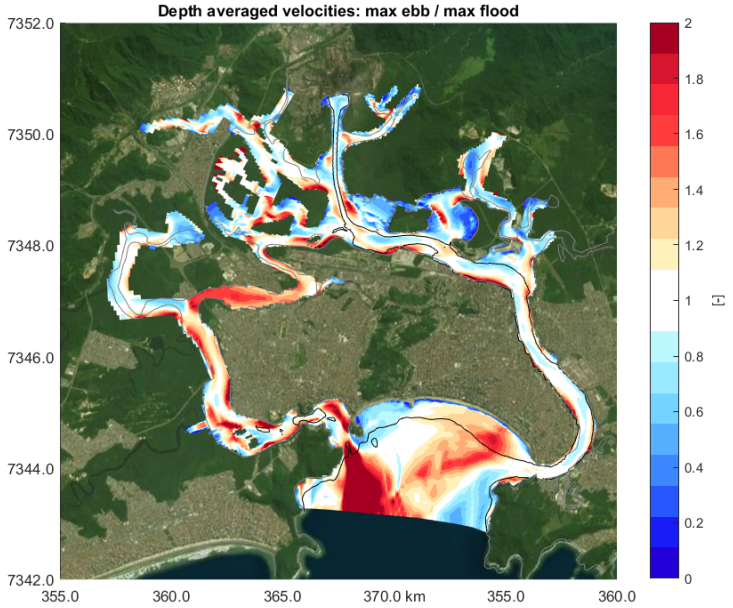

Figure 4.9: Asymmetry in the depth averaged flow velocities given by the ratio of the maximums during ebb and during flood. Shades of red indicate ebb dominance, shades of blue indicate flood dominance.

- The salt wedge intrudes deeper in the estuary in winter conditions. This is due to the reduced river discharges, and consequently, a reduced amount of fresh water moving in the outer direction of the estuary opposing the salt water traveling in the up-estuary direction;
- Stratification between bottom and surface layer reaches up to 10 ppt both in summer and winter conditions for spring tide. The largest salinity differences are found around station 4. Barnabé, area where the largest input of fresh water in the system is located; and around station 5. COSIPA, where the system also receives considerable volumes of fresh water;
- During neap tides, intrusion of the salt wedge is less pronounced, and it can be seen that gradients in the salt wedge are milder for both summer and winter periods. These reduced gradients are a result of smaller tidal amplitude variations in neap tide and probably of a larger period for the mixing of salt and fresh waters; and
- During ebb the same patterns described for flood conditions are found with exception of a larger stratification for spring neap tide when compared to winter neap tide. Again as a result of fresh water discharges in relation to tidal discharges.

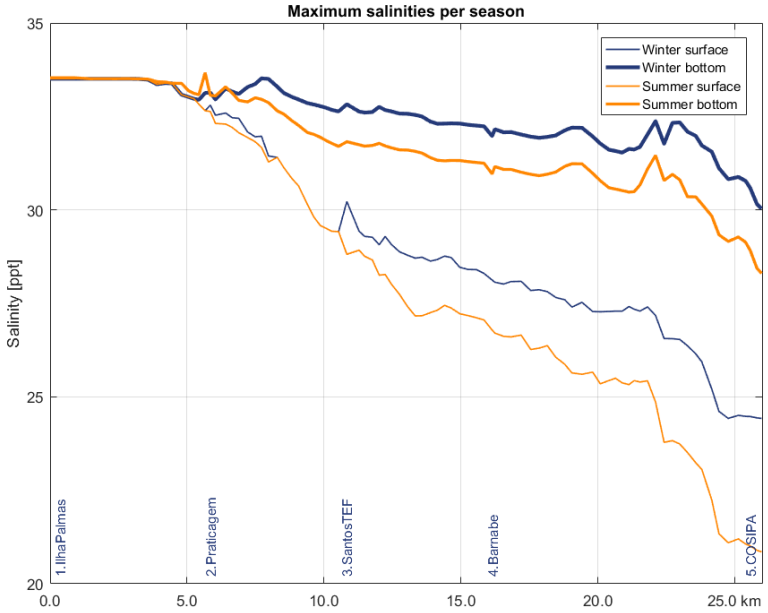

Figure 4.10: Maximum salinity per season.

4.3.3 Bed shear stress

Erosion characteristics are important for the understanding of sediment dynamics. When the bed shear stress becomes larger than the critical bed shear stress for erosion of the sediment, sediment becomes mobile. The critical bed shear stress for erosion ($\tau_{cr,er}$) depends on factors as the median diameter of the bed forming flocks, the time that the time-varying bed shear stress exceeds the cohesive forces within the bed, cohesion due to interparticle forces, and mean bed shear stress and its variance. Critical bed shear stress for erosion can vary from 0.1 N/m^2 to 5 N/m^2. For freshly deposited mud it typically ranges between 0.1 N/m^2 and 0.5 N/m^2 [Winterwerp and van Kersteren, 2004] [Winterwerp, 1989].

The percentage of time that the bed shear stress exceeds the sediment critical bed shear stress for erosion gives an indication of the probability that sediment will erode. This is computed by summing up the number of recorded time steps of the model when the bed shear stress exceeds a given threshold. The thresholds applied in this study were the typical lowest and highest $\tau_{cr,er}$ for freshly deposited mud (0.1 and 0.5 N/m^2 respectively) and the correspondent $\tau_{cr,er}$ of sediment fraction M2, 0.3 N/m^2.

Figure 4.11 presents the computed maximum bed shear stresses in the estuary. Along the Santos navigation channel, the bed shear stresses are above 0.1 N/m^2, indicating that fresh deposited mud with $\tau_{cr,er} \approx 0.1$ N/m^2 very probably will become mobile

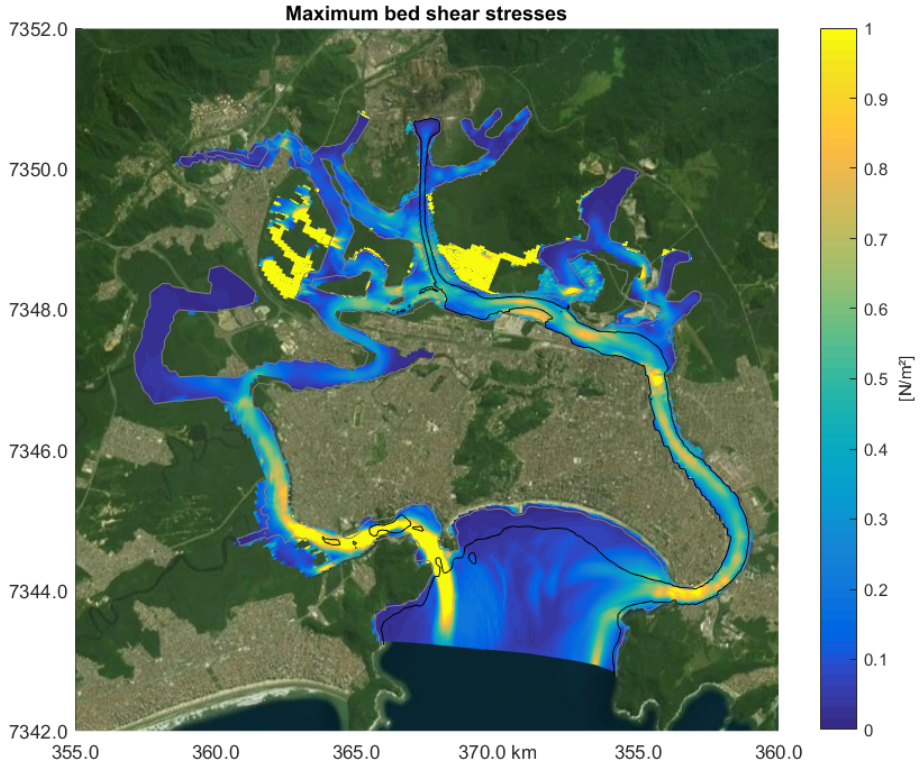

Figure 4.11: Maximum bed shear stresses found in the estuary.

within a tidal cycle and erosion will take place.

Figures D.1 to D.3 provided in Appendix D present the time exceedance for $\tau_{cr,er}$. It can be seen that the in the bay, where fine sediment deposits are present, erosion takes place from 90% to 100% of the time for sediment with $\tau_{cr,er}$ from 0.1 to 0.3 N/m^2. It is therefore very likely that in every tidal cycle eroded particles with such $\tau_{cr,er}$ will travel in the up-estuary direction.

Along the navigation channel, erosion also takes place with a similar rate. Particles with $\tau_{cr,er}$ = 0.5 N/m^2 are subject to erosion along S1, S2, and in some areas of S3 to S4. Roughly, if the depth averaged peak flow velocity is 0.5 m/s, and the mean velocity is 0.35 m/s, and a tidal cycle lasts 12 h, a particle at the bay, just in the entrance of the channel, will travel 7,6 km in half tidal cycle, reaching the second half of S3 during flood conditions.

4.3.4 Sediment concentration

The initial condition of the simulation is zero sediment in the system. With the start of the six-month period simulation, three fractions of fine sediment were constantly added in the estuary. The marine fractions M1 and M2 enter via the open boundary with the tidal forcing with concentration of 0.025 kg/m^3 each. The only difference between these fractions is the critical bed shear stress for erosion: $\tau_{\text{cr,er M1}} = 0.1$ N/m^2 and $\tau_{\text{cr,er M1}} = 0.3$ N/m^2. The fluvial fraction F1 was added to the system with a constant discharge of 0.5 kg/m^3 applied to the fresh water discharge locations. The characteristics of fine sediment F1 are the same as M1.

In the cross-section plot of Appendix C it can be seen that sediment reaches the end of Piaçaguera channel, traveling with the salt wedge. The concentration of sediment in the water column varies within the tidal cycle. In the concentration map plots it can be seen that in the navigation channel a layer with characteristics of fluid mud is formed around high water and almost destroyed around low water. During winter larger concentrations are found in the final stretches of the channel in comparison to summer. That is explained by the reduced fresh water discharge during winter, leading to a deeper penetration of the salt wedge together with sediment.

Figures 4.14a presents the amount of sediment available at the bed by the end of the simulated period. It indicates a greater accumulation in S1 and beginning of S2. This is in accordance with the flood and ebb dominance characters found in the estuary and the trapping of sediment between this zones, as discussed in Section 2.1.1.

Fraction M1 reaches further in the estuary [3], depositing not only in S1 and S2 but also in some areas of S3 and S4. Due to the small critical bed shear stress for erosion of this fraction, it is more easily reworked and transported, as modeled bed shear stresses are higher then 0.1 N/m^2 for more than 90% of the time. Source M2 likewise greatly accumulates in S1 and S2 [4], although found in S3 and S4 in negligible quantities. This is explained by the higher critical bed shear stress required to rework this fraction.

After a six-month period, riverine sediment deposits mostly close to fresh water discharge locations [5]. Less than 5% in mass of this fraction reaches the navigation channel. At the end of the simulation the contribution of the riverine sediment to the total sediment available in the bed is almost negligible when compared to the marine sources contribution.

It must be noted that a cold start is applied and no sediment is available in the system in the start of simulation. The system might need a longer period to stabilize the deposition pattern of the riverine fraction. Probably for longer simulation periods and/or higher input of river sediment, larger quantities of this fraction will deposit in the channel.

To control the up-estuary sediment transport, monitoring cross-sections are assigned in the model (Figure 4.12), positioned in the entrance of the estuary and in the beginning

[3] see Appendix D, Figure D.44
[4] see Appendix D, Figure D.45
[5] see Appendix D, Figure D.46

of each of the channel sections. The cumulative transport in each of this cross-sections is presented in Figure 4.13. It can be seen the influence of spring and neap tidal cycles over the sediment transport. During spring tide, when the system is more energetic, cumulative sediment transport wiggles within the tidal cycles, with a net import of sediment.

With respect to marine sediment, a slight variability is found for summer and winter conditions. This fraction presents very low critical bed shear stress for erosion and it almost equally reworked in both conditions. Sediment fraction M2 (dashed lines) is equally transported through the entrance during summer and winter conditions. In the beginning of S2 however, the cumulative transport through this cross-section is twice as larger in summer than in winter. This is probably due to more energetic conditions resultant from fresh water discharges, promoting the erosion of this sediment in this stretch and its transport further upstream.

Table 4.2 presents an overview of the cumulative sediment transport through the cross sections. Model results are given in volume but mass is preferred for the purposes of this study. Therefore the total sediment mass transport through each section is computed by applying a γ_{mud} of 1,600 kg/m^3, correspondent of the specific density for fine sediment of 2,600 kg/m^3 set in the model and 40% of voids.

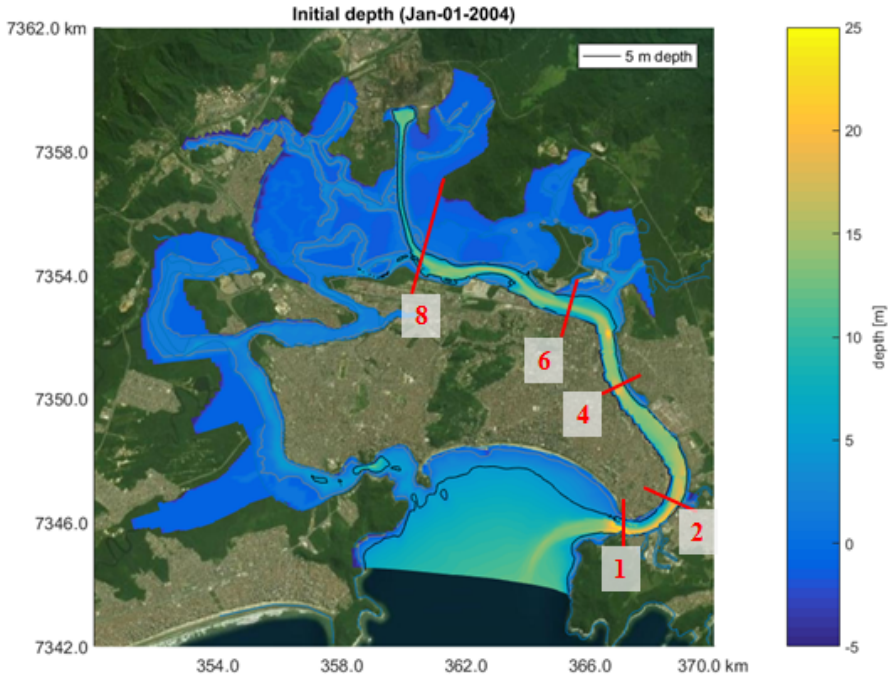

Figure 4.12: Observation cross-sections assigned to control the cumulative sediment transport along the channel.

Table 4.2: Cumulative sediment transport through cross-sections after a six-months simulation (January 01 to July 01, 2004.

Cross section / sediment fraction	M1 [Kton]	M2 [Kton]	F1 [Kton]	Total [Kton]
1. Entrance of Santos	170	370	-1	540
2. Beginning S2	150	220	-1	370
4. Beginning S3	70	10	-4	80
6. Beginning S4	40	2	10	50
8. Beginning Piaçaguera	20	-	3	20

Proxy for fluid mud formation

Fluid mud consists of *a high-concentration suspension of fine sediment particles where settling is substantially hindered by the closeness of particles and flocs, however has not formed and interconnected matrix of bonds strong enough to eliminate the potential for mobility* [van Rijn, 2016]. Fluid mud can be formed from rapid deposition, liquefaction and/or fluidization of the sediment bed, and is in a transient state. It consists of a consolidating water mud-mixture, which is expected to consolidate, unless external energy is supplied to the mixture, as externally induced shear stresses generated by strong currents and/or wave action [Winterwerp, 2011].

According to van Rijn [2016] in systems with high flow velocities, i.e. larger than 1 m/s, several high-concentration layers of mud may be present in the water column. These layers are influenced by gravity processes that oppose mixing processes. A three-layer system can be distinguished in the vertical direction:

- Consolidated mud layer at the bed surface. Concentrations of fine sediment larger than 200 to 300 kg/m^3;
- Fluid mud suspension layer with concentrations ranging from 10 to 300 kg/m^3. Typically the layer thickness is between 0.1 and 1 m, but reaches 3 m in conditions of high tidal velocities (larger than 15 m/s) as in the Amazon shelf.; and
- Dilute mud suspension with concentrations of up to 10 kg/m^3.

The presence of fluid mud in the SE is known and is studied in Ferreira [2013]. An analysis on the cross-sectional plots and map plots of the model results indicates that the system offers conditions for fluid mud formation due to high sediment concentrations found in the water column, close to the bottom. A variation of sediment concentration is seen within the tidal cycles and between the different scenarios. High concentrations (up to 0.4 g/l) are found near the edge of the salt wedge, moving up and down the estuary during the tidal cycle. Around low water, little concentrations are found in the estuary, indicating that, if formed, the fluid mud layer might be destroyed and will appear again in the following tidal cycle.

The described process consists of a type of supply/settling dominated fluid-mud formation and deposition. van Rijn [2016] also describes locally-generated layers of fluid mud. A process that might occur in the SE is the mobile fluid mud, result of erosion and settling of mud suspension in accelerating/decelerating tidal flow. During slack water

a temporary layer can be formed from the concentrations settling out from above, specially during neap tide. This can be derived from the map plots: during neap tide larger concentrations are found in the entrance of the estuary. This area also corresponds to the primary region of sediment deposition, i.e, the transient layer eventually turns to a layer of deposited sediment.

Further discussion on the formation of fluid mud is out of the scope of this project. Results presented above aim to encourage further investigation on dredging strategies and navigation in fluid mud.

No salinity

The model is rerun to evaluate the influence of salinity in the sediment transport and deposition. Salinity is switched off in this second simulation. The initial condition is fresh water in the entire domain and no salinity is assigned to the open boundary.

In the cross-sectional results provided in the Appendix C it can be seen that suspended sediment does not reach further than Barnabé station, S3. This in an indication that the up-estuary sediment transport is not only dependent on the tidal motion, but also on the density driven currents.

The concentration map-plots of Appendix D.4, corroborate the salinity driven sediment transport. Maximum sediment concentration in the layer above the bed is half of the maximum sediment concentration found in the run with salinity on. Sediment deposition is reduced in this condition, as it can be seen in Figure 4.14b. This is, among others, result of the 69% reduction of cumulative sediment transport through the entrance of the estuary.

Table 4.3 presents the cumulative mass transport through the cross-sections and the percentage of reduction in comparison to the run with salinity. Besides the reduction of net import of sediment in the estuary, it is also found a 95% reduction of net sediment import after S2. This highlights the influence of the salt wedge in the sedimentation of the middle and upper areas of the SE.

Table 4.3: Cumulative sediment transport through cross-sections after a six-months simulation (January 01 to July 01, 2004. Run with salinity switched off.

Cross section / sediment fraction	M1 [Kton]	M2 [Kton]	F1 [Kton]	Total [Kton]	Total - salinity on [Kton]	Reduction
1. Entrance of Santos	29	137	-	167	540	69%
2. Beginning S2	17	50	-	66	370	82%
4. Beginning S3	3	2	1	4	80	95%
6. Beginning S4	1	-	-	2	50	97%
8. Beginning Piaçaguera	-	-	-	-	20	99%

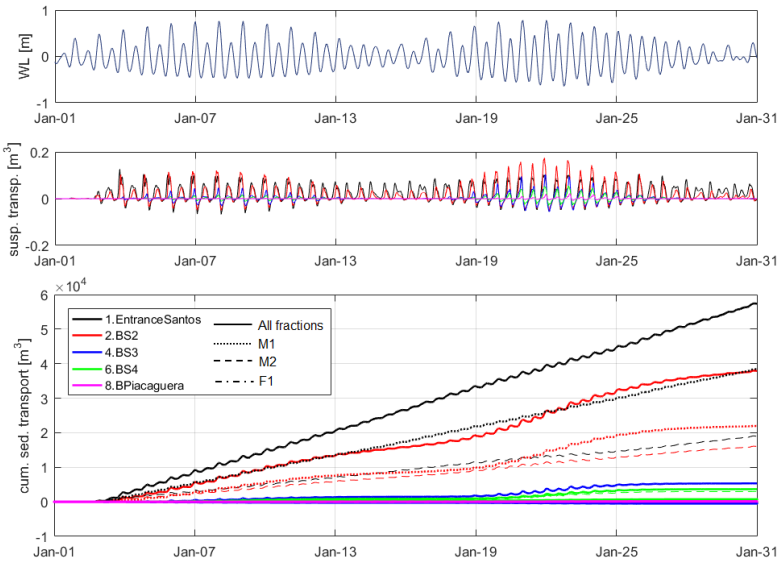

(a) Summer conditions.

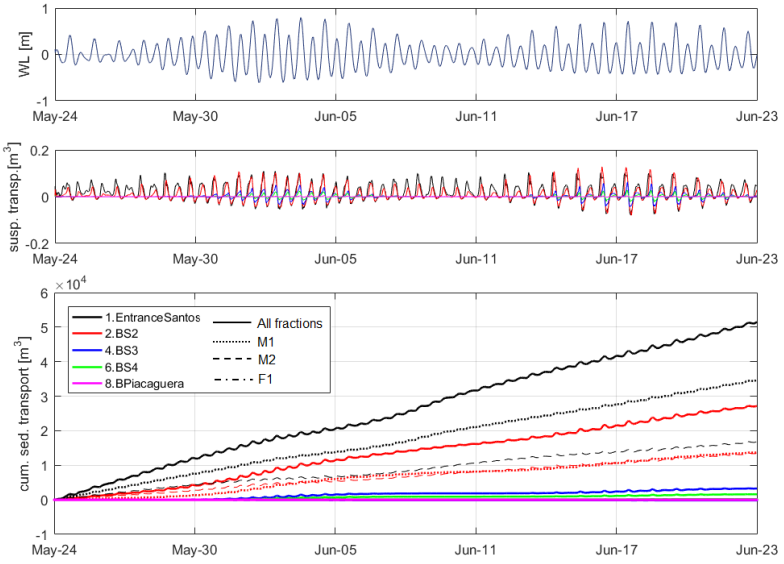

(b) Winter conditions.

Figure 4.13: Cumulative sediment transport over the cross sections during summer and winter conditions. Solid line corresponds to the sum of all fractions, dashed line to M1, dotted line to M2, and dash-dot to F1.

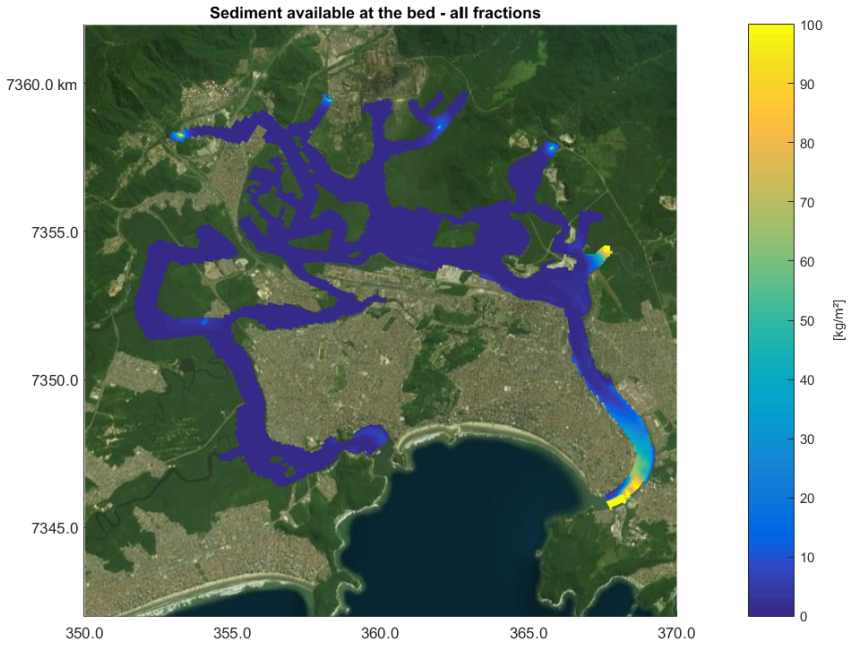

(a) Main run (salinity on).

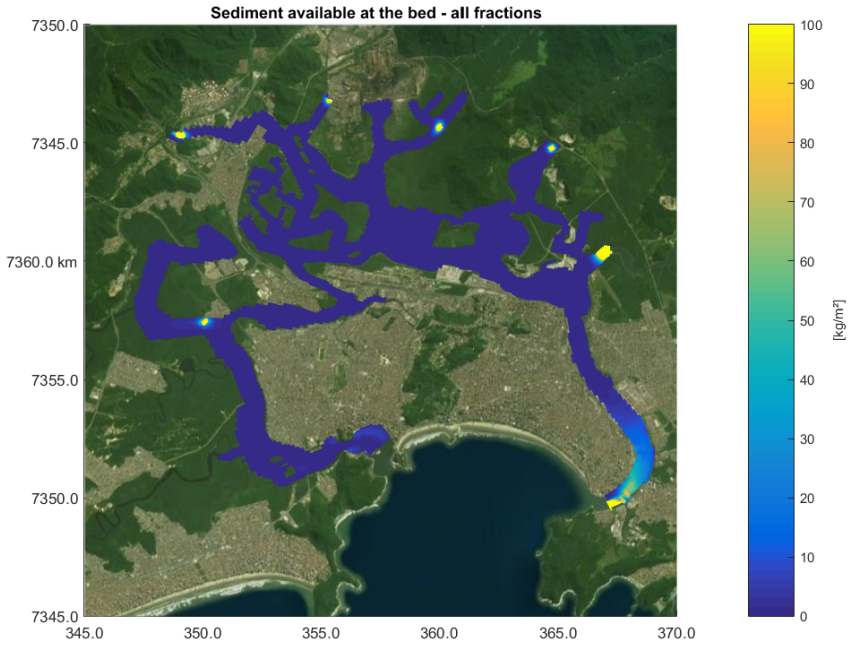

(b) Run with salinity switched off.

Figure 4.14: Available sediment at the bed after six months. Sum of all sediment fractions.

5

Main findings

The objective of this MSc thesis is to improve the understanding of the sedimentation origins and patterns in the Santos Estuary. Focus has been given to fine sediment. This research was conducted by means of a extensive literature review on the Santos Estuary, assessment of sediment sources and sinks, and the set-up of an explorative process based numerical model for the system. The main findings are summarized below and a modified sediment balance is proposed based on the interpretation of model results.

5.1 Main findings

Sediment transport

- A literature research and an analysis of the tidal constituents of the measurement stations along the Santos estuary provide that the system presents a dominant flood character [Alfredini and Lavieri, 2013]. The interpretation of model results for circulation, mean depth averaged residual currents, sedimentation pattern, among others, support this statement;
- Sediment transport into the estuary appears to be, mainly salinity driven, especially in the mid and upper areas of the Santos Estuary. Fine sediment supplied from the marine boundary is transported further upstream due to density driven circulation. This implies that the deeper the penetration of the salt wedge, the larger is the amount of fines brought in the upper area (assuming unlimited supply of fine sediment downstream). This finding is supported not only by comparing cross-sectional plots of the runs with and without salinity, but also by comparing summer and winter conditions when salinity is in the model. During winter, the salt wedge reaches further up-stream due to less fresh water discharge in the system, thus, larger concentration of fines is found in the upper areas of the estuary, when compared to summer conditions. Moreover, it is seen that once salinity is switched off in the model, negligible concentrations are found from S3 on, while in reality, S3, S4, and the Piaçaguera channel can present concentrations in the order of 80 mg/l [Elfrink et al., 2008];

- The two considerations above suggest that deepening the channels and/or reclaiming intertidal areas might enhance the flood character and the import of fine sediment into the system;
- Results indicate a little capacity of the system in pumping out fine sediment, interpreted from the cumulative net sediment transport results through the entrance of the Santos Estuary. It is known that the model run has a cold start and that the simulated period might be shorter than the time required to the system to reach a dynamic equilibrium regarding sediment transport. Moreover, to optimize the computational time, the open boundary was not placed so far from the entrance of the channel (3 km). Complicated flow patterns are found in the bay, it might have influenced the morphological behavior in the bay. Nonetheless, in fact Santos bay is subject to wave action and highly energetic winter storms, providing a large transport of coarse and fine sediment. Therefore, it is likely than in reality negligible export of fine sediment takes place;
- If deposits of fine sediment are existent in the bottom of Santos bay, they can be reworked by tidal currents and by wave agitation, providing a potential source of fines to be transported in the up-estuary direction. Fine sediment already in suspension in the water column can also be transported upstream within the salt wedge; and
- In the model, critical bed-shear stresses for sediment are found to be exceeded at most of the time, especially in S1 and S2. This indicates that freshly deposited sediment layers may not last longer than a tidal cycle. Moreover, high-concentration of sediment (up to 400 mg/l) are found, indicating that conditions for fluid mud formation might exist. As concentrations vary within a tidal cycle, from 400 mg/l during high water to less than 100 mg/l during low water, it is likely that, if formed, this fluid mud layer builds up and then breaks down within a tidal cycle.

Sediment balance

- Model results suggest that little mass of fine sediment reaches the navigation channel after a year, opposing what is considered in the literature-based sediment mass balance (0.9 Mton/year). Given that fluvial sediment loads discharged in the Santos Estuary are unknown and that, if available, a considerable mass of fine sediment supplied from the marine boundary can reach the upper areas of the estuary, this study suggests that fine sediment present in S2 to S4 and, perhaps in the Piaçaguera channel, is mainly provided from marine sources, while in in previous studies it is attributed to riverine sources; and
- Interpretation of model output indicates a strong capacity for import of marine sediment, with a cumulative sediment transport in order of 1.1 Mton/year, if this sediment source is available. This quantity is larger than the *other sources*, namely the import of fines from the sea, assessed in the literature-based mass sediment balance. In the referred mass balance, this sediment source is computed from the deficit of sources (rivers and winter storms) and sinks (maintenance dredging and trapping in the mudflats). Therefore, the *other sources* term is highly sensitive to the accuracy of the previous terms. A modified sediment mass

balance is proposed based on the model findings: the lower band of river input is shifted to the best estimate. As a result, the modified mass balance provides an annual import of sediment of of 0.7 Mton into the Santos Estuary, which is more consistent with the model results. A reviewed sediment mass balance is proposed in Figure 5.1, assuming a sufficient source of fine sediment in the bay.

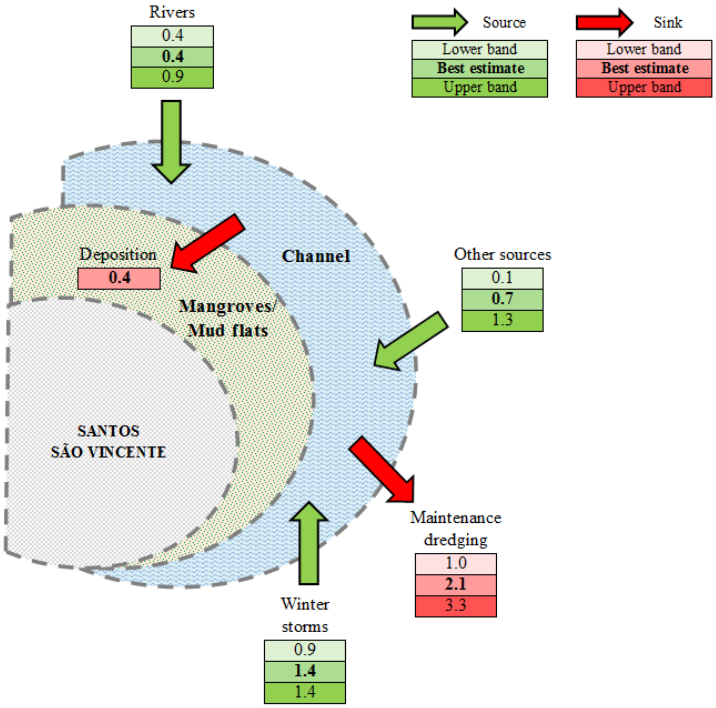

Figure 5.1: Modified sediment mass balance [Mton/year], averaged over the period of 2005 to 2012. Dredging ranges are attributed to different densities of the dredged material.

6

Dredging strategies

The observations and findings derived from this study provide potential insights in dredging strategies for the Port of Santos with respect to fine sediment. Three aspects are here discussed: the source of fine sediment in the bay and its up-estuary transport, overdredging, and water injection dredging (WID).

6.1 Fine sediment in the bay

This project assumes a sufficient source of fine sediment in the bay. A strong capacity of import of this material is suggested by the modelling resuts (circa 1.1 Mton/year). It is recommended therefore to assess the presence and size of this source and conduct further research in its implication in the import of fines into the estuary. A soil investigation campaign is recommended for the bay and the navigation channel. These areas are indicated Figure 6.1. The area in the bay is selected based on the results of the soil campaign of the FRF [2008], presented earlier in Figure 2.10.

In the bay, the availability of fine sediment can be assessed by submitting extracted soil samples to sediment grain size analysis. The magnitude of consolidation of these deposits is also of interest, as it gives an indication of which energetic conditions might promote the mobilization of the bed material. In the navigation channel however, the purpose of the soil investigation is to confirm if the deposited fines are originated from the deposits in the sea. This can be achieved by a comparison of the soil samples extracted from the channel and from the bay.

Provided that extensive data on contaminated sediment in the Piaçaguera channel is available due to the environmental studies carried for its maintenance dredging, an additional analysis is suggested. It consists in evaluating the presence of those contaminants in the bay. If identical contaminants are found in the bay, it could indicate a capacity of the system in exporting sediment and in trapping this material in the bay. Logically, other possible sources of these pollutants should be investigated in order to not wrongly assume the system exported fine sediment from the estuary.

6.1.1 Implication of test results

Four different scenarios can arise from the suggested investigation campaign:

- There is a great source of fine sediment in the bay and the fine sediment present in the channel are provided from the sea. In this case it is recommended to investigate the feasibility of removal of the fine sediment layer in the bay and/or wash out of the mixture of sand and fine sediment, otherwise it is very likely that this source will keep feeding the estuary in the present configuration of the system;
- There is a great source of fine sediment in the bay but the fine sediment found in the navigation channel is not from this source. For this scenario it is suggested to investigate river loads and suspended matter in the water column of the bay. The latter one comprises the possibility of other deposits in the offshore area of Santos platform that are subject to erosion;
- Negligible or little deposits of fine sediment are found in the bay and the fine sediment present in the channel are compatible with marine sources. It might be valuable to investigate the exhaustion of the source in the bay and assess the presence of fines in other areas of Santos platform; and Negligible or little deposits of fine sediment are found in the bay, however, the fine sediment present in the navigation channel is not compatible with marine sediment. Then it is very likely that the sediment comes from rivers and this source should be investigated in aspects of loads, seasonality, sediment excursion once discharged in the estuary, among others. Another possibility is the lateral erosion of mudflats and release of fine sediment from these areas.

6.2 Overdredging

Overdredging is the depth of dredged material removed from below a required level [Kinlan, 2015]. This is usually related to vertical and horizontal dredging tolerances, result of the accuracy obtained with the dredging works. Overdredging can be used as a deposit for sediment between maintenance dredging operations.

In the case of the SE, overdredging allowances must be careful considered. The system is salinity driven and it is very likely that deepening the channel will increase sedimentation volumes due to a deeper penetration of the salt wedge in the system and enhanced turbulent mixing and up-estuary sediment transport [van Maren et al., 2015]. Yet, a trade-off can be made between the frequency of maintenance dredging and the increased sedimentation due to overdredging, as mobilization costs may exceed an allowance in extra sedimentation volumes.

6.3 Water injection dredging

Water injection dredging is a hydrodynamic dredging technique developed by Van Oord. It consists in the use of natural processes and forces to allow the fluidised sediment layer to flow horizontally out of a system. The water injection dredger turns the solid sediment layer to a density current. The horizontal transport of this layer is

Figure 6.1: Suggested soil sampling areas.

induced by the combined forces of pressure difference in the water and gravitational forces [IADC, 2013]. This technique has been used worldwide in the maintenance dredging of ports and rivers, including a 19-year contract covering the maintenance of a port in São Luís, ES Brazil [Van Ooord, 2017].

In the SE water injection dredging seems promising from the execution perspective and relatively low costs, as in this study density driven currents prove to be capable of transporting large quantities of sediment in and out of the system. However, model results also suggest that once in the bay, the fine sediment can be soon deposited back in the estuary. In this sense, WID appears to be a short-term solution.

Related to fluidised sediment layers, navigation in fluid mud might be of interest. This aspect has been discussed by Ferreira [2013] and is of practice in several ports worldwide (Indonesia, the Netherlands, United Kingdom, Brazil). Further studies on fluid mud formation in the SE and navigation policies in such conditions might provide a feasible dredging strategy for the Port of Santos.

Bibliography

CODESP. Termo de Referência - Contratação dos serviços de dragagem de manutenção dos trechos 1, 2, 3 e 4 do canal de acesso e dos acessos aos berços de atracação do Porto de Santos (processo nº 25402/1620), 2016a.

D.S. van Maren, T. van Kessel, K. Cronin, and L. Sittoni. The impact of channel deepening and dredging on estuarine sediment concentration. *Continental Shelf Research*, 95:1–14, 2015.

FRF. EIA-RIMA da dragagem de aprofundamento do canal de navegação, bacia de evolução e berços de atracação do Porto Organizado de Santos - São Paulo. Technical report, FRF - Fundação Ricardo Franco, 2008.

D. H. Schoellhamer and J. R. Burau. `https://sfbay.wr.usgs.gov/sediment/circulation/est_physics.html`, 2007.

F. Roversi. Estudo Hidrodinâmico e de Renovação das Águas do Sistema Estuarino de Santos. Master's thesis, COPPE-UFRJ, 2012.

P.G. Lopes. As assimetrias de Maré no Estuário de Santos, SP, Brasil. Master's thesis, UFRJ/COPPE, 2015.

J. Harari, C.A.S. França, and R. Camargo. *Perspectives on Integrated Coastal Zone Management in South America, Chapter: Climatology and hydrography of Santos Estuary*. IST press, 2008.

DAEE. Banco de dados hidrológicos. `http://www.hidrologia.daee.sp.gov.br/`, 2016.

B. Elfrink, K. Bundgaard, U. Lumborg, and C.B.M. Rocha. Porto de Santos - Modelagem do transporte de sedimentos. Technical report, DHI, 2008.

FEMAR. `https://www.fundacaofemar.org.br/biblioteca/emb/indice.html#saopaulo`, 2017.

CODESP. Porto de Santos. `http://www.portodesantos.com.br/`, September 2016b.

P. Alfredini and R. Lavieri. Estimativa da taxa de dragagem anual de manutenção do canal de acesso e bacias de evolução do Porto de Santos após obra de dragagem

de aprofundamento para cota -15,00 m (DHN) e alargamento. Technical report, Argonáutica Engenharia e Pesquisas, 07 2013.

CODESP. Resposta esclarecimentos Van Ooord processo nº 25402/1620., 2016c.

Van Ooord. Recurso pregão eletrônico nº 45/2016 (processo nº 25402/1620)., 2016.

T.M. Coelho. Análise do transporte de sedimentos na região central da Baixada Santista (SP) através de modelagem numérica. Master's thesis, Universidade de São Paulo, 2008.

T.R.S. Ferreira. Ocorrência de lama fluida no Porto de Santos. Master's thesis, COPPE-UFRJ, 2013.

D.V. Hansen and Jr. M. Rattray. New dimensions in estuary classification. *Limnology and Oceanography*, 11(3):319–326, 1966a.

D.V. Hansen and Jr. M. Rattray. Gravitational circulation in straits and estuaries. Technical report, University of Washington - Department of Oceanography, 1966b.

J. Bosboom and M.J.F. Stive. *Coastal Dynamics I*. VSSD, 2015.

P. MacCready and J. Keister. Pudget sound oceanography : Estuarine processes. `https://faculty.washington.edu/pmacc/Classes/Est2011/syllabus.html`, 2011.

L.B. Miranda, E.D. Olle, and A.L. Bérgamo. Circulation and salt intrusion in the Piaçaguera channel, Santos (SP). *Brazilian Journal of Oceanography*, 60(1):11–23, 2012.

S. Pond and G. Pickard. *Introductory Dynamical Oceanography*. Oxford Pergamon Press, 1978.

D.S. van Maren and J.C. Winterwerp. The role of flow asymmetry and mud properties on tidal flat sedimentation. *Continental Shelf Research*, 60:S71–S84, jun 2013. doi: http://dx.doi.org/10.1016/j.csr.2012.07.010.

CT Friedrichs. *Tidal flat morphodynamics: a synthesis*, volume 3. Treatise on Estuarine and Coastal Science, 2012.

C.T. Friedrichs and D.G. Aubrey. Non-linear tidal distortion in shallow well-mixed estuaries: a synthesis. *Estuarine, Coastal and Shelf Science*, 27:521–545, 1988.

E.C. Truccolo. *Maré meteorológica e forçantes atmosféricas locais em São Francisco do Sul - SC*. PhD thesis, UFSC, 1998.

Ricardo Martins Campos, Ricardo de Camargo, and Joseph Harari. Caracterização de eventos extremos do nível do mar em Santos e sua correspondência com as reanálises do modelo do NCEP no sudoeste do Atlântico Sul. *Revista Brasileira de Meteorologia*, 25(2):175–184, 2010. ISSN 0102-7786. doi: http://dx.doi.org/10.1590/S0102-77862010000200003. URL `http://www.scielo.br/scielo.php?script=sci_arttext&pid=S0102-77862010000200003`.

FAPESP. http://agencia.fapesp.br/inundacoes_costeiras_em_santos_podem_causar_prejuizos_bilionarios_/21997/, 2015.

B.M. Castro. *Subtidal Response To Wind Forcing In The South Brazil Bight During Winter (models, Shelf, Coastal)*. PhD thesis, University of Miami, 1985.

P.S. Yoshikawa S.N. Hurtado M.G. Tessler, S.C. Goya. *Erosão e Progradação do Litoral Brasileiro*. Ministério do Meio Ambiente, 2006.

P. Alfredini. O clima de agitação ondulatória na Baía de São Vicente (SP). Technical report, -, 2003.

A. Farinnaccio, S.C. Goya, and M.G. Tessler. Variações da linha de costa nas baías de Santos e São Vicente / Variations of the shoreline on Santos and São Vicente bays. *Quaternary and Environmental Geosciences*, 01(1):42–48, 2009.

B. Elfrink K. Bundgaard. Porto de Santos - Modelagem Hidrodinâmica. Technical report, DHI, 2008.

INPH. Anteprojeto de dragagem de manutenção e de readequação da geometria do canal de acesso aquaviário e dos berços de acostagem do complexo portuário de Santos - sp. Technical report, INPH/SEP, 2013.

CBH. Minuta preliminar do relatório da situação dos recursos hídricos da Baixada Santista. Technical report, CBH - Comitê da Bacia Hidrográfica da Baixada Santista, 2000.

IBGE. http://mapas.ibge.gov.br/fisicos, 2017. URL http://mapas.ibge.gov.br/fisicos.

A.H.V. Titarelli. A Serra do Mar. *Orientação*, (7):86–93, 1986.

Sonia Maria Flores Gianesella. *Produção primária da Baia de Santos, estado de São Paulo - aspectos sobre a eficiência fotossintética num ambiente marinho poluído*. PhD thesis, USP, 1978.

V.J. Fúlfaro and W.L. Poçano. Sedimentação atual do estuário e baía de Santos: um modelo geológico aplicado a projetos de expansão da zona portuária. In Congresso Brasileiro de Geologia de Engenharia, editor, -, volume 2, pages 67–90, 1976.

L.R. Tommasi. 6. Programa de monitoramento e modelagem de parâmetros hidrodinâmicos e oceanográficos. Technical report, FUNDESPA, 2008.

KR Dyer. The typology of intertidal mudflats. *Geological Society, London, Special Publications*, 139(1):11–24, 1998.

Deltares. *Delft3D-FLOW User Manual*, 3.15 edition, 10 2016.

J. C. Winterwerp and W. G. M. van Kersteren. *Introduction on the physics of cohesive sediment in the marine environment*. Elsevier, 2004.

J. C. Winterwerp. Flow induced erosion of cohesive beds: a literature study, 1989.

B. Beardsley R. Pawlowicz and S. Lentzb. Classical tidal harmonic analysis including error estimates in matlab using ttide. *Computers & Geosciences*, 28:929–937, 2002.

L. van Rijn. Fluid mud formation. http://www.leovanrijn-sediment.com/papers/Fluidmudformation2016.pdf, 11 2016.

J. C. Winterwerp. The physical analysis of muddy sedimentation processes, 2011.

D. Kinlan. Contractor or client: who pays for over-dredging. http://www.iadc-dredging.com/ul/cms/terraetaqua/document/4/4/7/447/447/1/article-contractor-or-client-who-pays-for-overdredging-terra-et-aqua-139-3.pdf, June 2015.

IADC. Water Injection Dredging. https://www.iadc-dredging.com/ul/cms/fck-uploaded/documents/PDF%20Facts%20About/facts-about-water-injection-dredging.pdf, 2013.

Van Ooord. Water injection dredger. http://www.vanoord.com/activities/water-injection-dredger, 2017.

A

FEMAR Tables

This appendix provides the tables containing the tidal astronomical components measured in five stations along the Santos Estuary and Santos bay (Figure A.1).

Figure A.1: Location of the measurement stations (Google Earth ®).

FEMAR-FUNDAÇÃO DE ESTUDOS DO MAR *Catálogo de Estações Maregráficas Brasileiras*

Nome da Estação :	**ILHA DAS PALMAS – SP**		
Localização :	Barra do Porto de Santos - no Trapiche do Clube de Pesca		
Organ. Responsável :	DHN / INPH		
Latitude :	24° 00,5' **S**	**Longitude :**	46 ° 19,6' **W**
Período Analisado :	28/03/90 a 27/04/90	**Nº de Componentes :**	24
Análise Harmônica :	Método Almirante Santos Franco		
Classificação :	Maré de Desigualdades Diurnas		
Estabelecimento do Porto: (HWF&C)	III H 31 min	**Nível Médio (Zo):**	77 cm acima do NR.
Média das Preamares Superiores (MHHW) :	140 cm acima do NR.	**Média das Preamares Inferiores (MLHW) :**	130 cm acima do NR
Média das Baixa-mares Superiores (MHLW) :	29 cm acima do NR.	**Média das Baixa-mares Inferiores (MLLW) :**	9 cm acima do NR.

CONSTANTES HARMÔNICAS SELECIONADAS

Componentes	Semi-amplitude (H) cm	Fase (g) graus (°)	Componentes	Semi-amplitude (H) cm	Fase (g) graus (°)
Sa	-	-	MU_2	-	-
Ssa	-	-	N_2	4,6	149
Mm	-	-	NU_2	0,9	140
Mf	-	-	M_2	35,3	081
MTM	-	-	L_2	-	-
Msf	-	-	T_2	1,3	076
Q_1	3,2	033	S_2	22,9	075
O_1	9,6	084	K_2	6,2	075
M_1	-	-	MO_3	-	-
P_1	2,2	104	M_3	4,5	198
K_1	6,7	106	MK_3	3,1	080
J_1	-	-	MN_4	-	-
OO_1	-	-	M_4	1,7	351
MNS_2	-	-	SN_4	-	-
$2N_2$	0,6	217	MS_4	1,6	105

Referências de Nível: RN instalada numa pedra junto à rampa de acesso ao Clube.

Obs: Outros Períodos: 01/06/73 a 02/07/73; 01/09/73 a 02/10/73; 01/03/74 a 01/04/74; 09/05/79 a 09/06/79, 01/05/90 a 22/07/90 .

Código BNDO: 50230

- 239 -

Figure A.2: 1. Ilha das Palmas [FEMAR, 2017].

Nome da Estação :	**PRATICAGEM (SANTOS) - SP**		
Localização :	Porto de Santos, no Trapiche da Praticagem		
Organ. Responsável :	DHN		
Latitude :	23° 59,7' **S**	**Longitude :**	46° 18,0' **W**
Período Analisado :	05/09/95 a 07/10/95	**Nº de Componentes :**	26
Análise Harmônica :	Método Almirante Santos Franco		
Classificação :	Maré de Desigualdades Diurnas		
Estabelecimento do Porto: (HWF&C)	11 H 50 min	**Nível Médio (Zo):**	80 cm acima do NR.
Média das Preamares Superiores (MHHW) :	144 cm acima do NR.	**Média das Preamares Inferiores (MIHW) :**	134 cm acima do NR
Média das Baixa-mares Superiores (MHLW) :	34 cm acima do NR.	**Média das Baixa-mares Inferiores (MLLW) :**	8 cm acima do NR.

CONSTANTES HARMÔNICAS SELECIONADAS

Componentes	Semi-amplitude (H) cm	Fase (g) graus (°)	Componentes	Semi-amplitude (H) cm	Fase (g) graus (°)
Sa	-	-	**MU_2**	-	-
Ssa	-	-	**N_2**	4,7	147
Mm	-	-	**NU_2**	0,9	138
Mf	-	-	**M_2**	33,9	079
MTM	16,5	156	**L_2**	2,7	097
Msf	-	-	**T_2**	1,5	086
Q_1	4,8	043	**S_2**	24,9	086
O_1	12,9	087	**K_2**	6,8	087
M_1	-	-	**MO_3**	-	-
P_1	2,2	148	**M_3**	5,2	213
K_1	6,5	153	**MK_3**	-	-
J_1	-	-	**MN_4**	-	-
OO_1	-	-	**M_4**	-	-
MNS_2	-	-	**SN_4**	-	-
$2N_2$	0,6	214	**MS_4**	2,3	100

Referências de Nível: RN-1 no trapiche ao lado da bomba de combustível
RN-2 no início da passarela de acesso ao trapiche

Obs: Não há referências a outros períodos

Código BNDO: 50227

- 238 -

Figure A.3: 2. Praticagem Santos [FEMAR, 2017].

FEMAR-FUNDAÇÃO DE ESTUDOS DO MAR *Catálogo de Estações Maregráficas Brasileiras*

Nome da Estação :	**SANTOS (PORTO) – SP**		
Localização :	Na torre de passagem dos cabos elétricos pelo canal (Torre Grande)		
Organ. Responsável :	INPH / CODESP / DHN		
Latitude :	23° 57,3' **S**	**Longitude :**	46 ° 18,6' **W**
Período Analisado :	01/01/56 a 23/12/56	**Nº de Componentes :**	32
Análise Harmônica :	Método Tidal Liverpool Institute		
Classificação :	Maré de Desigualdades Diurnas		
Estabelecimento do Porto: (HWF&C)	II H 55 min	**Nível Médio (Zo):**	77 cm acima do NR.
Média das Preamares Superiores (MHHW) :	141 cm acima do NR.	**Média das Preamares Inferiores (MLHW) :**	130 cm acima do NR
Média das Baixa-mares Superiores (MHLW) :	29 cm acima do NR.	**Média das Baixa-mares Inferiores (MLLW) :**	7 cm acima do NR.

CONSTANTES HARMÔNICAS SELECIONADAS

Componentes	Semi-amplitude (H) cm	Fase (g) graus (°)	Componentes	Semi-amplitude (H) cm	Fase (g) graus (°)
Sa	10,2	025	**MU_2**	2,1	122
Ssa	5,0	180	**N_2**	5,4	149
Mm	4,2	289	**NU_2**	0,4	139
Mf	1,7	141	**M_2**	36,4	088
MTM	-	-	**L_2**	1,6	037
Msf	1,5	121	**T_2**	0,8	020
Q_1	2,5	058	**S_2**	22,5	091
O_1	11,5	081	**K_2**	7,4	082
M_1	0,8	095	**MO_3**	0,7	096
P_1	2,3	136	**M_3**	4,9	234
K_1	6,3	143	**MK_3**	2,5	117
J_1	0,8	192	**MN_4**	1,3	318
OO_1	0,2	133	**M_4**	2,6	355
MNS_2	0,2	189	**SN_4**	0,6	061
$2N_2$	2,0	149	**MS_4**	2,2	143

Referências de Nível: RN Alfândega, situada na Praça da República, no meio fio em frente ao prédio da Delegacia da Receita Federal (antiga Alfândega).
RN 2 implantada na sapata da torre do lado do porto.

Obs: Outros Períodos: 01/01/51 a 04/01/51; 14/11/59 a 15/12/59; 07/02/78 a 23/02/78; 27/02/78 a 27/03/78; 05/09/95 a 07/10/95.

Existem outros períodos no INPH e na CODESP

Consta das Tábuas das Marés.

Código BNDO: 50225

- 237 -

Figure A.4: 3. Santos Port (TEF) [FEMAR, 2017].

Nome da Estação :	**ILHA BARNABÉ – SP**		
Localização :	Porto de Santos, no antigo trapiche de acesso à Ilha		
Organ. Responsável :	CODESP / DHN		
Latitude :	23° 55,7' **S**	**Longitude :**	46 ° 19,9' **W**
Período Analisado :	27/09/74 a 29/11/74	**N° de Componentes :**	24
Análise Harmônica :	Método Almirante Santos Franco		
Classificação :	Maré de Desigualdades Diurnas		
Estabelecimento do Porto: (HWF&C)	11 H 59 min	**Nível Médio (Zo):**	74 cm acima do NR.
Média das Preamares Superiores (MHHW) :	142 cm acima do NR.	**Média das Preamares Inferiores (MLHW) :**	129 cm acima do NR.
Média das Baixa-mares Superiores (MHLW) :	23 cm acima do NR.	**Média das Baixa-mares Inferiores (MLLW) :**	2 cm acima do NR.

CONSTANTES HARMÔNICAS SELECIONADAS

Componentes	Semi-amplitude (H) cm	Fase (g) graus (°)	Componentes	Semi-amplitude (H) cm	Fase (g) graus (°)
Sa	-	-	MU_2	-	-
Ssa	-	-	N_2	5,1	146
Mm	-	-	NU_2	1,0	138
Mf	-	-	M_2	38,4	086
MTM	-	-	L_2	-	-
Msf	-	-	T_2	1,4	088
Q_1	2,5	051	S_2	23,3	088
O_1	11,4	083	K_2	6,3	088
M_1	-	-	MO_3	1,7	086
P_1	2,1	152	M_3	5,5	245
K_1	6,2	158	MK_3	3,4	105
J_1	-	-	MN_4	-	-
OO_1	-	-	M_4	2,7	348
MNS_2	-	-	SN_4	-	-
$2N_2$	0,7	206	MS_4	3,6	144

Referências de Nível: RN 1 implantada na escada do prédio da antiga Alfândega de Santos

Obs: Não há referências a outros períodos

Ver também a estação BNDO 50221 - Barnabé

Código BNDO: 50226

- 235 -

Figure A.5: 4.Barnabé [FEMAR, 2017].

FEMAR-FUNDAÇÃO DE ESTUDOS DO MAR *Catálogo de Estações Maregráficas Brasileiras*

Nome da Estação :	**PIAÇAGUERA – SP**		
Localização :	Em Santos, no Terminal da Cosipa (Canal de Piaçaguera)		
Organ. Responsável :	DHN		
Latitude :	23° 52,5' **S**	**Longitude :**	46 ° 22,6' **W**
Período Analisado :	24/01/68 a 24/12/68	**Nº de Componentes :**	36
Análise Harmônica :	Método Tidal Liverpool Institute		
Classificação :	Maré de Desigualdades Diurnas		
Estabelecimento do Porto: (HWF&C)	IV H 02 min	**Nível Médio (Zo):**	82 cm acima do NR.
Média das Preamares Superiores (MHHW) :	145 cm acima do NR.	**Média das Preamares Inferiores (MLHW) :**	142 cm acima do NR
Média das Baixa-mares Superiores (MHLW) :	34 cm acima do NR.	**Média das Baixa-mares Inferiores (MLLW) :**	7 cm acima do NR.

CONSTANTES HARMÔNICAS SELECIONADAS

Componentes	Semi-amplitude (H) cm	Fase (g) graus (°)	Componentes	Semi-amplitude (H) cm	Fase (g) graus (°)
Sa	-	-	**MU_2**	0,4	204
Ssa	-	-	**N_2**	6,5	187
Mm	7,6	330	**NU_2**	1,3	187
Mf	-	-	**M_2**	37,7	120
MTM	-	-	**L_2**	2,1	205
Msf	15,5	021	**T_2**	1,4	124
Q_1	3,7	068	**S_2**	23,7	124
O_1	13,1	102	**K_2**	6,4	124
M_1	0,9	104	**MO_3**	3,0	084
P_1	1,9	178	**M_3**	6,8	293
K_1	5,7	178	**MK_3**	3,1	204
J_1	1,1	134	**MN_4**	1,1	360
OO_1	0,3	125	**M_4**	3,2	041
MNS_2	-	-	**SN_4**	1,9	121
$2N_2$	0,9	254	**MS_4**	2,5	235

Referências de Nível: RN-1 no capeamento do cais da COSIPA

Obs: Não há referências a outros períodos.
Maré com influência fluvial e meteorológica

Código BNDO: 50215

- 234 -

Figure A.6: 5. Piaçaguera (COSIPA) [FEMAR, 2017].

B

Delft3D model set-up

This appendix provides additional information on the model set-up in Delft3D.

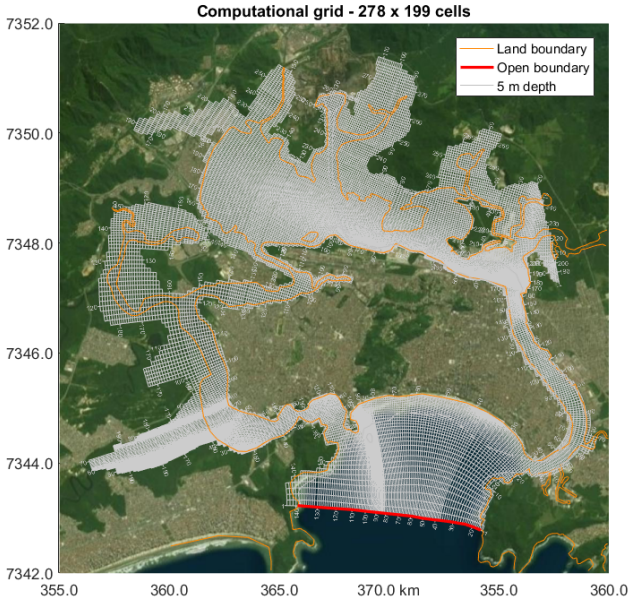

Figure B.1: Computational grid, 278x199 grid cells.

Table B.1: Model parameters.

DOMAIN				
Time step	min	1		
k-layers	-	12		
Grid points in M-direction	-	279		
Grid points in N-direction		200		
OPEN BOUNDARY		Marine 1 (M1)	Marine 2 (M2)	Fluvial (F1)
Transport condition	kg/m³	0.025	0.025	0
Transport condition salinity	ppt		29 (summer), 33 (winter)	
VISCOSITY				
Uniform background horizontal eddy viscosity	m²/s	1		
Uniform background horizontal eddy diffusivity	m²/s	1		
Uniform background vertical eddy viscosity	m²/s	1.0E-04		
Uniform background vertical eddy diffusivity	m²/s	1.0E-07		
SEDIMENT		Marine 1 (M1)	Marine 2 (M2)	Fluvial (F1)
Reference density for hindered settling	kg/m³	100		
Specific density	kg/m³	2,650		
Dry bed density	kg/m³	500		
Fresh settling velocity	mm/s	0.25		
Saline settling velocity	mm/s	0.25		
Critical bed shear stress for sedimentation at Santos bay	N/m²	1.0E-03		
Critical bed shear stress for sedimentation inside the estuary	N/m²	100		
Critical bed shear stress for erosion	N/m²	0.1	0.3	0.1
Erosion parameter	kg/m²/s	1.0E-03		
Initial layer thickness at bed	m	0		
MORPHOLOGY				
Morphological scale factor	-	1		
Spin-up before morphological changes	min	720		
Minimum depth for sediment calculation	m	0.1		

C

Model results - cross-sectional plots

The following figures present the magnitude and direction of currents, salinity conditions, stratification, and sediment concentration for each of the sixteen scenarios of Figure 4.7. Representative times of the simulations 1 and 2 (with and without salinity, respectively) were selected. The cross-section is placed in the center of the navigation channel, starting at the sea boundary and running until the end of the Piaçaguera channel, see Figure C.1).

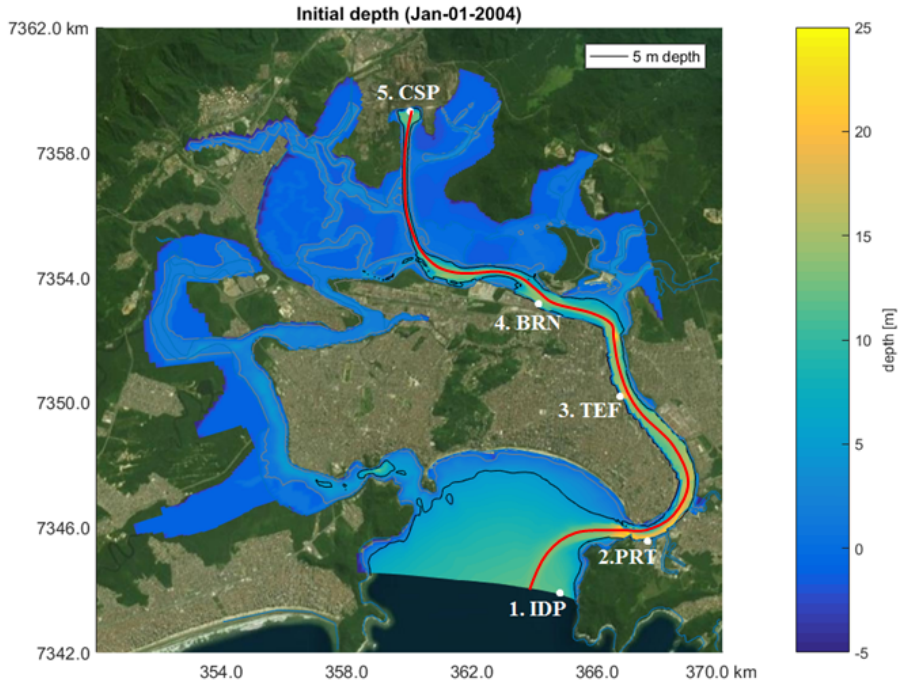

Figure C.1: Top view of the position of the longitudinal cross-section, represented by the red line.

C.1 Salinity on

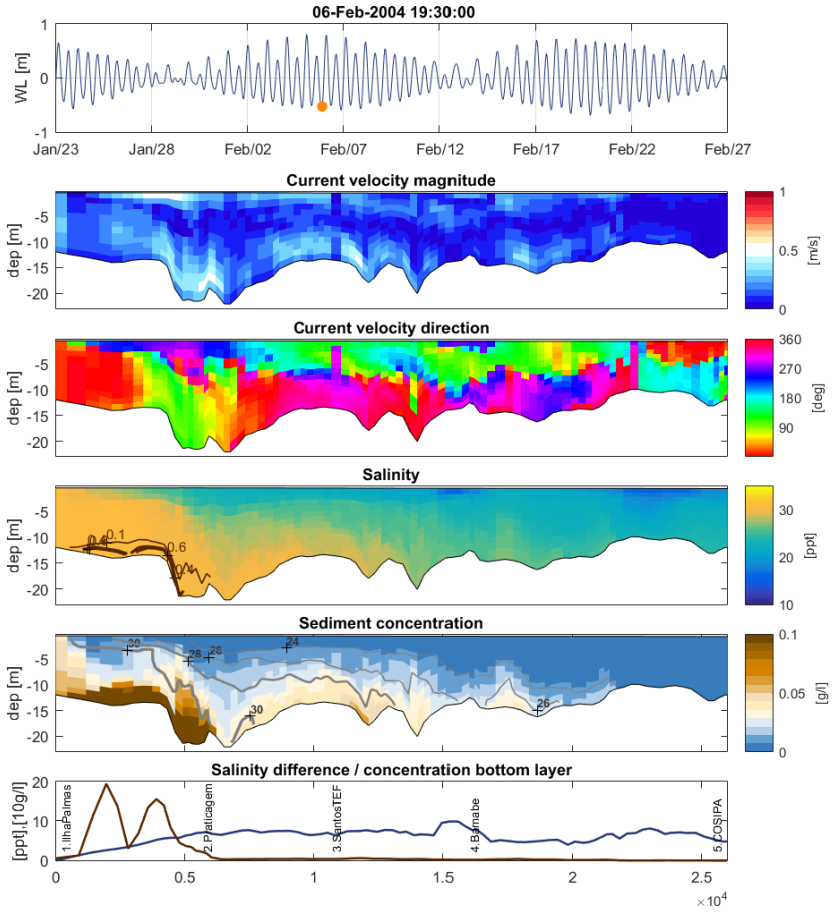

Figure C.2: Summer condition, spring tide, low water.

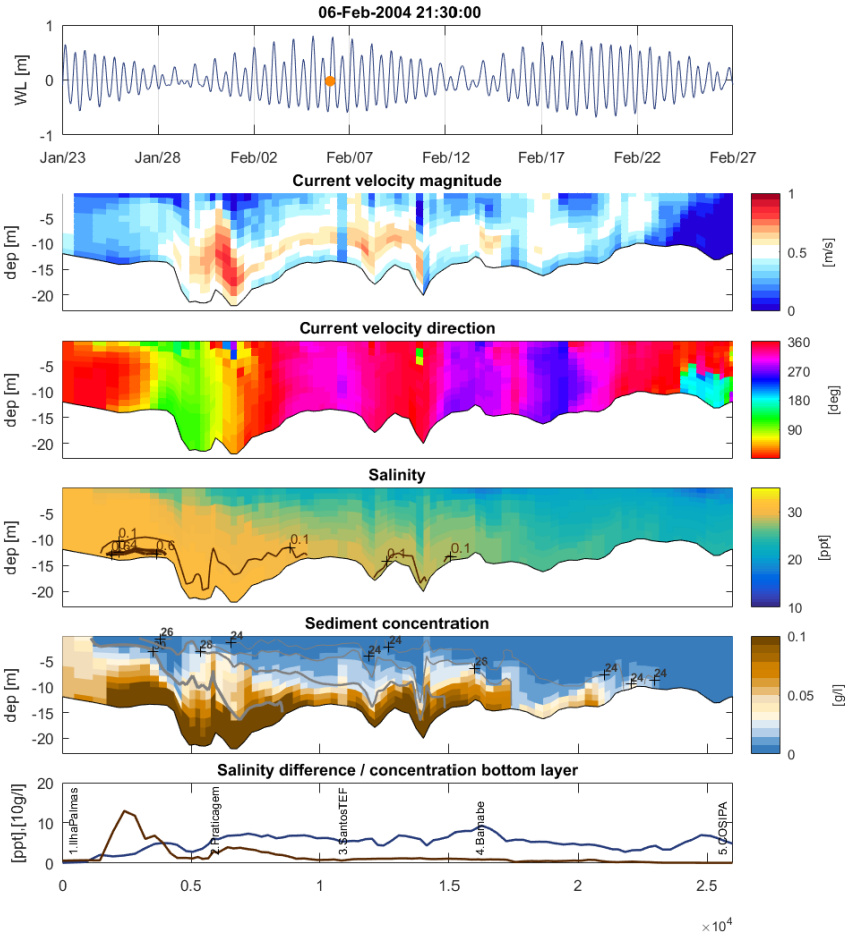

Figure C.3: Summer condition, spring tide, mean water, flood.

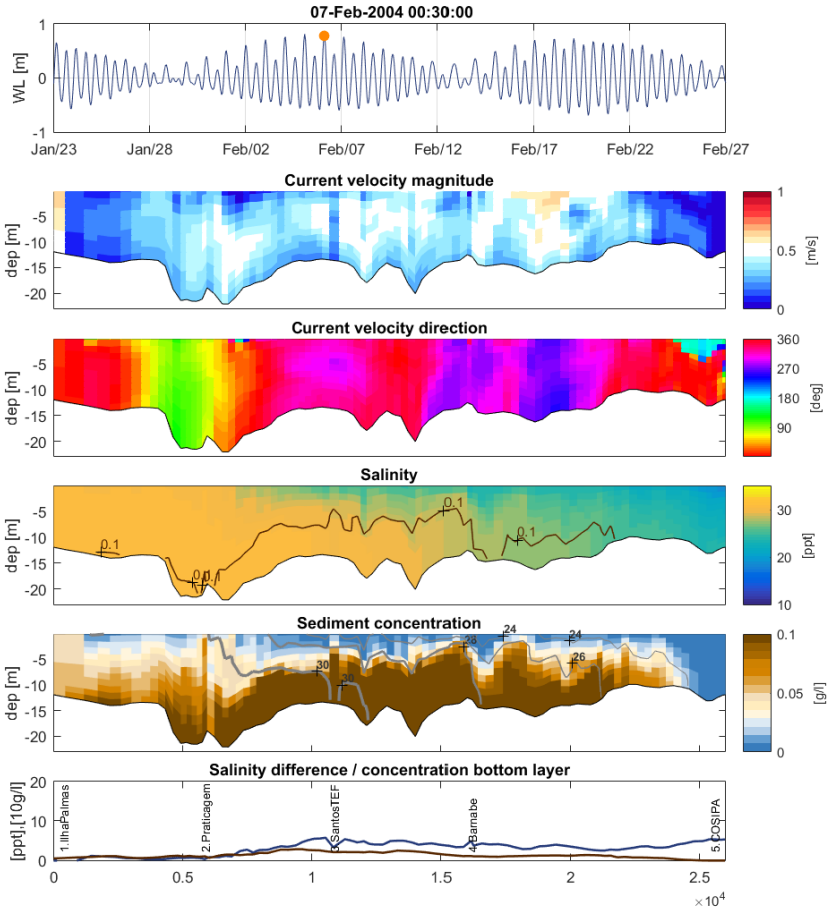

Figure C.4: Summer condition, spring tide, high water.

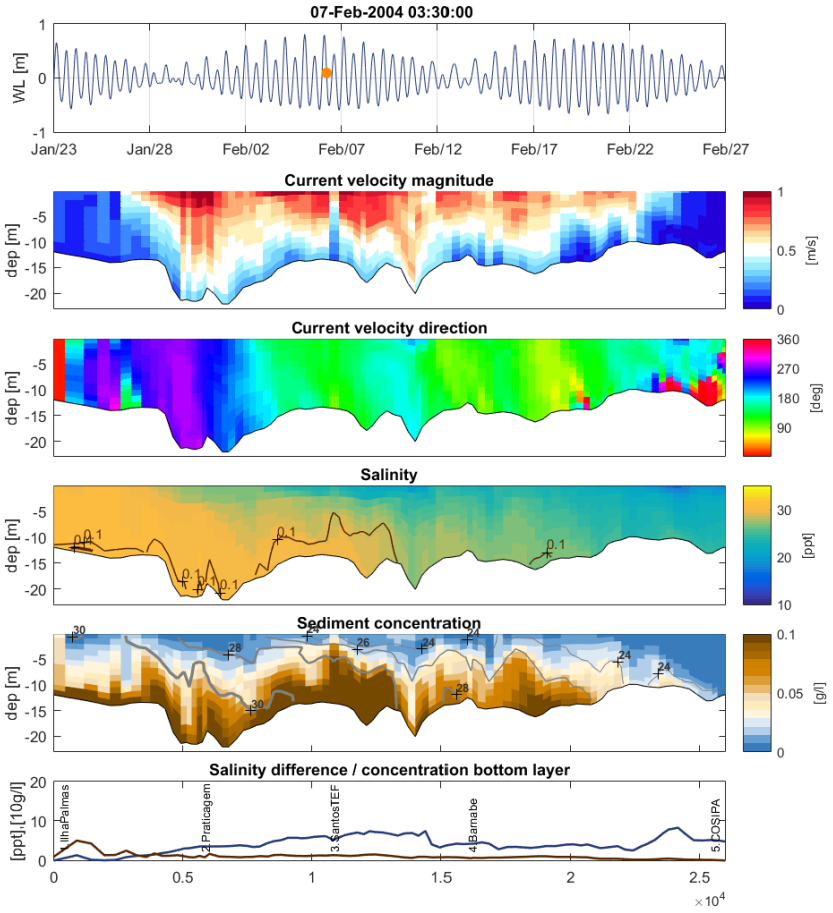

Figure C.5: Summer condition, spring tide, mean water, ebb.

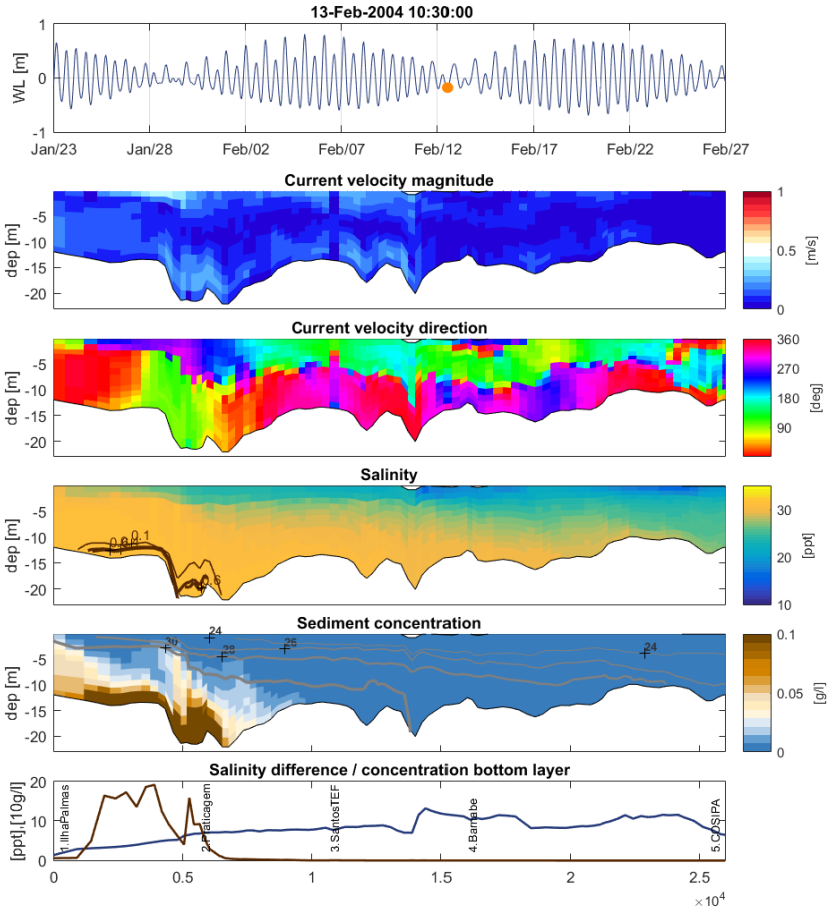

Figure C.6: Summer condition, neap tide, low water.

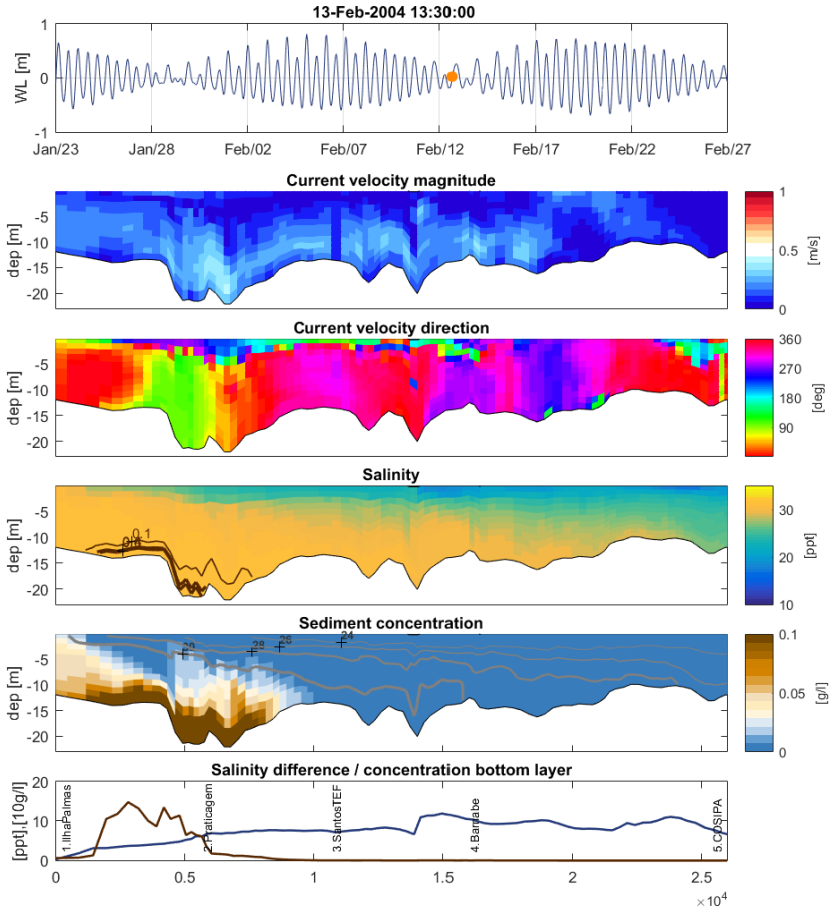

Figure C.7: Summer condition, neap tide, mean water, flood.

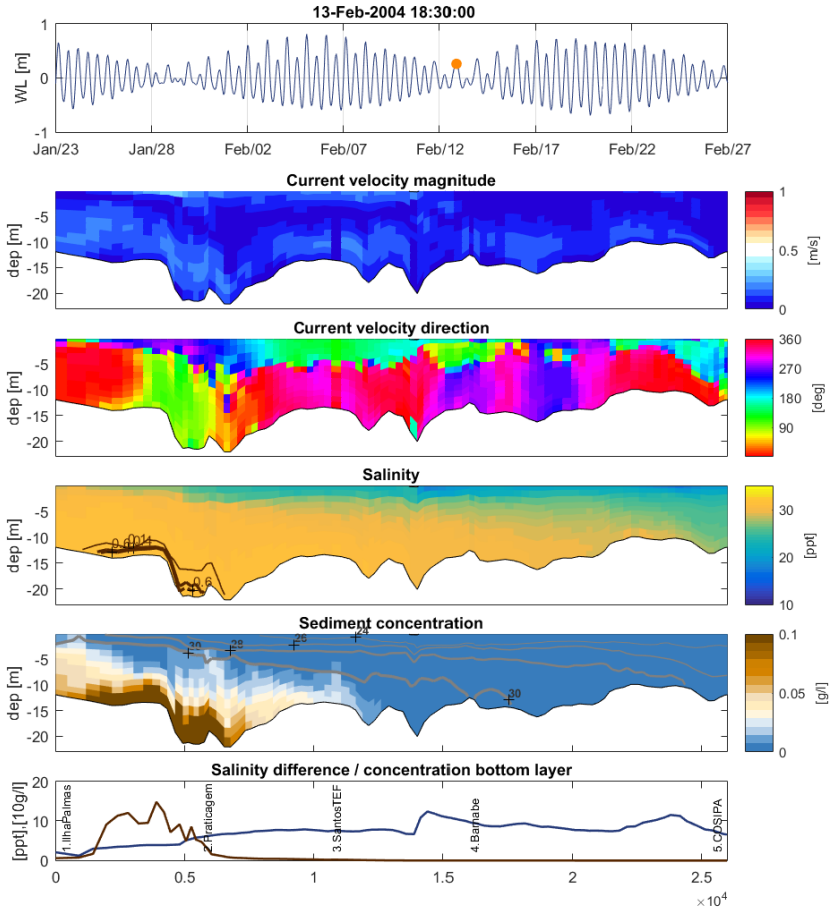

Figure C.8: Summer condition, neap tide, high water.

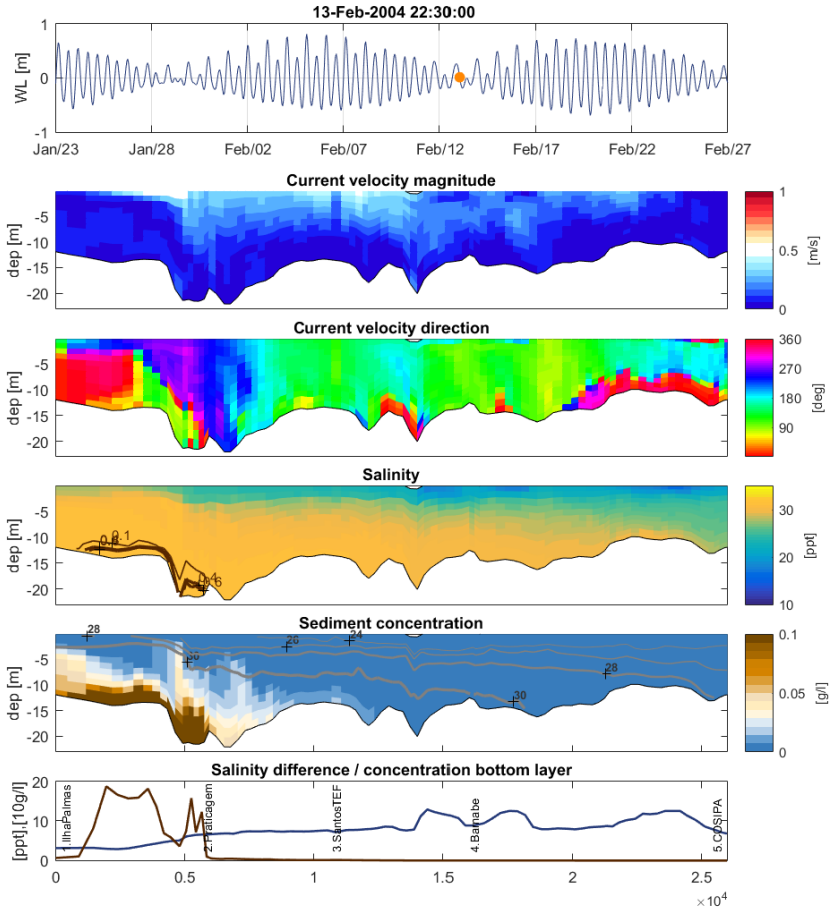

Figure C.9: Summer condition, neap tide, mean water, ebb.

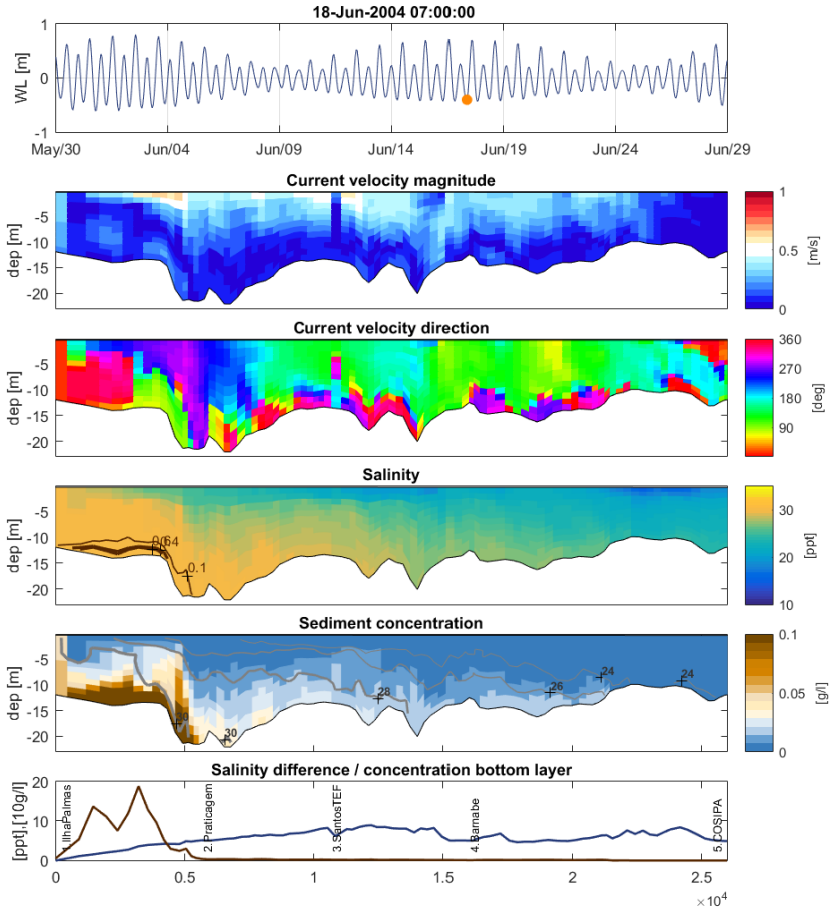

Figure C.10: Winter condition, spring tide, low water.

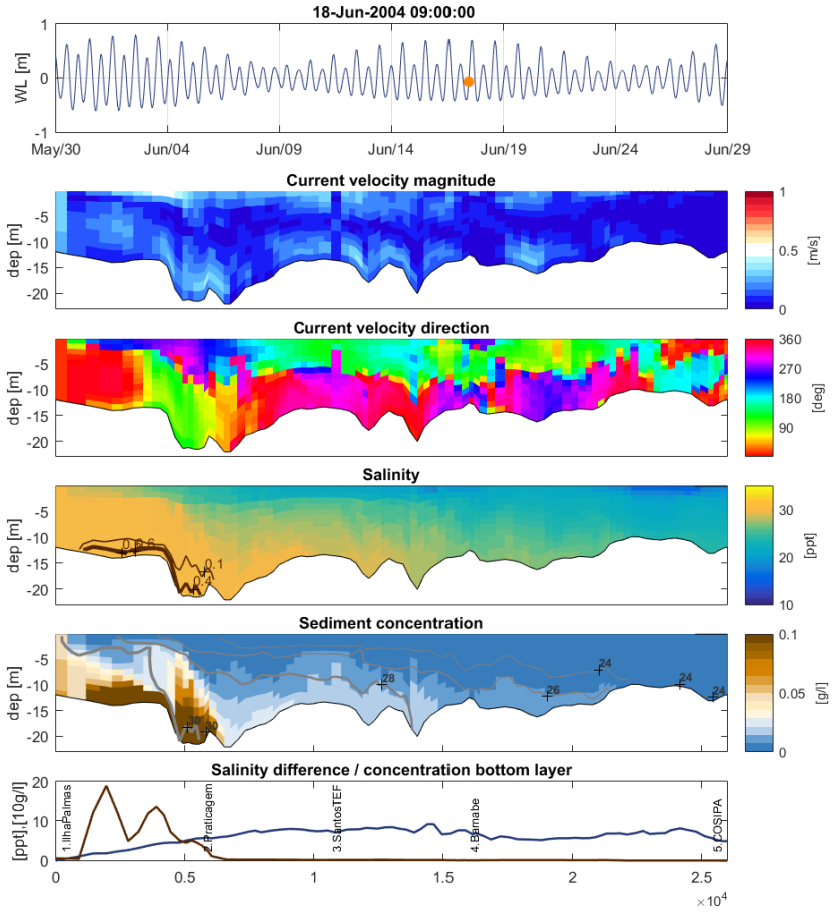

Figure C.11: Winter condition, spring tide, mean water, flood.

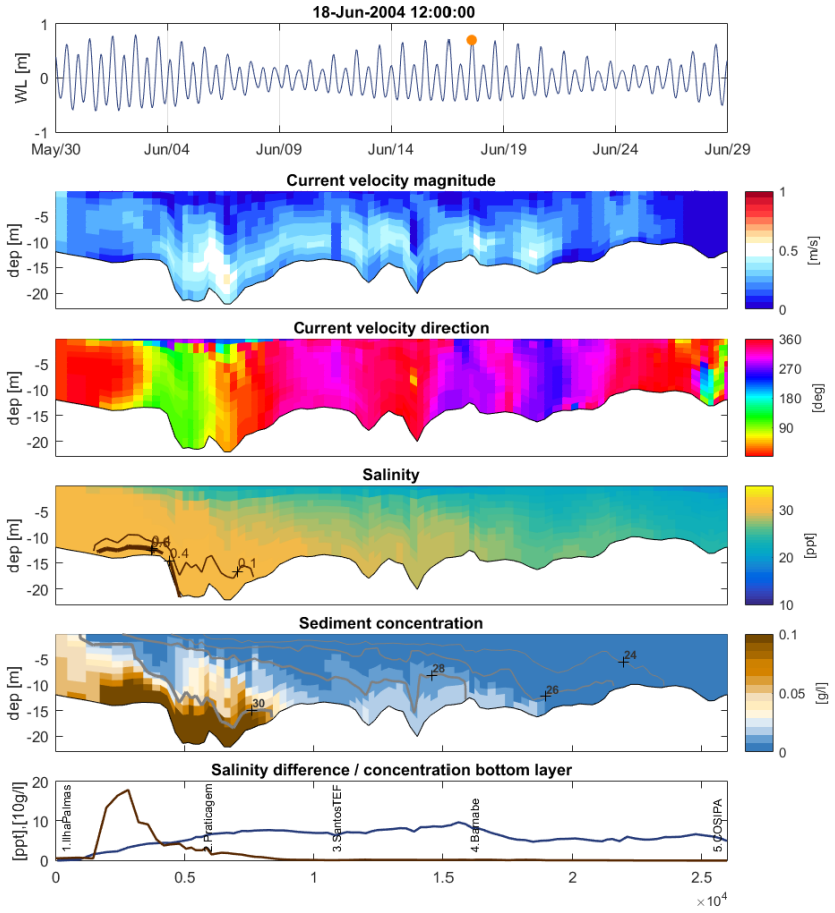

Figure C.12: Winter condition, spring tide, high water.

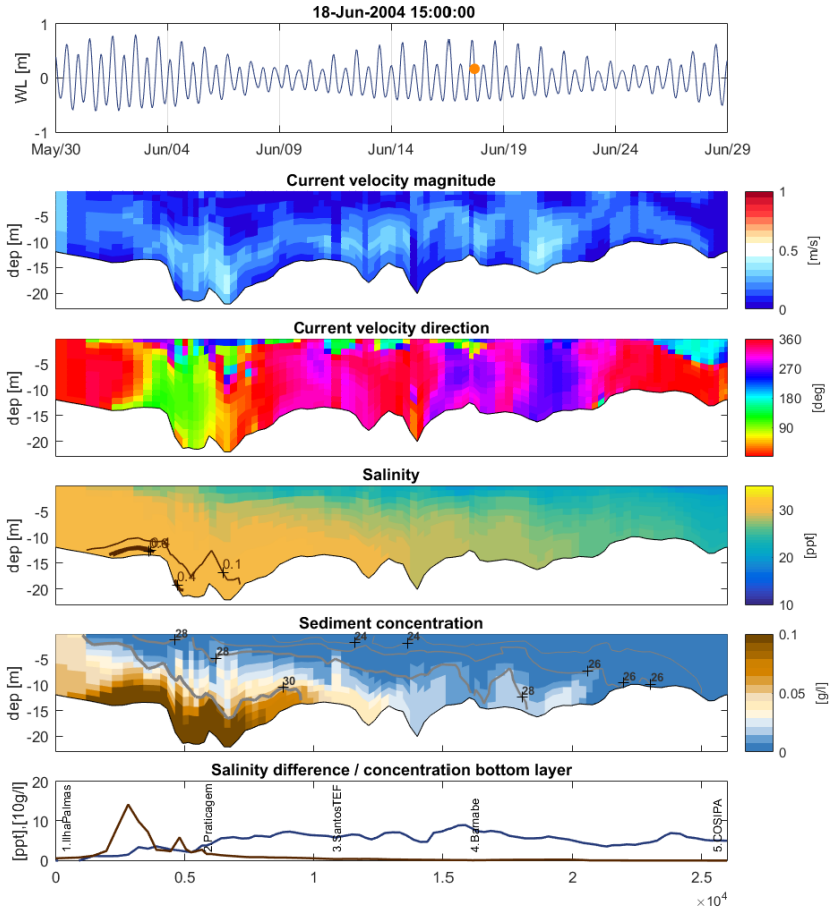

Figure C.13: Winter condition, spring tide, mean water, ebb.

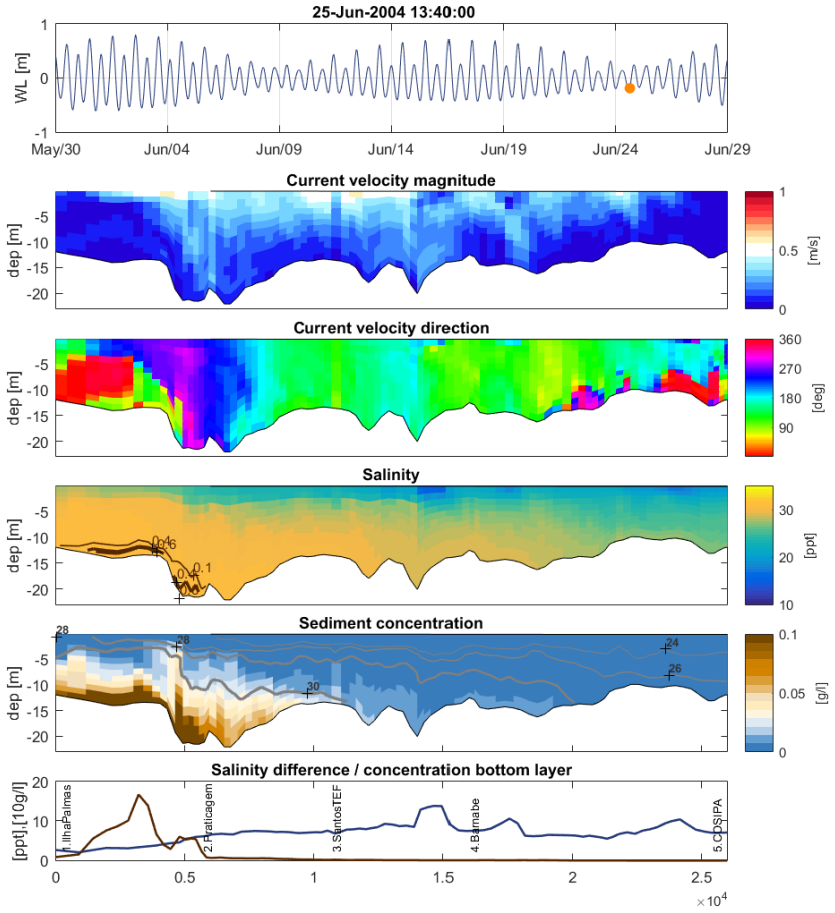

Figure C.14: Winter condition, neap tide, low water.

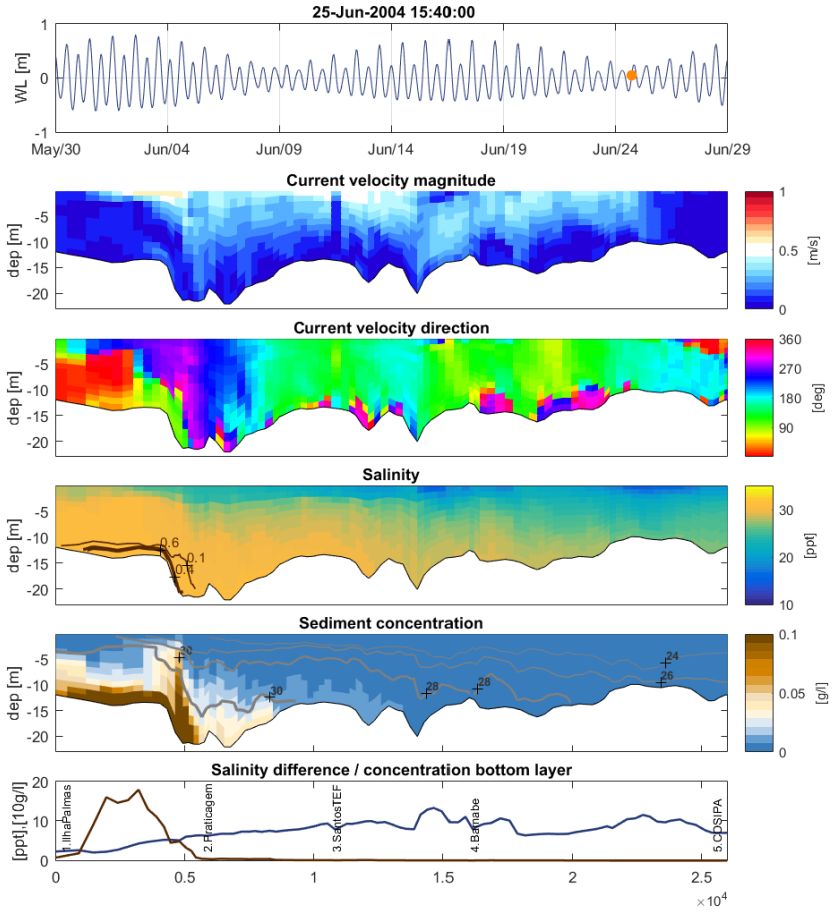

Figure C.15: Winter condition, neap tide, mean water, flood.

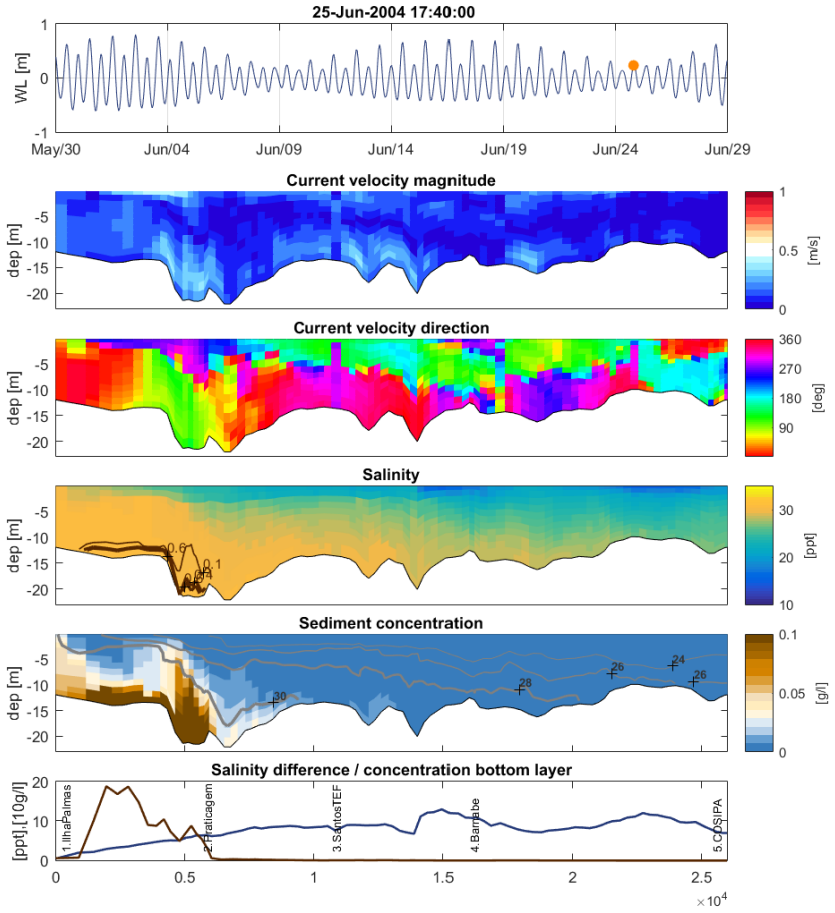

Figure C.16: Winter condition, neap tide, high water.

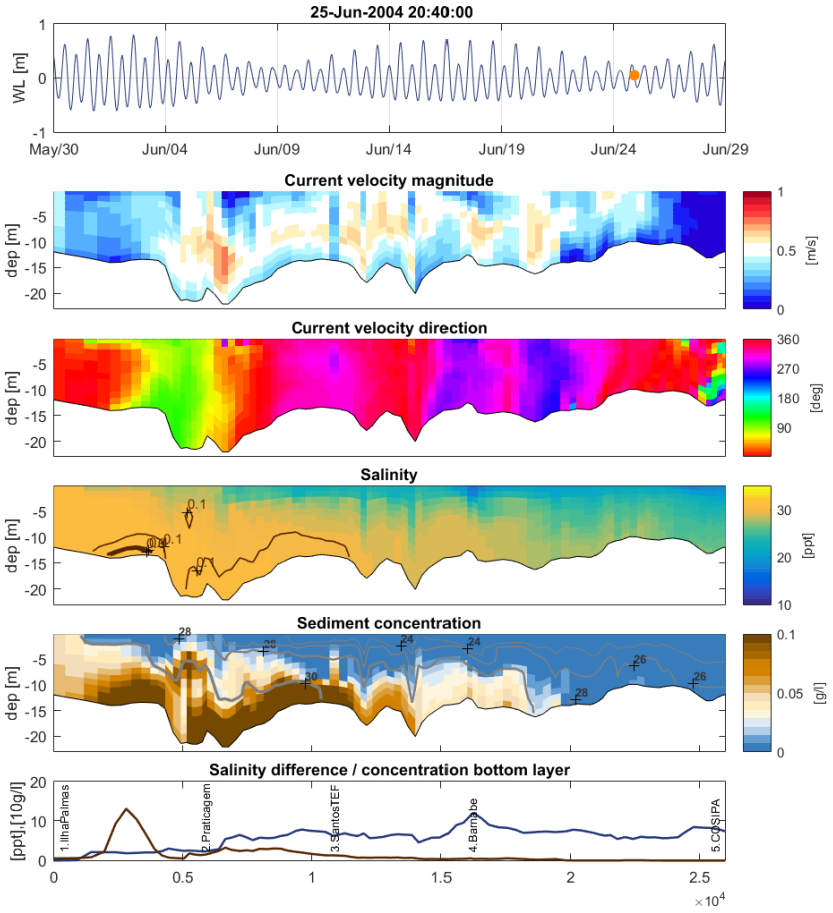

Figure C.17: Winter condition, neap tide, mean water, ebb.

C.2 Salinity off

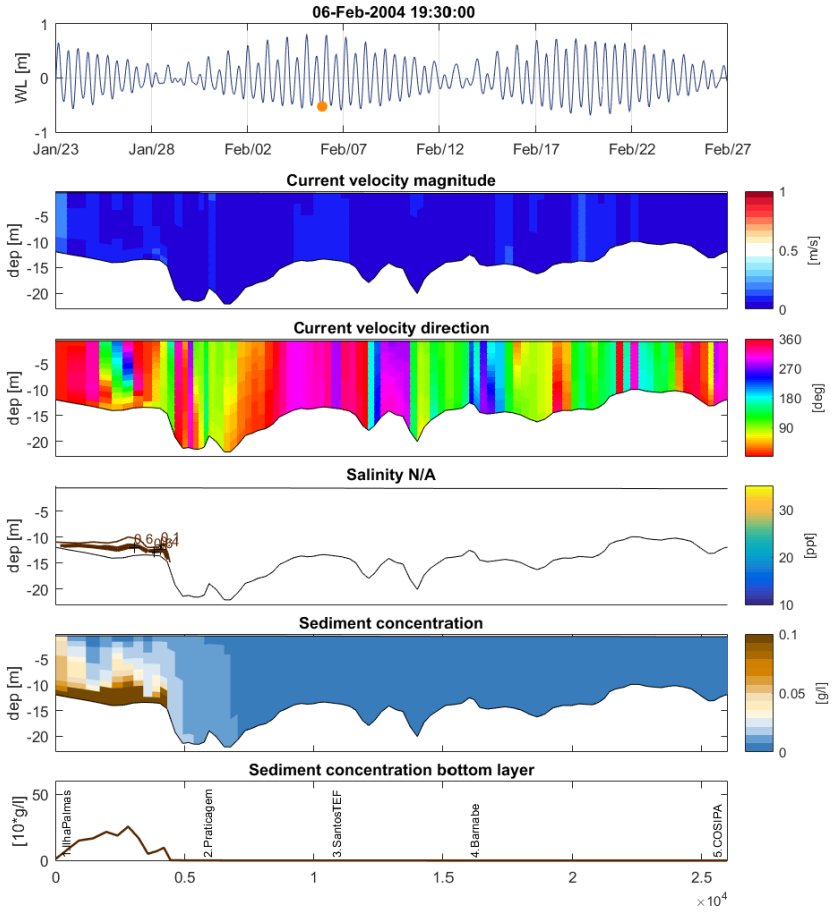

Figure C.18: Summer condition, spring tide, low water.

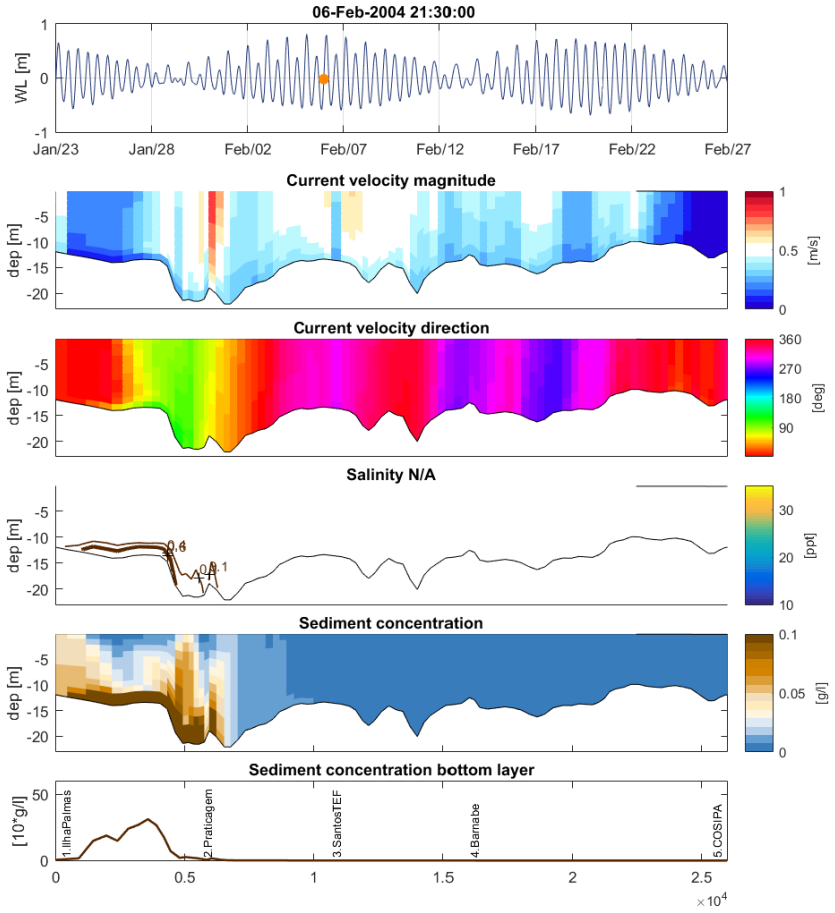

Figure C.19: Summer condition, spring tide, mean water, flood.

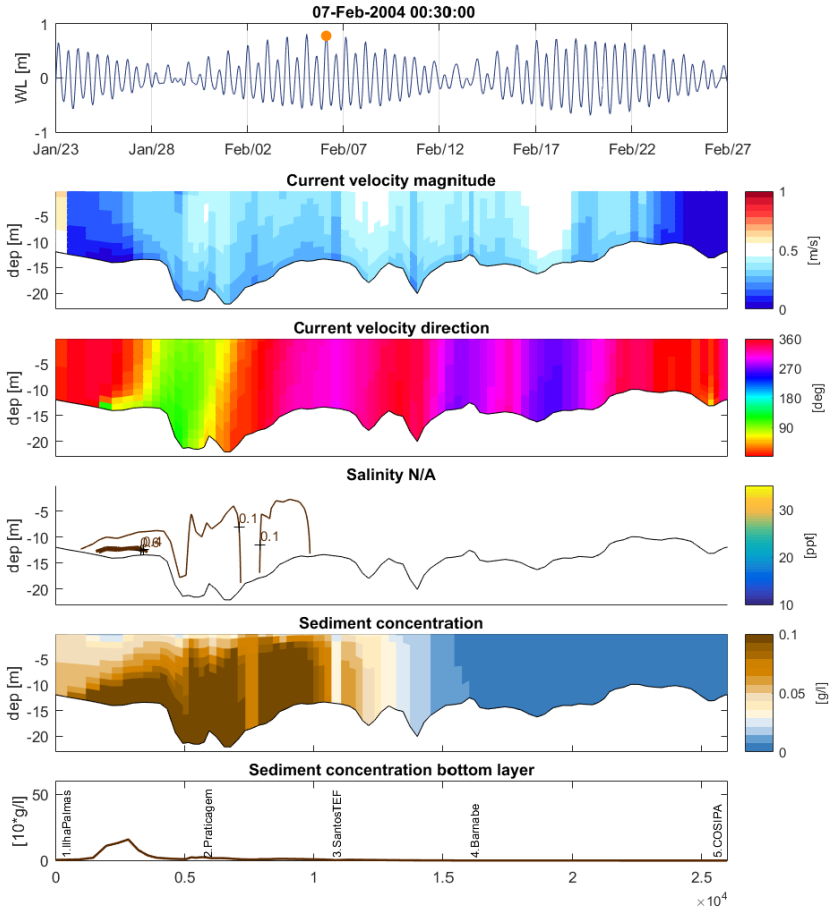

Figure C.20: Summer condition, spring tide, high water.

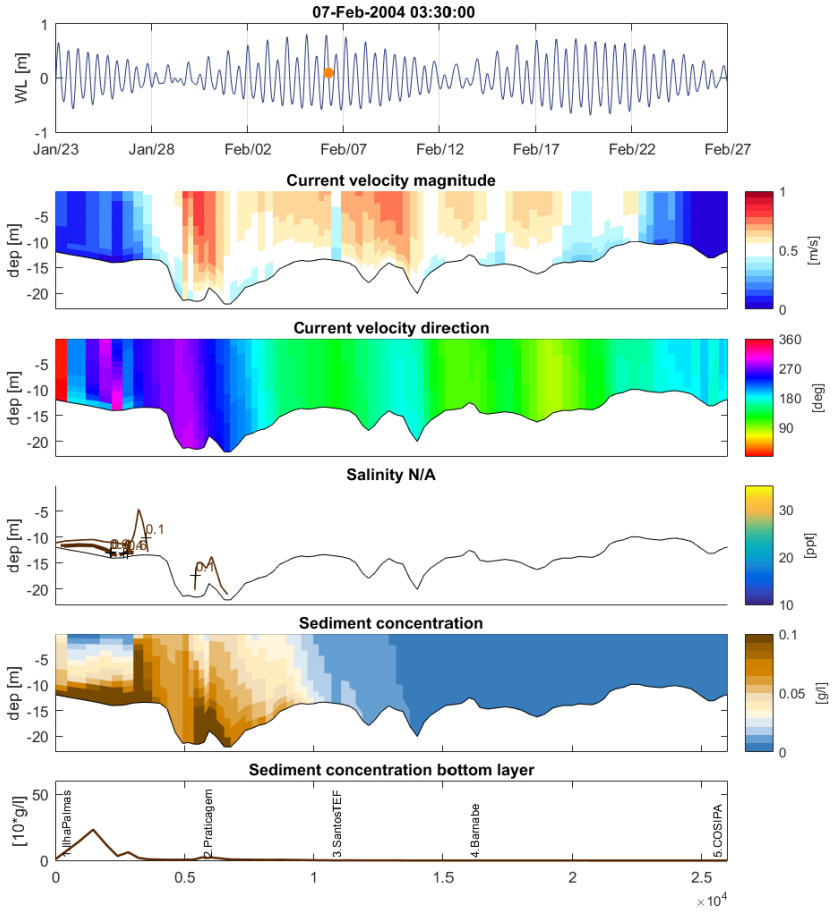

Figure C.21: Summer condition, spring tide, mean water, ebb.

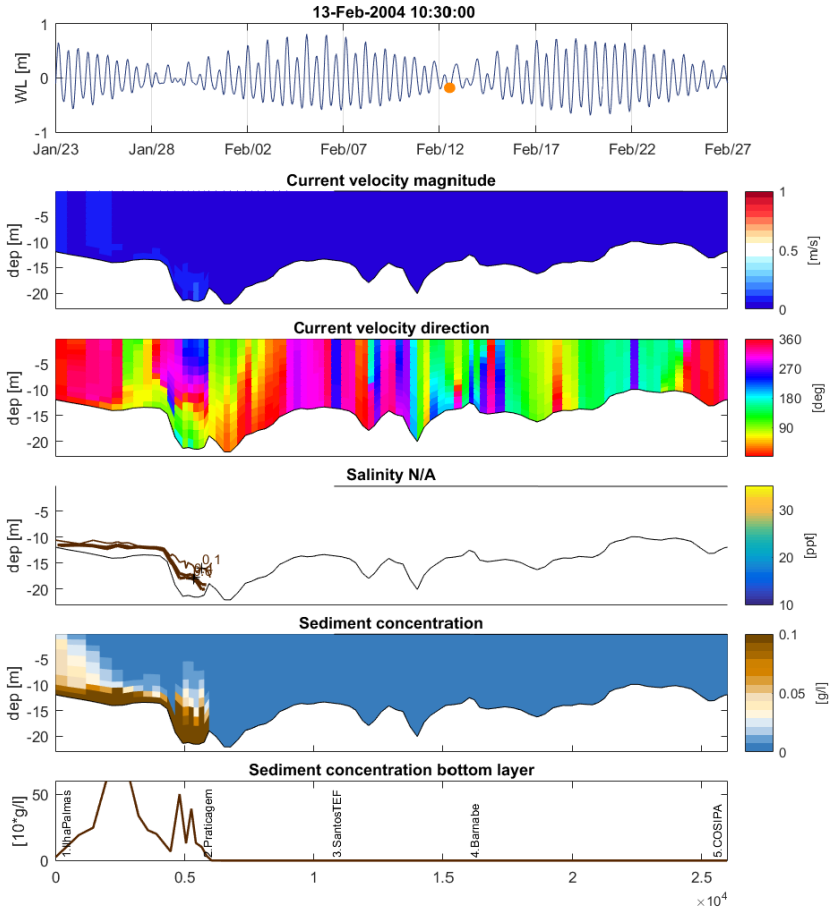

Figure C.22: Summer condition, neap tide, low water.

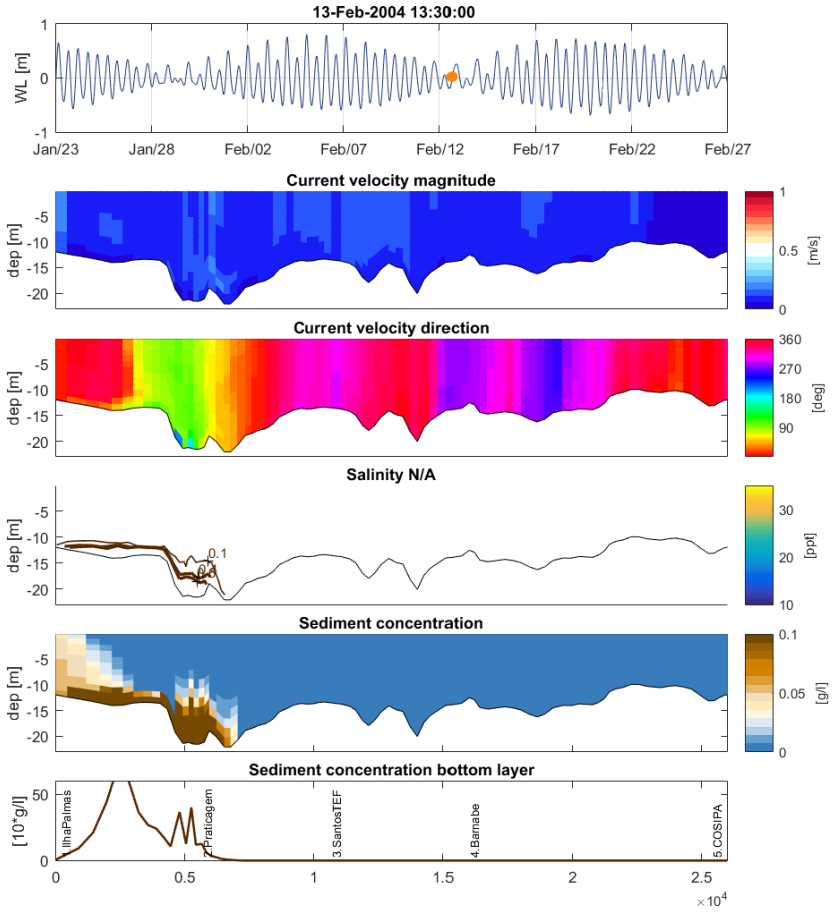

Figure C.23: Summer condition, neap tide, mean water, flood.

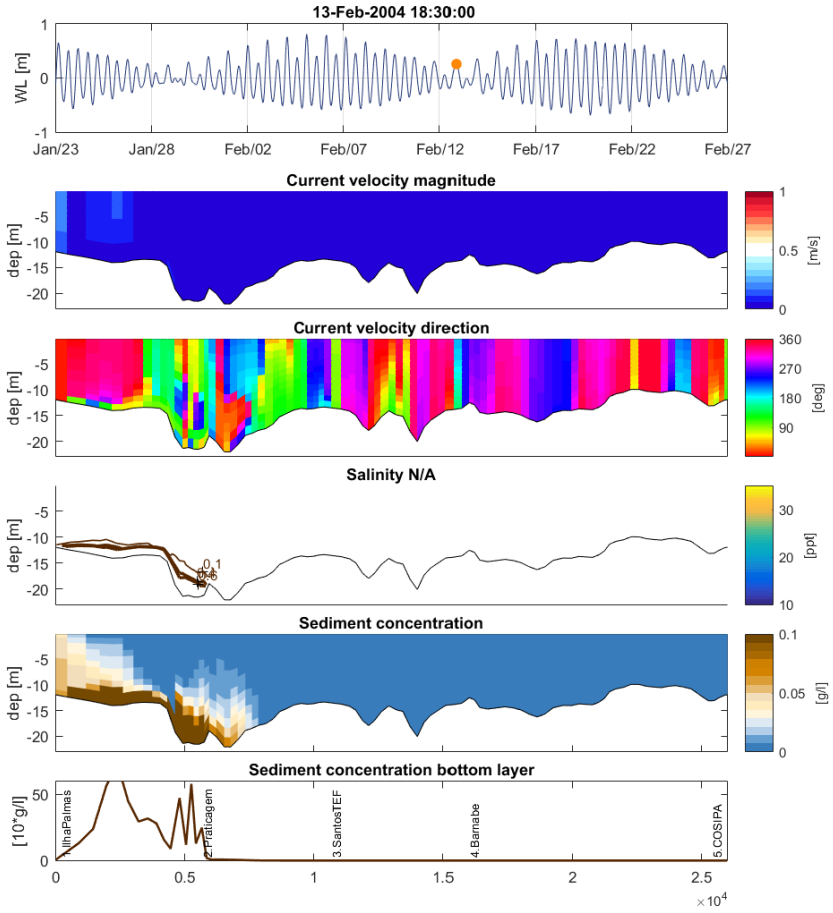

Figure C.24: Summer condition, neap tide, high water.

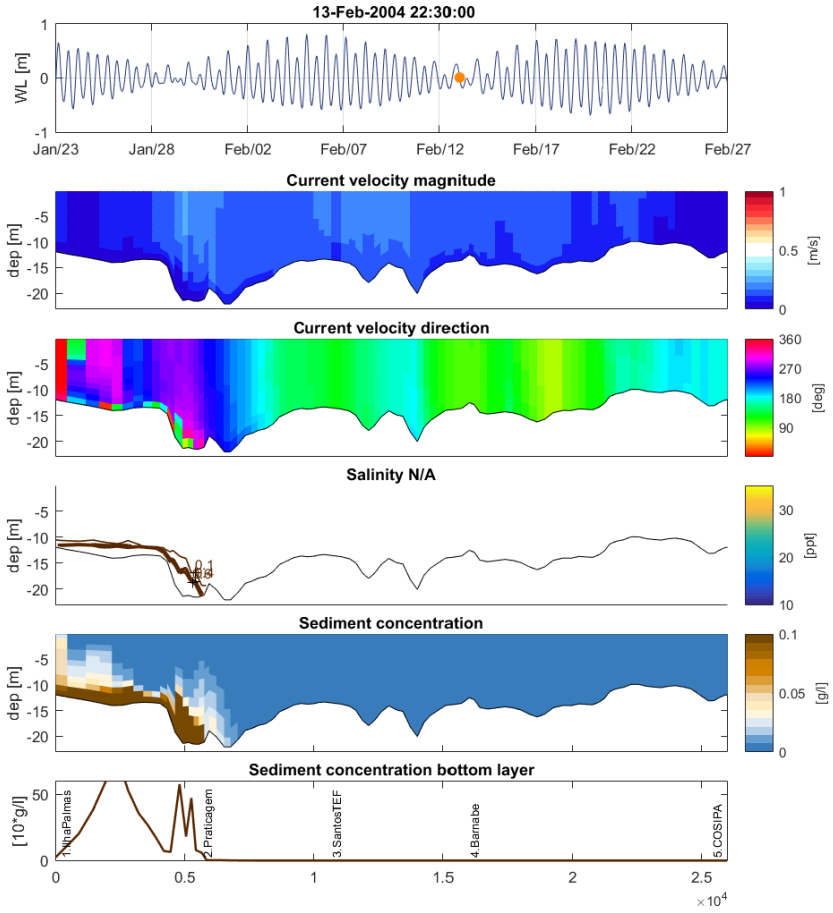

Figure C.25: Summer condition, neap tide, mean water, ebb.

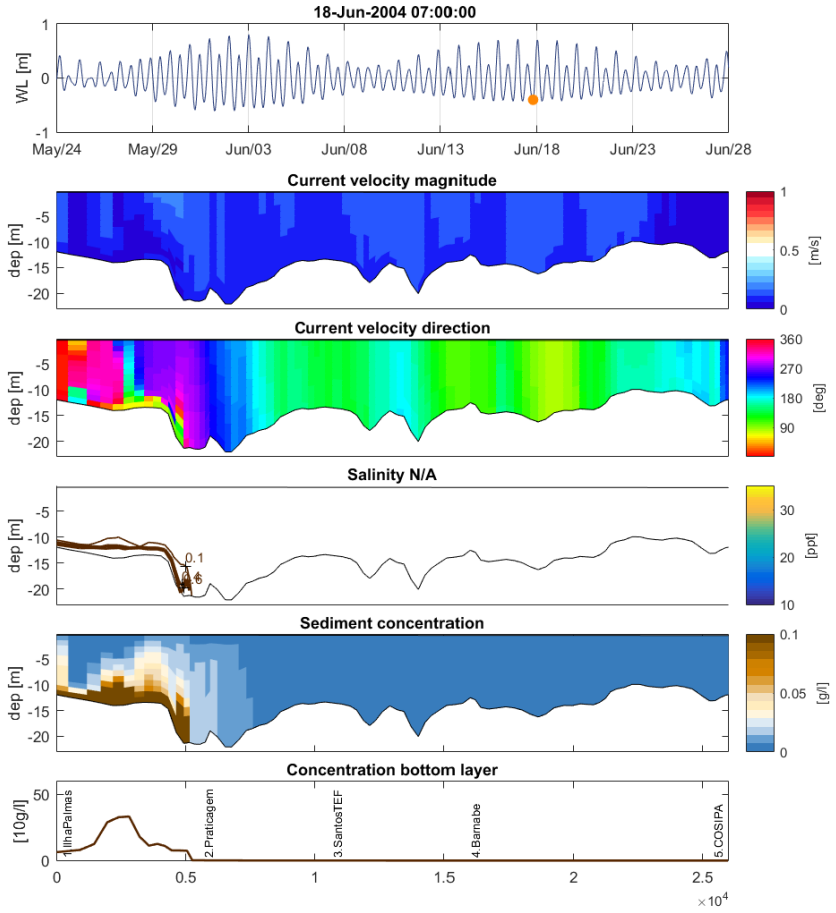

Figure C.26: Winter condition, spring tide, low water.

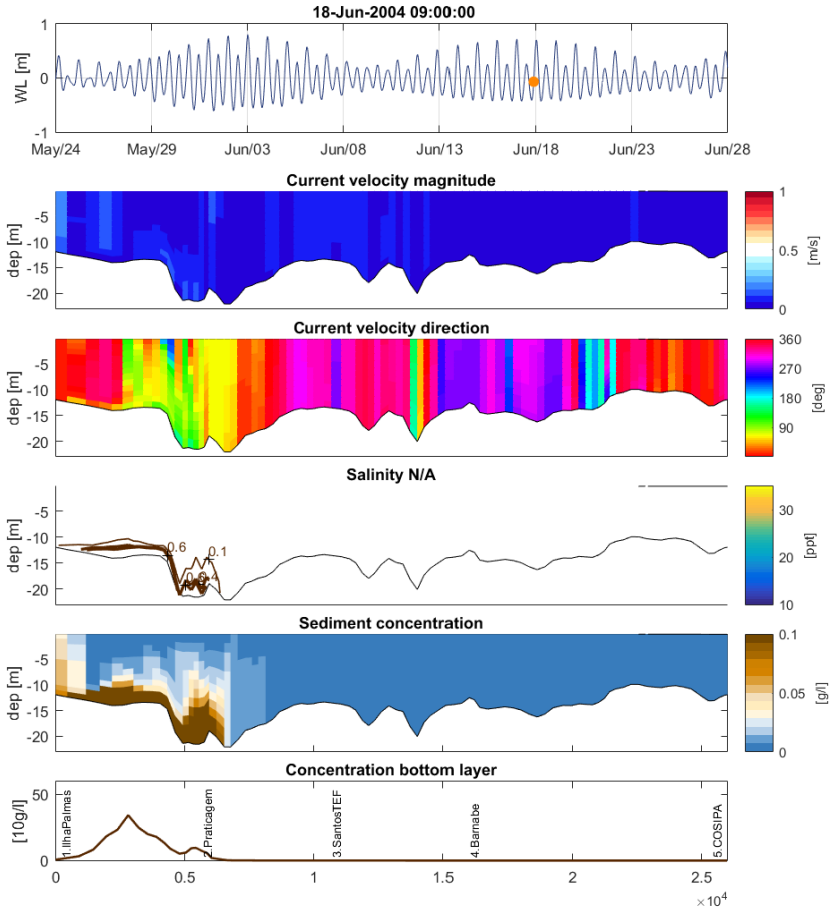

Figure C.27: Winter condition, spring tide, mean water, flood.

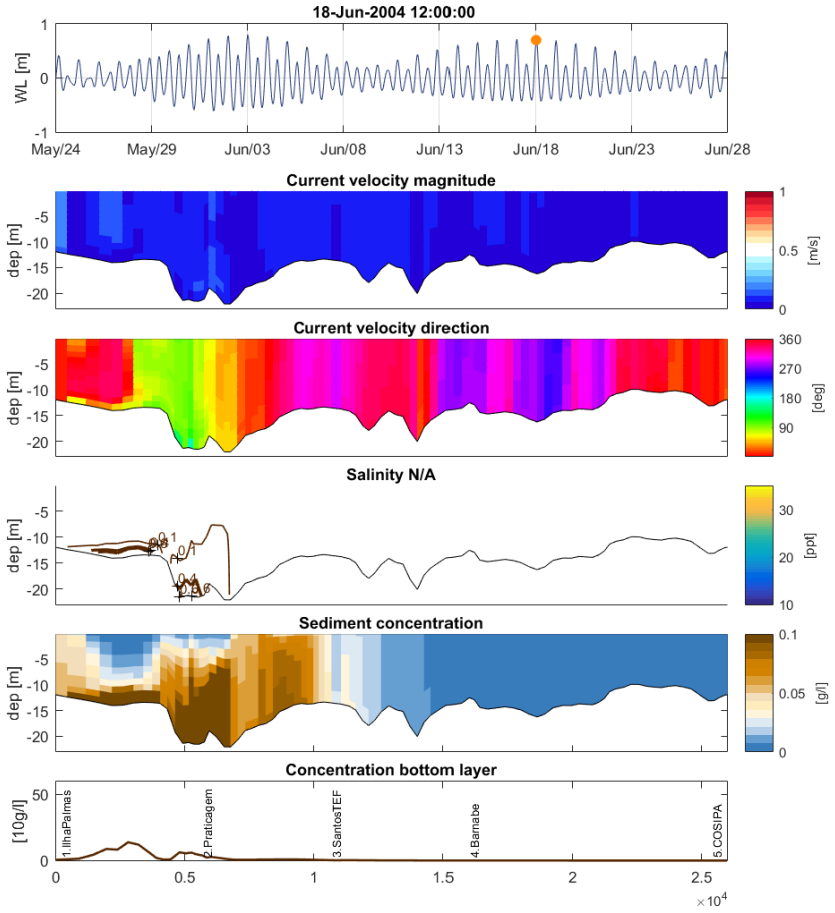

Figure C.28: Winter condition, spring tide, high water.

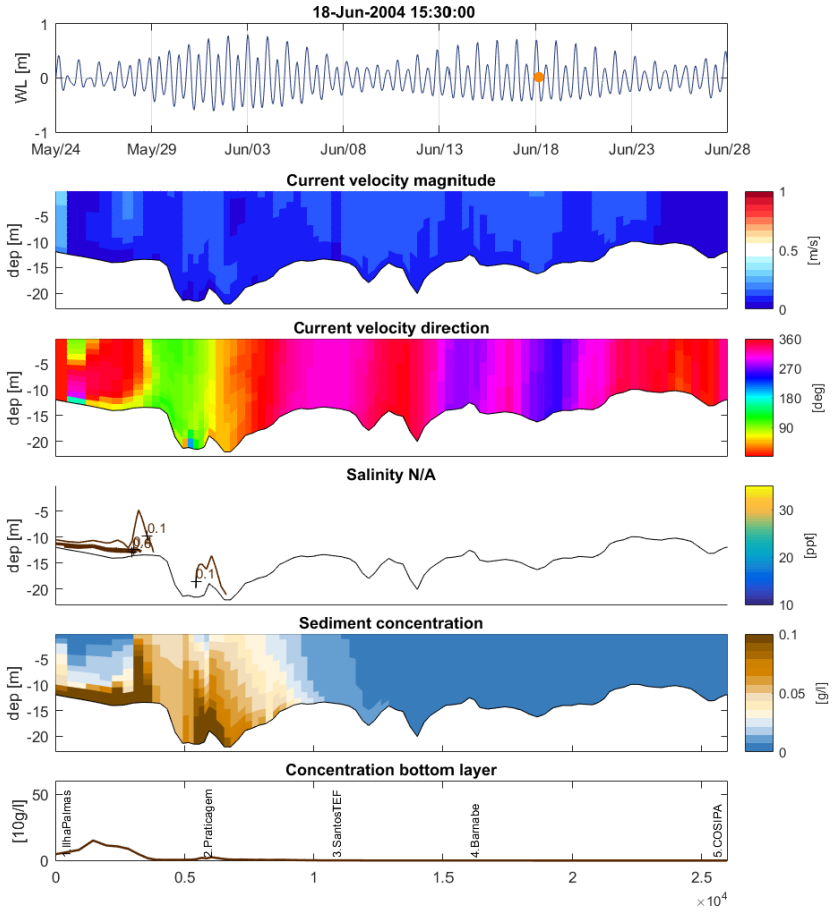

Figure C.29: Winter condition, spring tide, mean water, ebb.

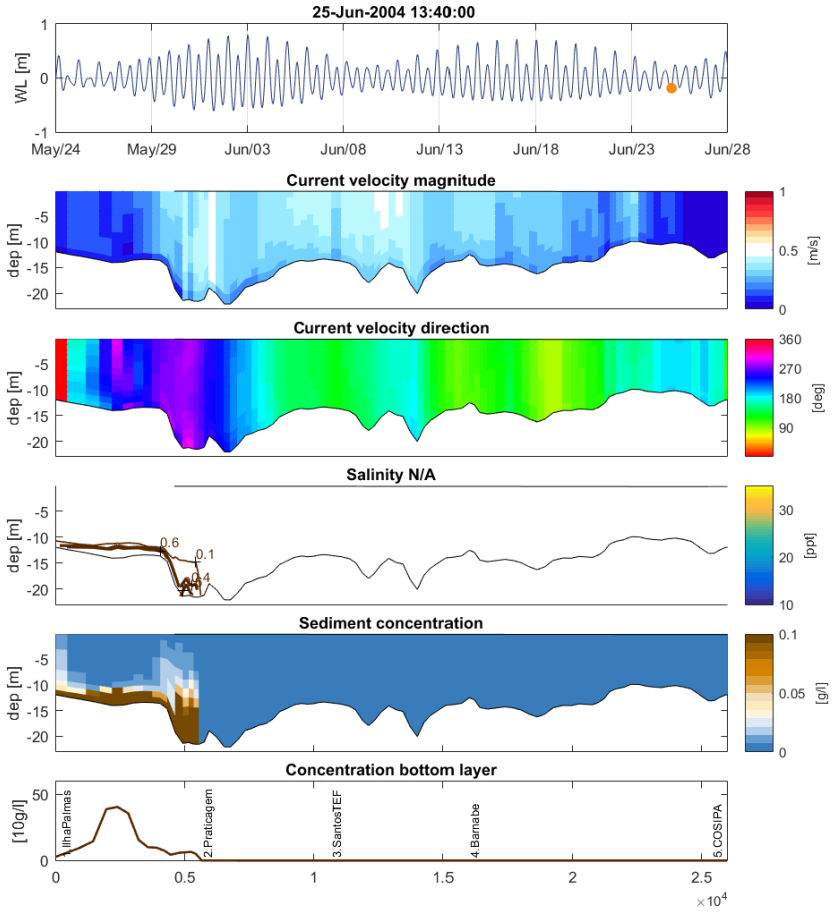

Figure C.30: Winter condition, neap tide, low water.

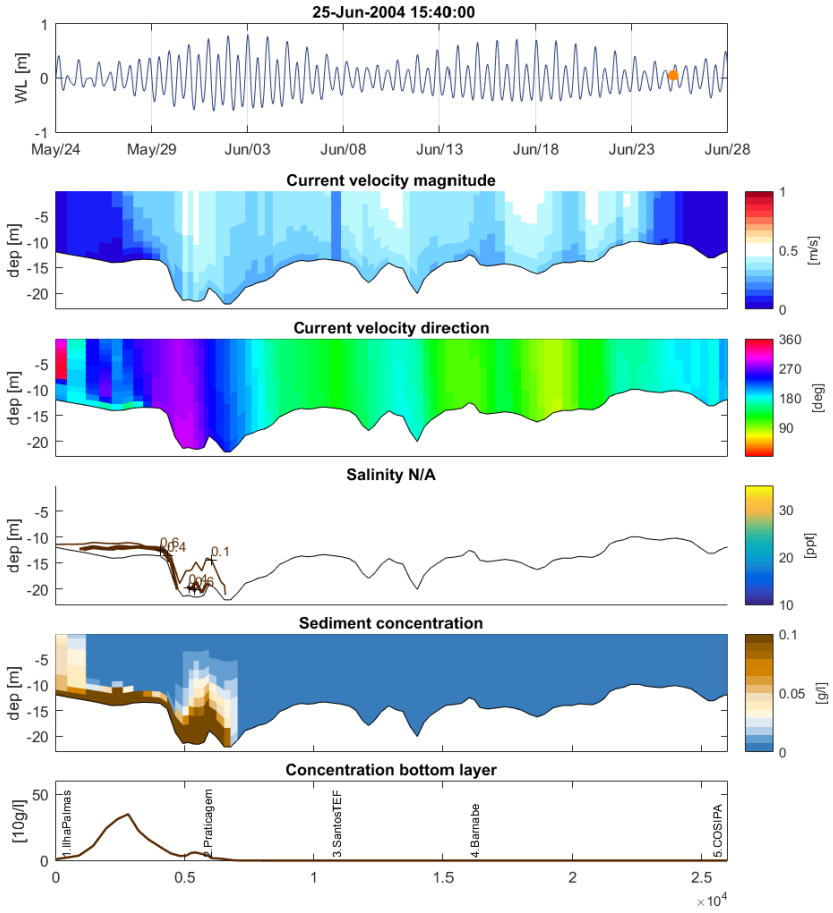

Figure C.31: Winter condition, neap tide, mean water, flood.

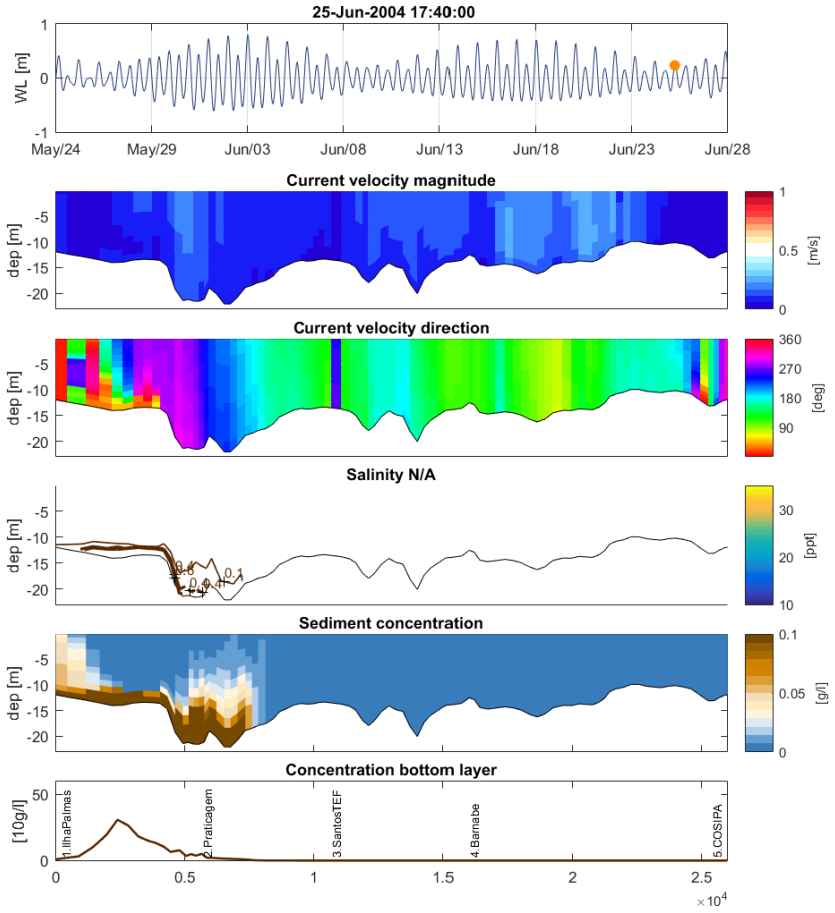

Figure C.32: Winter condition, neap tide, high water.

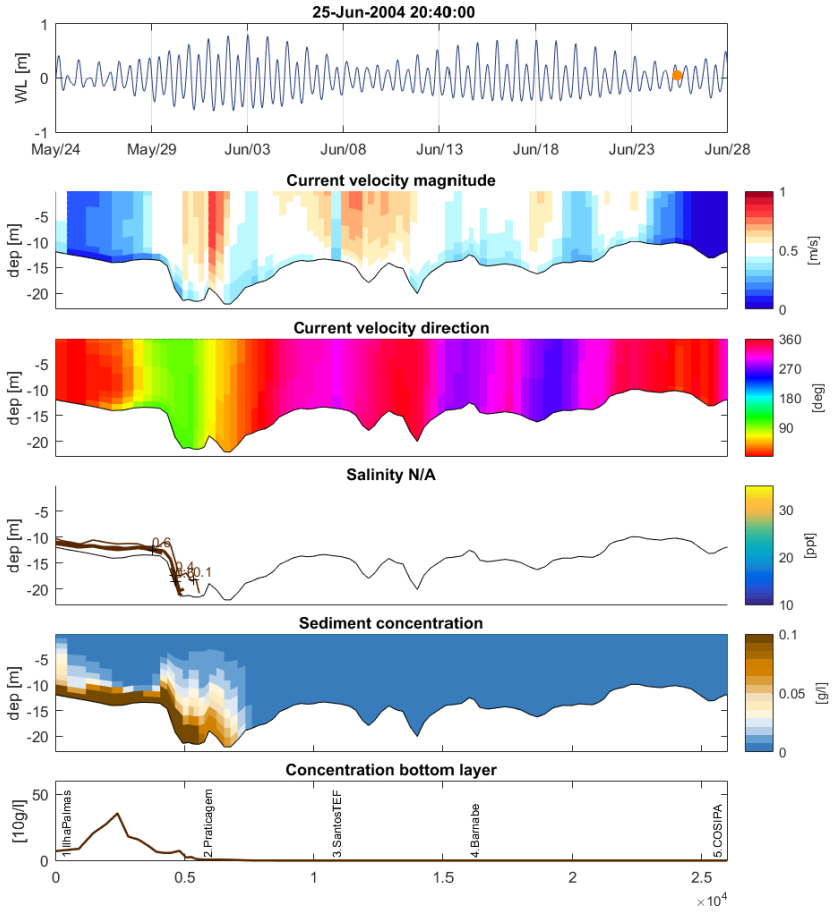

Figure C.33: Winter condition, neap tide, mean water, ebb.

D

Model results - map plots

D.1 Bed shear stress

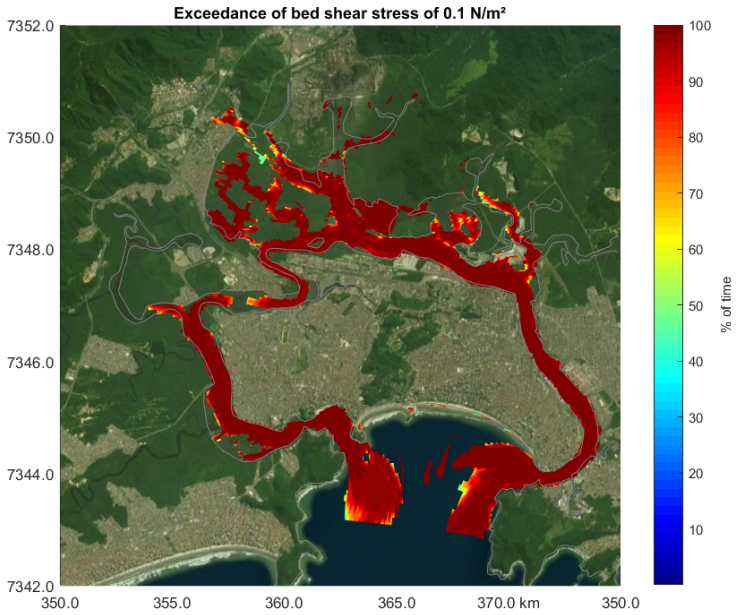

Figure D.1: % of time $\tau \geq 0.1$ N/m^2

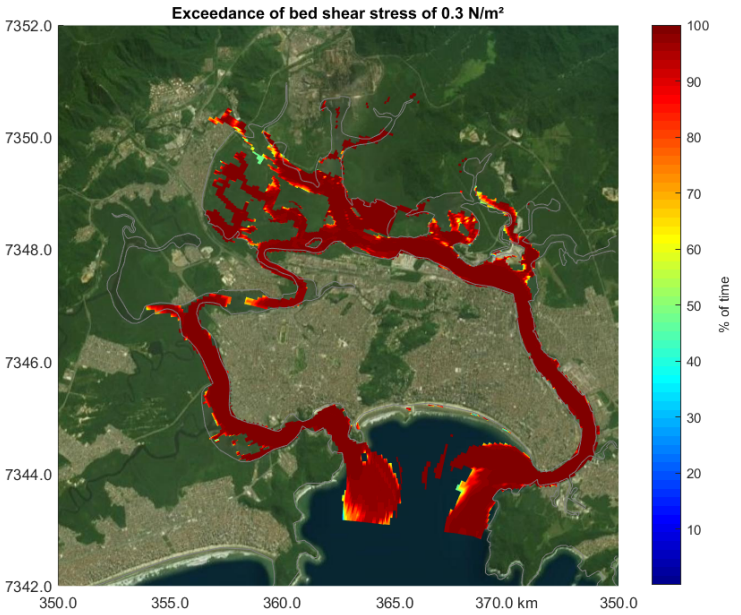

Figure D.2: % of time $\tau \geq 0.3$ N/m^2

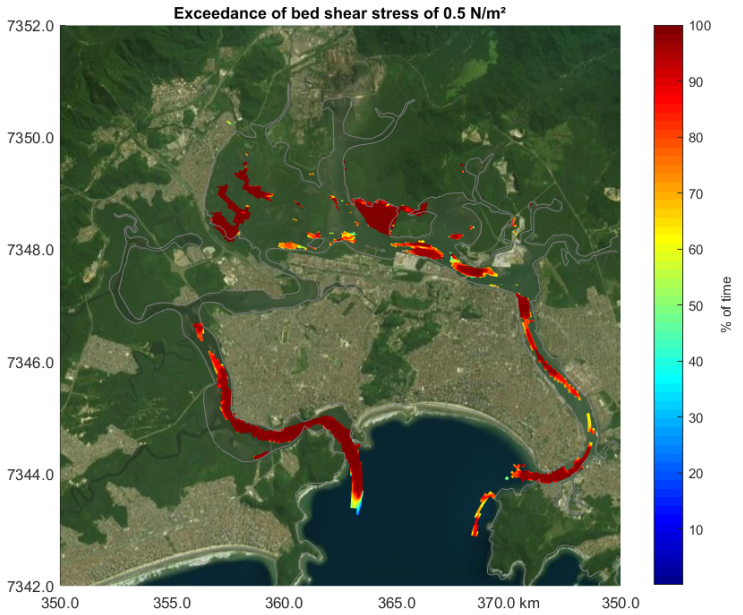

Figure D.3: % of time $\tau \geq 0.5$ N/m^2

D.2 Residual currents

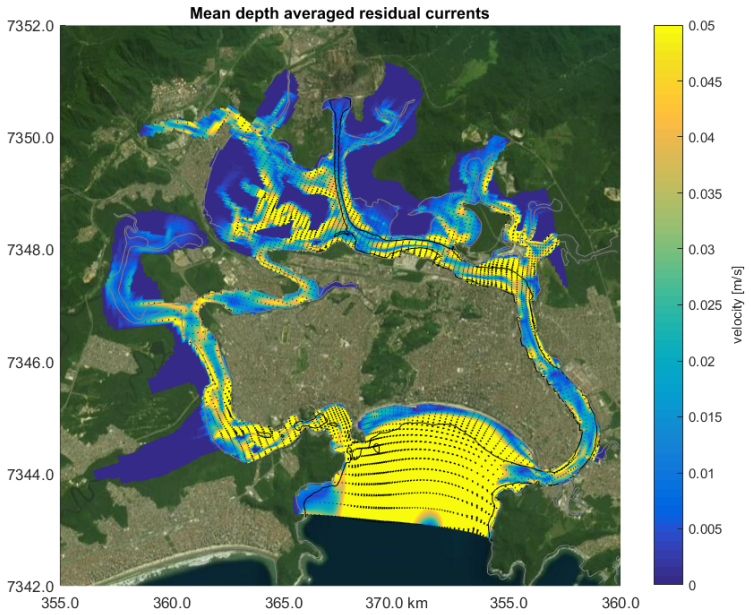

Figure D.4: Mean depth averaged residual currents. Summer, spring tide conditions.

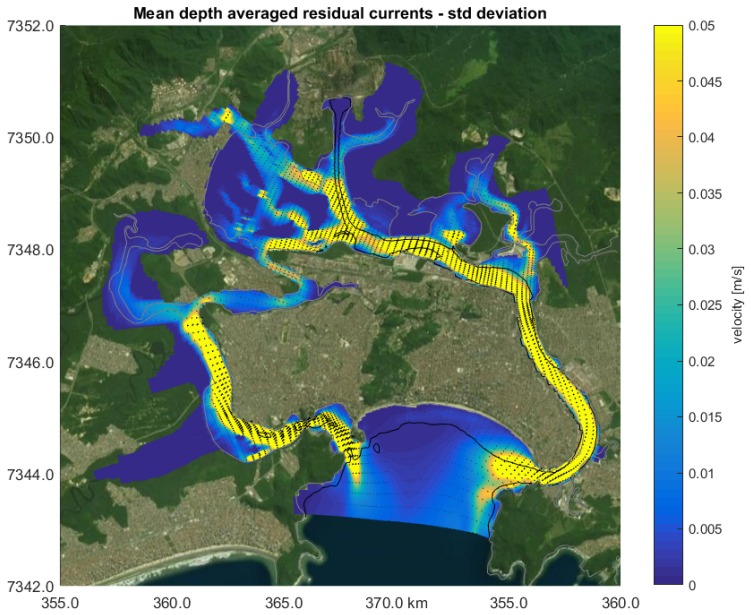

Figure D.5: Depth averaged residual currents standard deviation. Summer, spring tide conditions.

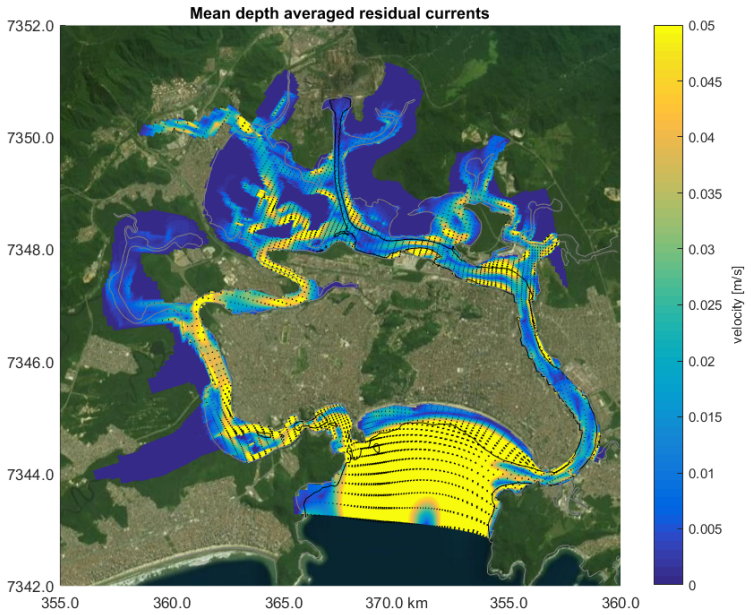

Figure D.6: Mean depth averaged residual currents. Summer, neap tide conditions.

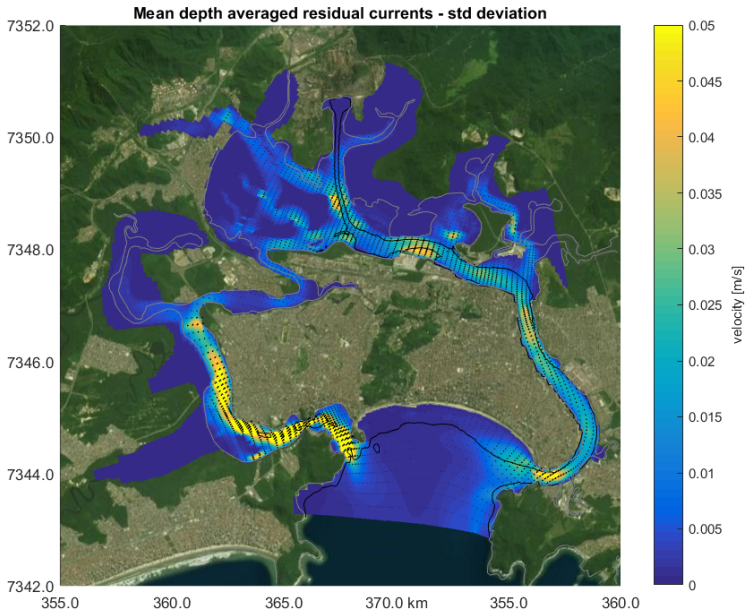

Figure D.7: Depth averaged residual currents standard deviation. Summer, neap tide conditions.

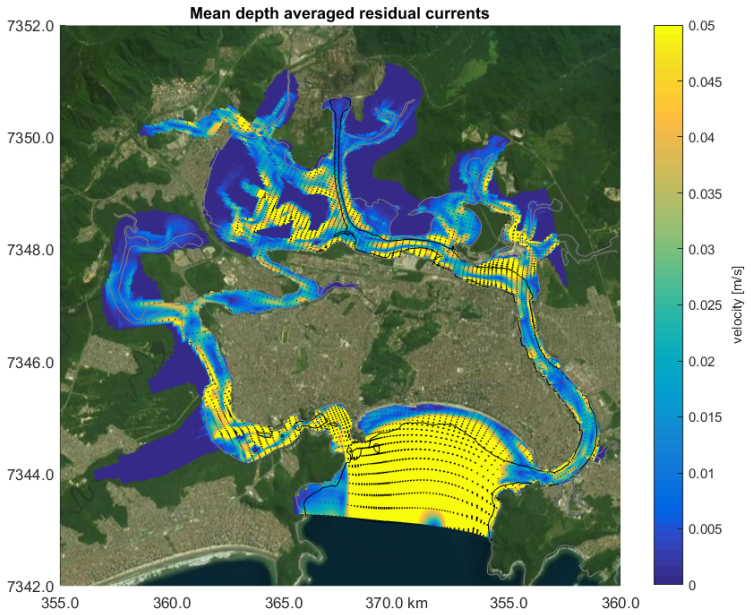

Figure D.8: Mean depth averaged residual currents. Winter, spring tide conditions.

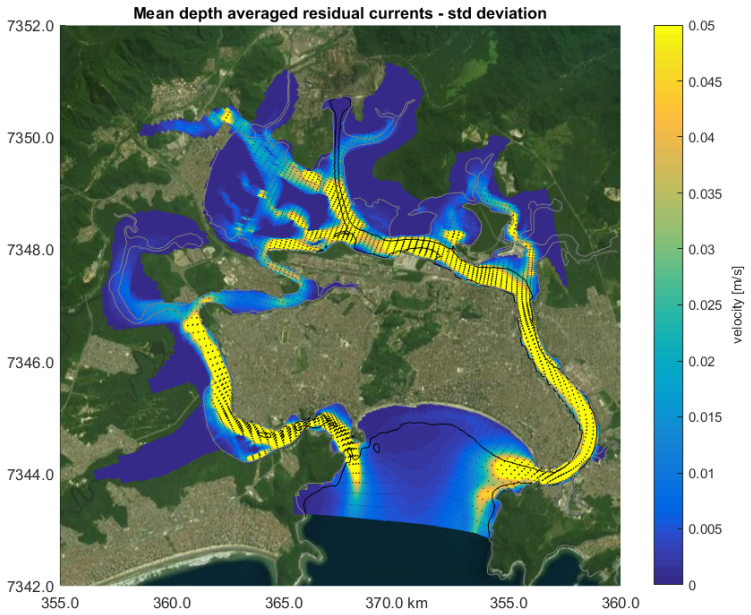

Figure D.9: Depth averaged residual currents standard deviation. Winter, spring tide conditions.

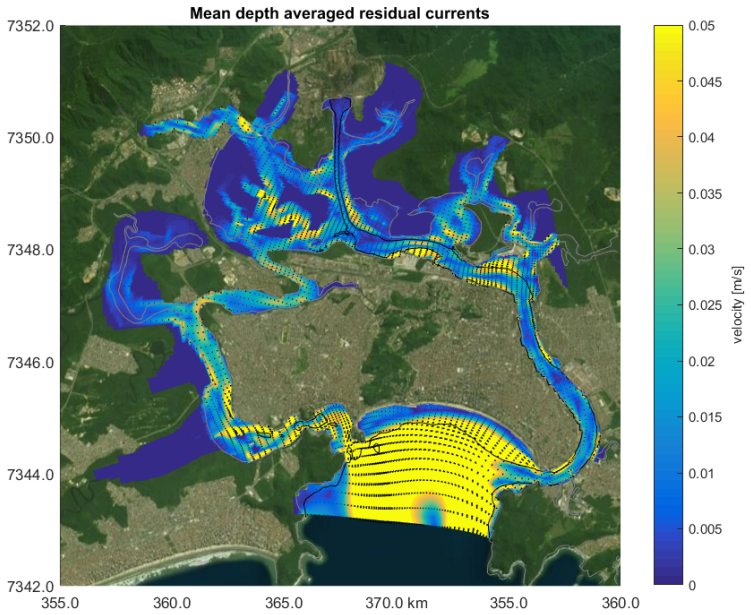

Figure D.10: Mean depth averaged residual currents. Winter, neap tide conditions.

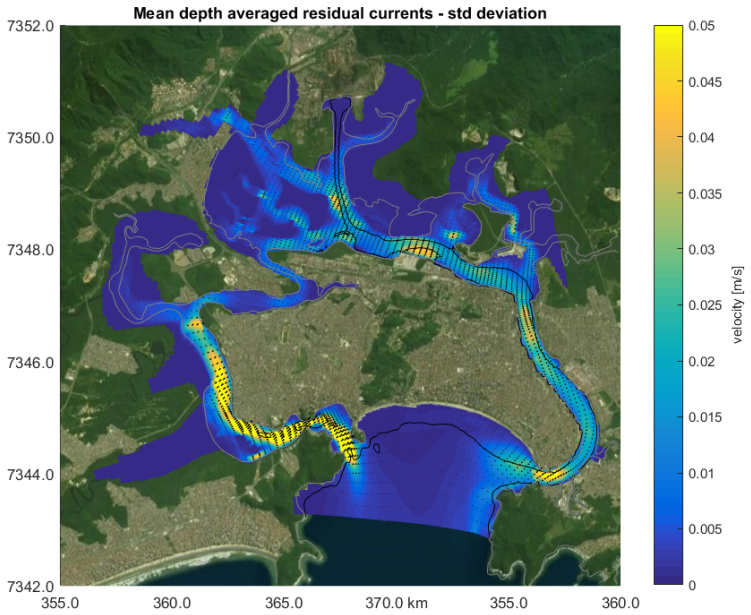

Figure D.11: Depth averaged residual currents standard deviation. Winter, neap tide conditions.

D.3 Sediment concentration close to the bed - salinity on

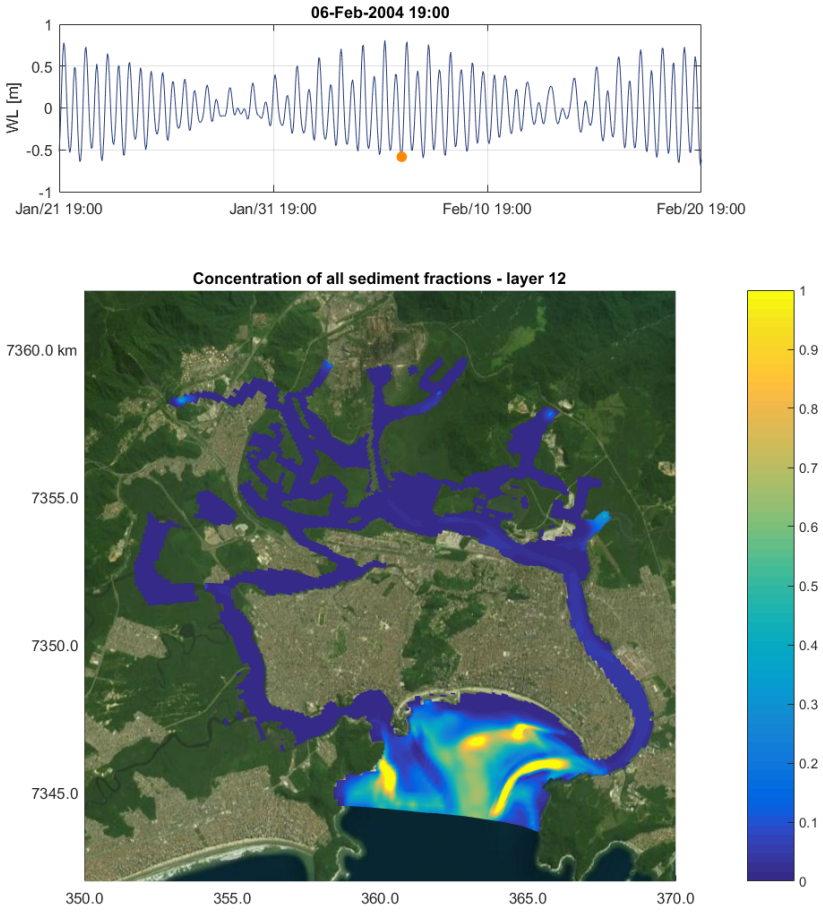

Figure D.12: Sediment concentration [g/l] in the first layer above the bed during summer, spring tide, low water. All fractions.

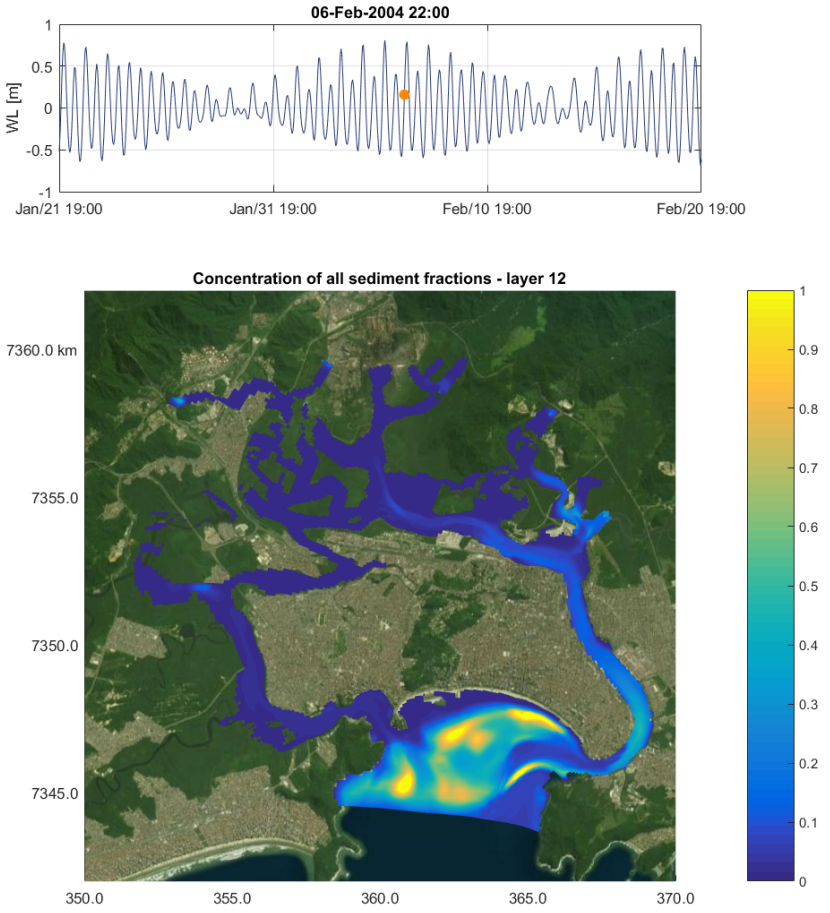

Figure D.13: Sediment concentration [g/l] in the first layer above the bed during summer, spring tide, mean water, flood. All fractions.

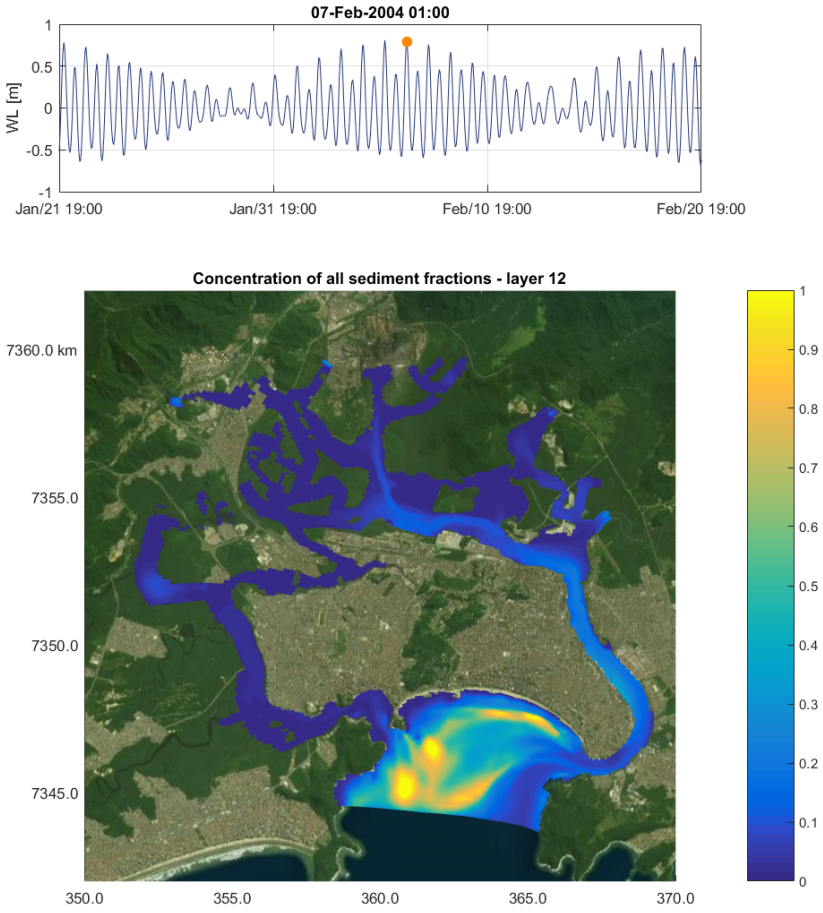

Figure D.14: Sediment concentration [g/l] in the first layer above the bed during summer, spring tide, high water. All fractions.

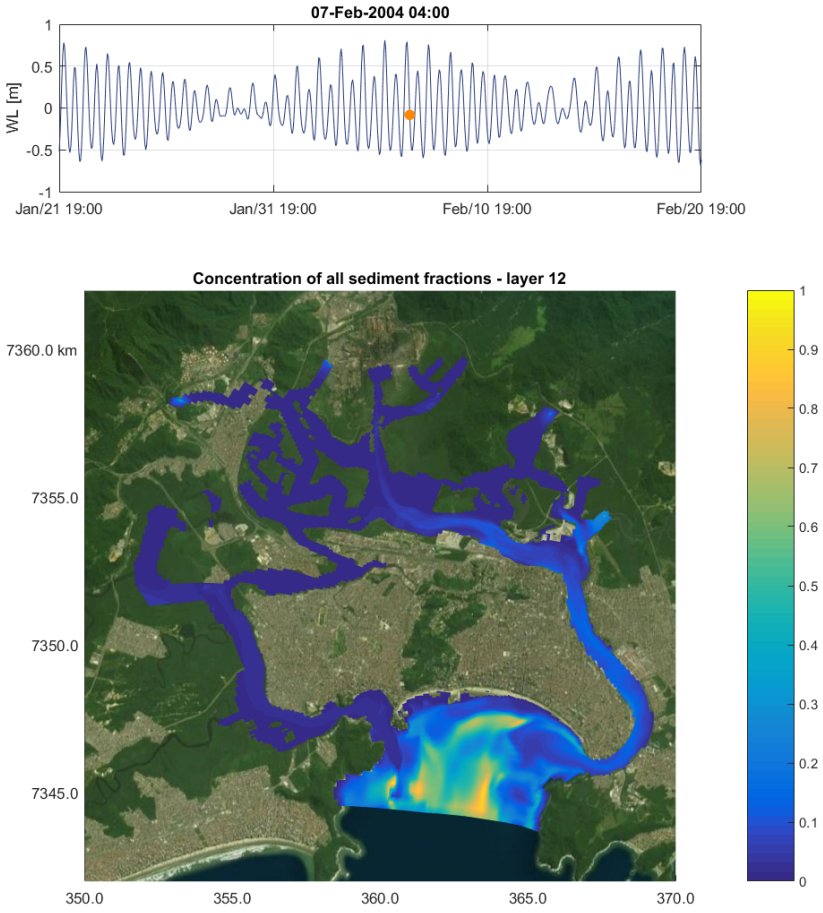

Figure D.15: Sediment concentration [g/l] in the first layer above the bed during summer, spring tide, mean water, ebb. All fractions.

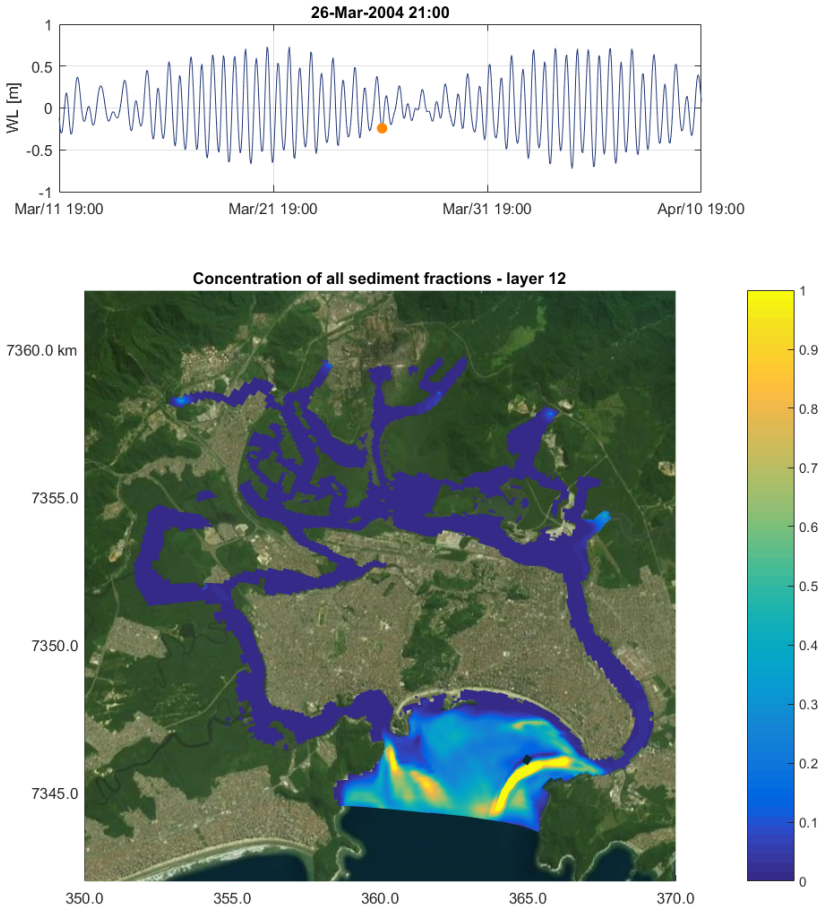

Figure D.16: Sediment concentration [g/l] in the first layer above the bed during summer, neap tide, low water. All fractions.

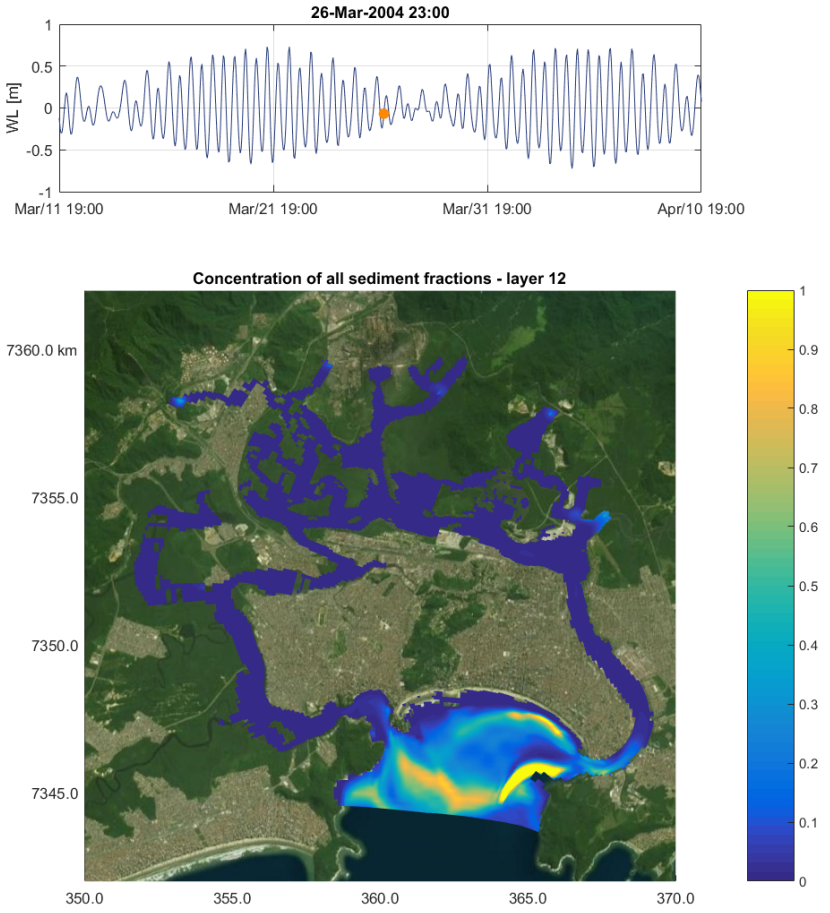

Figure D.17: Sediment concentration [g/l] in the first layer above the bed during summer, neap tide, mean water, flood. All fractions.

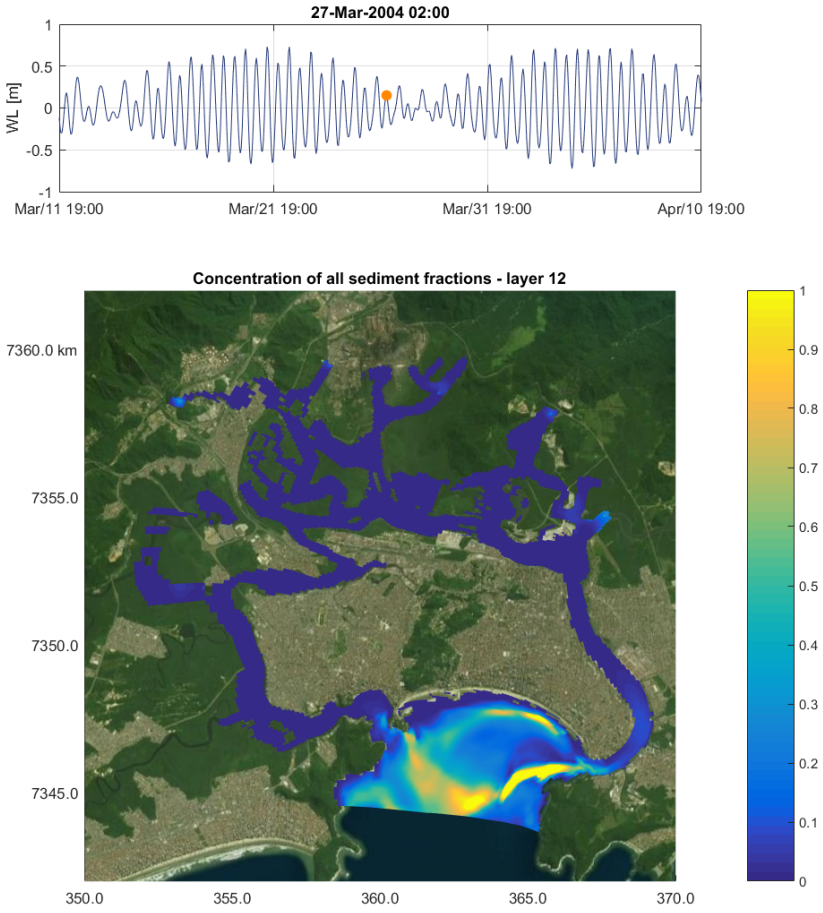

Figure D.18: Sediment concentration [g/l] in the first layer above the bed during summer, neap tide, high water. All fractions.

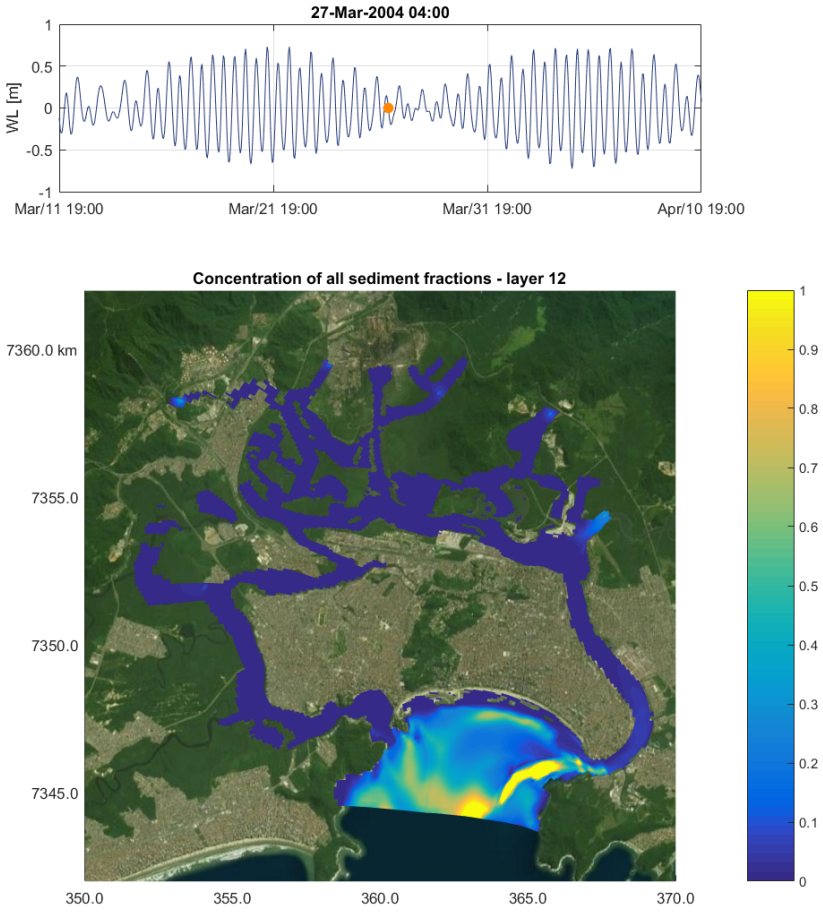

Figure D.19: Sediment concentration [g/l] in the first layer above the bed during summer, neap tide, mean water, ebb. All fractions.

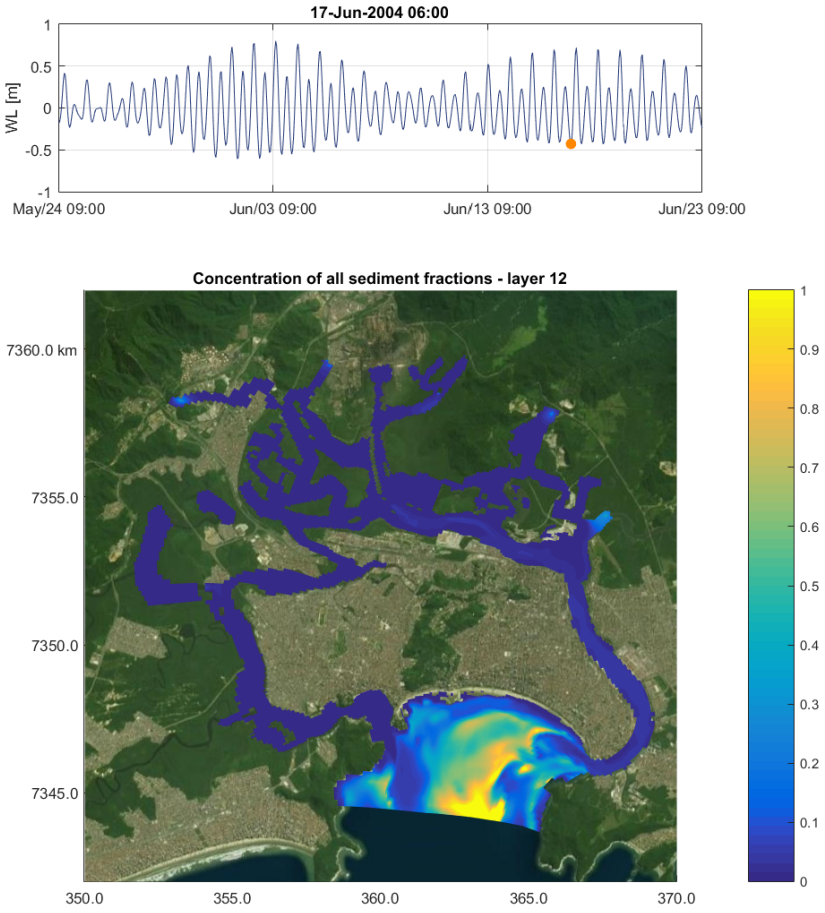

Figure D.20: Sediment concentration [g/l] in the first layer above the bed during winter, spring tide, low water. All fractions.

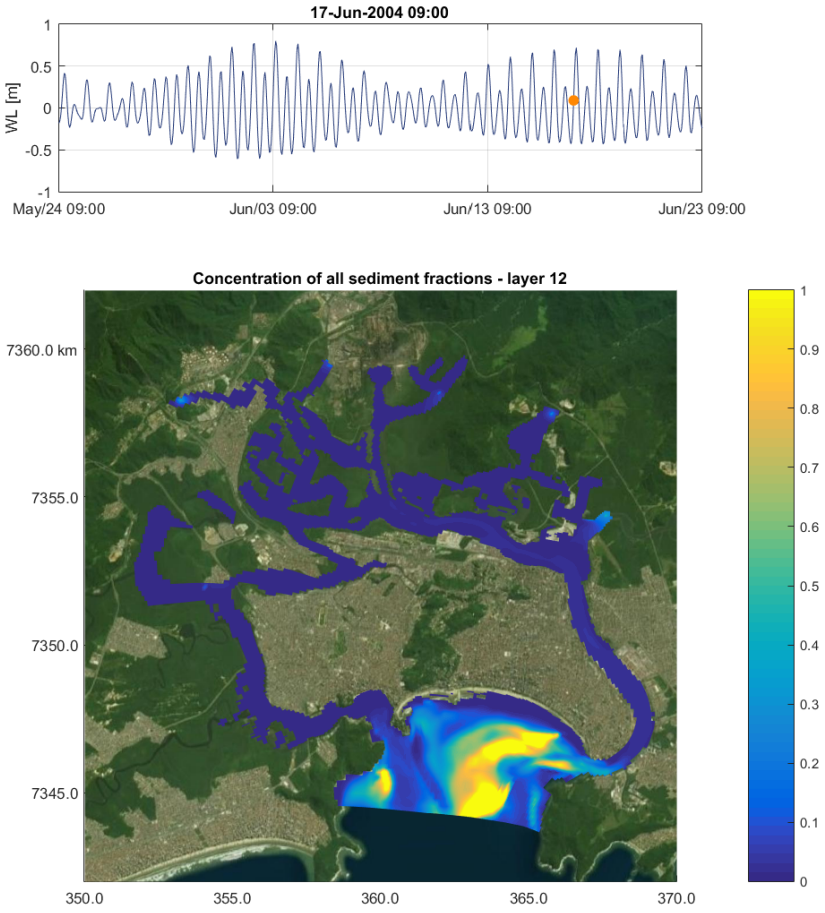

Figure D.21: Sediment concentration [g/l] in the first layer above the bed during winter, spring tide, mean water, flood. All fractions.

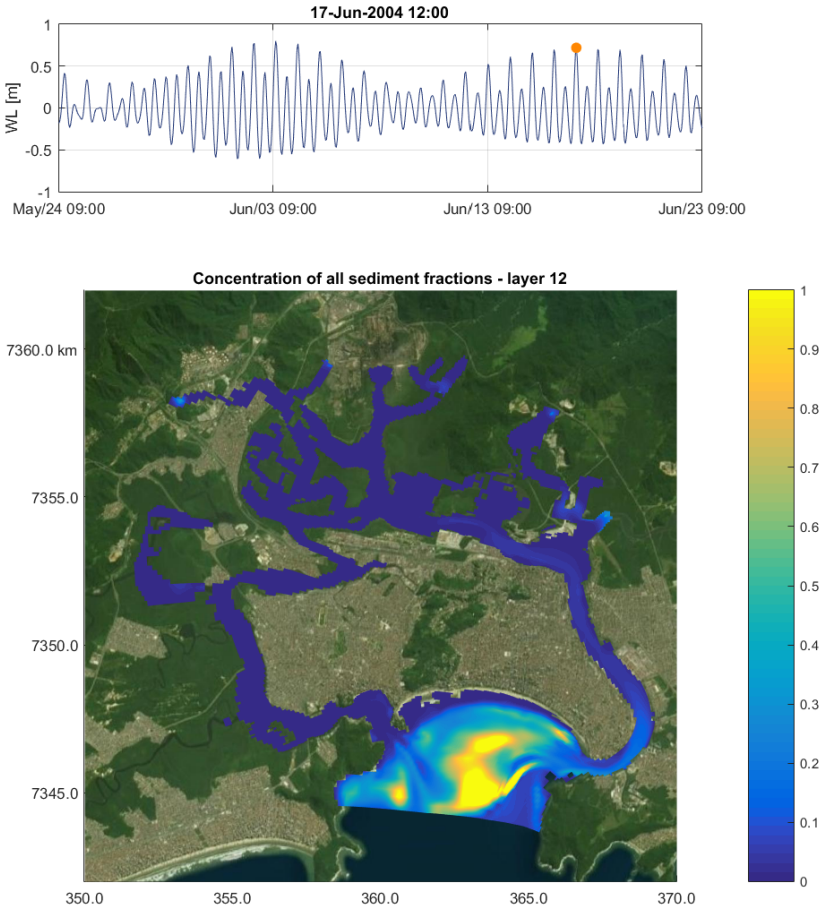

Figure D.22: Sediment concentration [g/l] in the first layer above the bed during winter, spring tide, high water. All fractions.

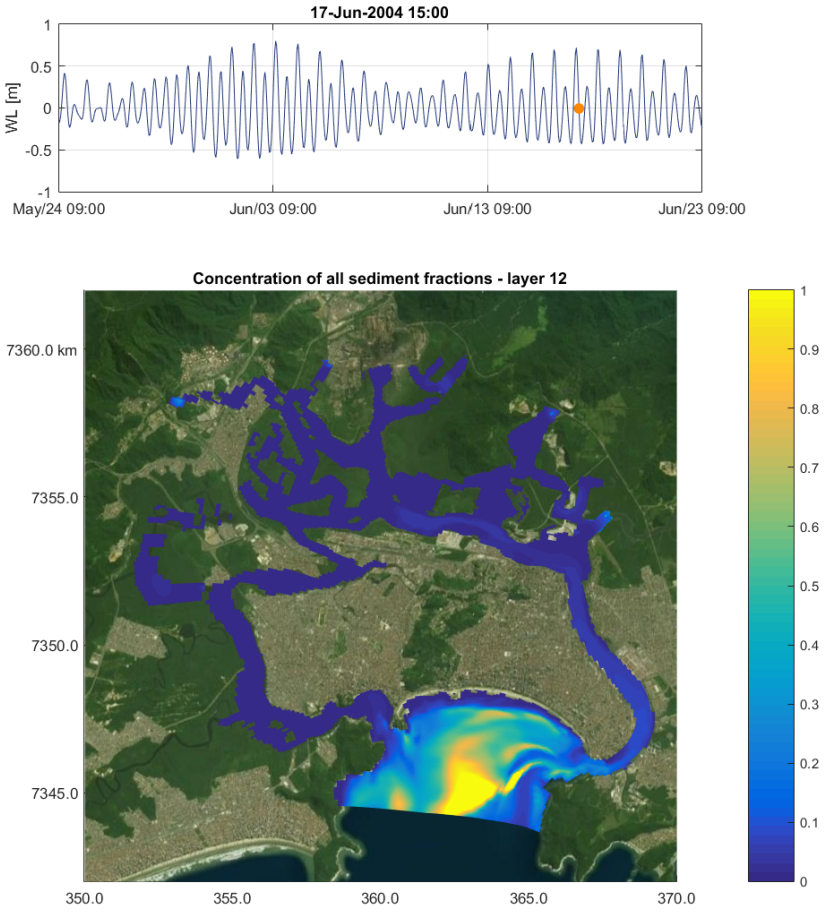

Figure D.23: Sediment concentration [g/l] in the first layer above the bed during winter, spring tide, mean water, ebb. All fractions.

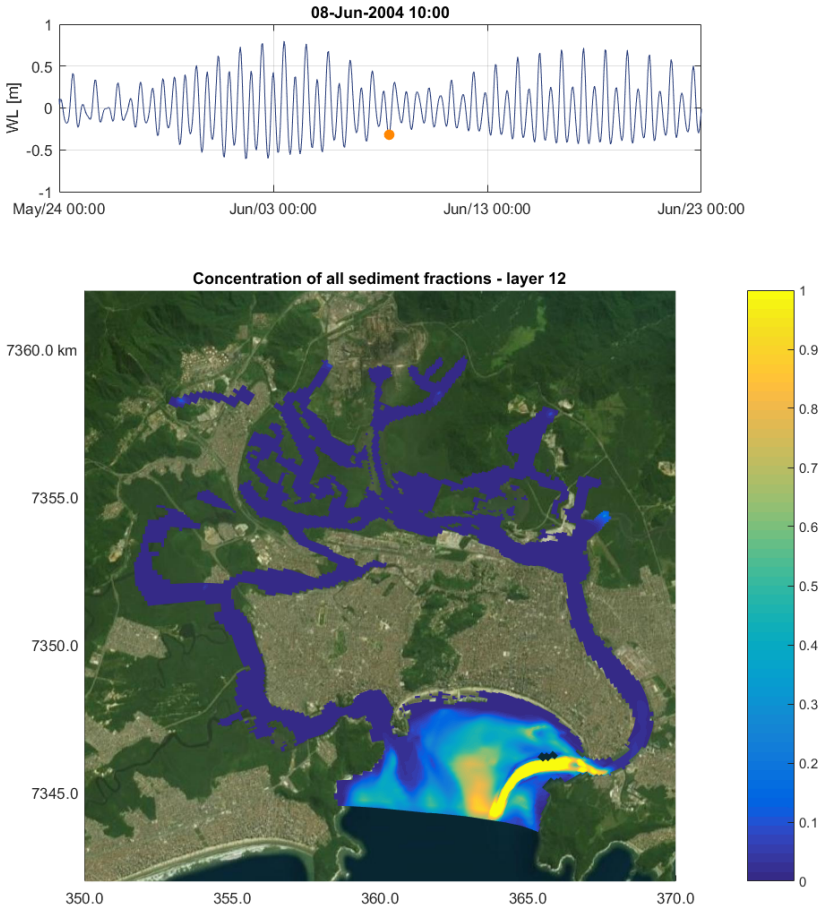

Figure D.24: Sediment concentration [g/l] in the first layer above the bed during winter, neap tide, low water. All fractions.

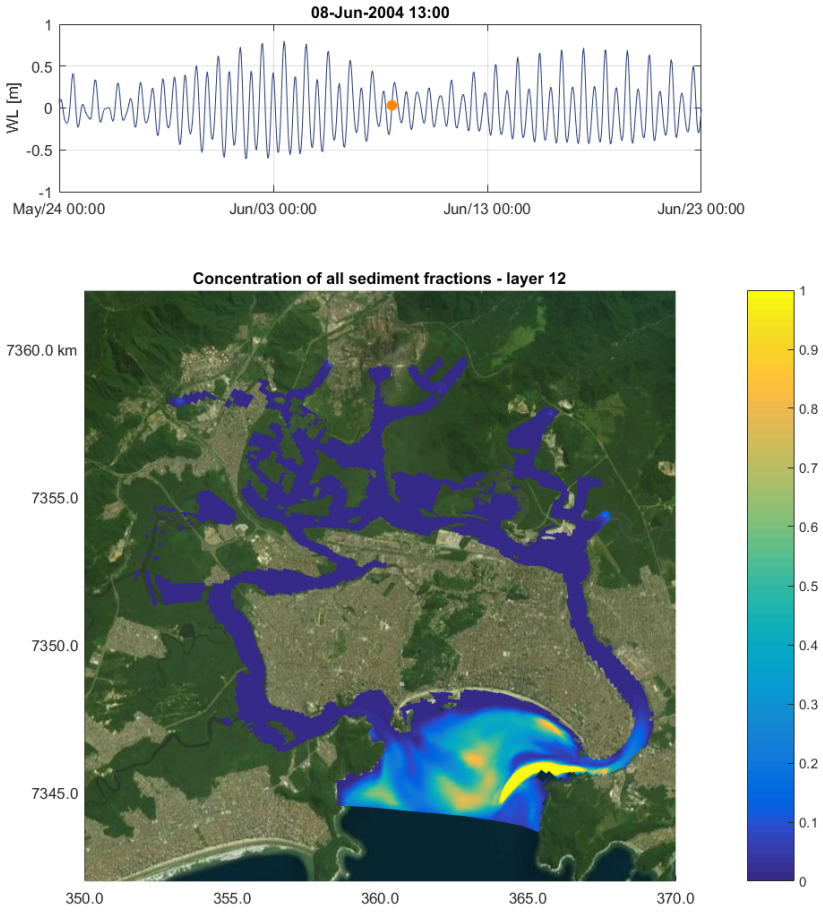

Figure D.25: Sediment concentration [g/l] in the first layer above the bed during winter, neap tide, mean water, flood. All fractions.

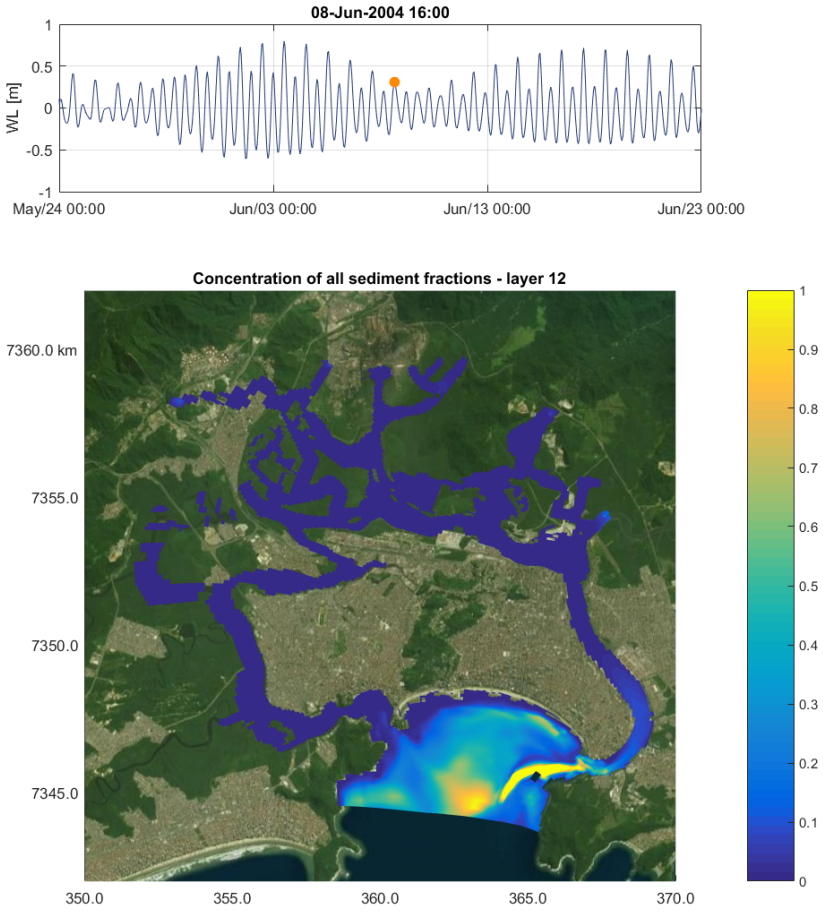

Figure D.26: Sediment concentration [g/l] in the first layer above the bed during winter, neap tide, high water. All fractions.

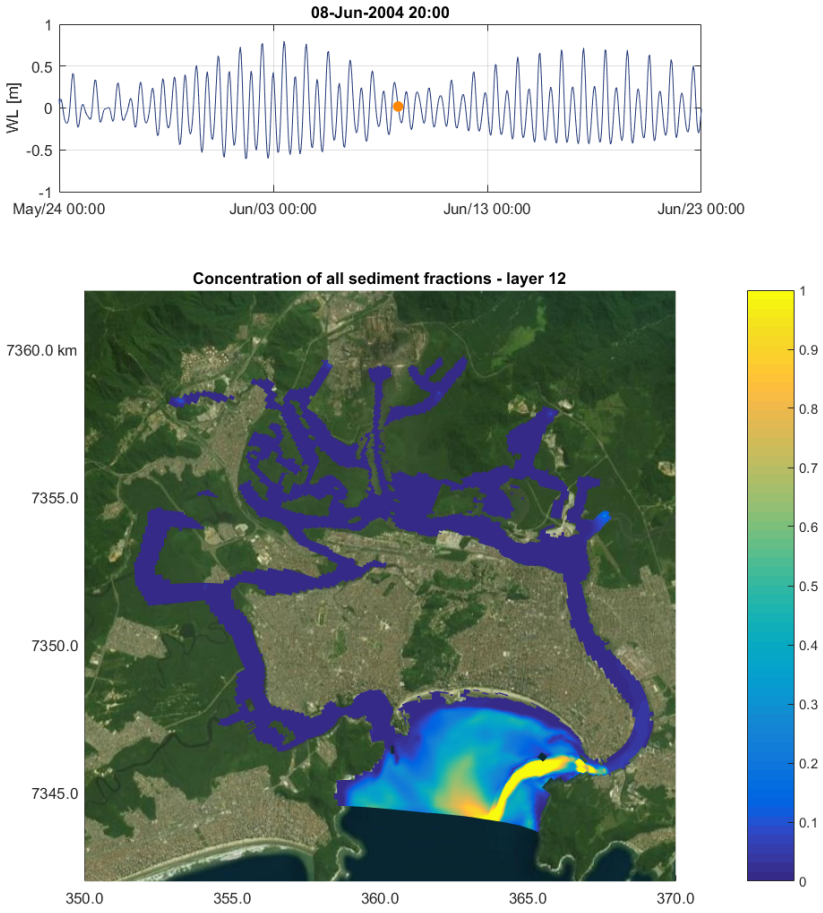

Figure D.27: Sediment concentration [g/l] in the first layer above the bed during winter, neap tide, mean water, ebb. All fractions.

D.4 Sediment concentration close to the bed - salinity off

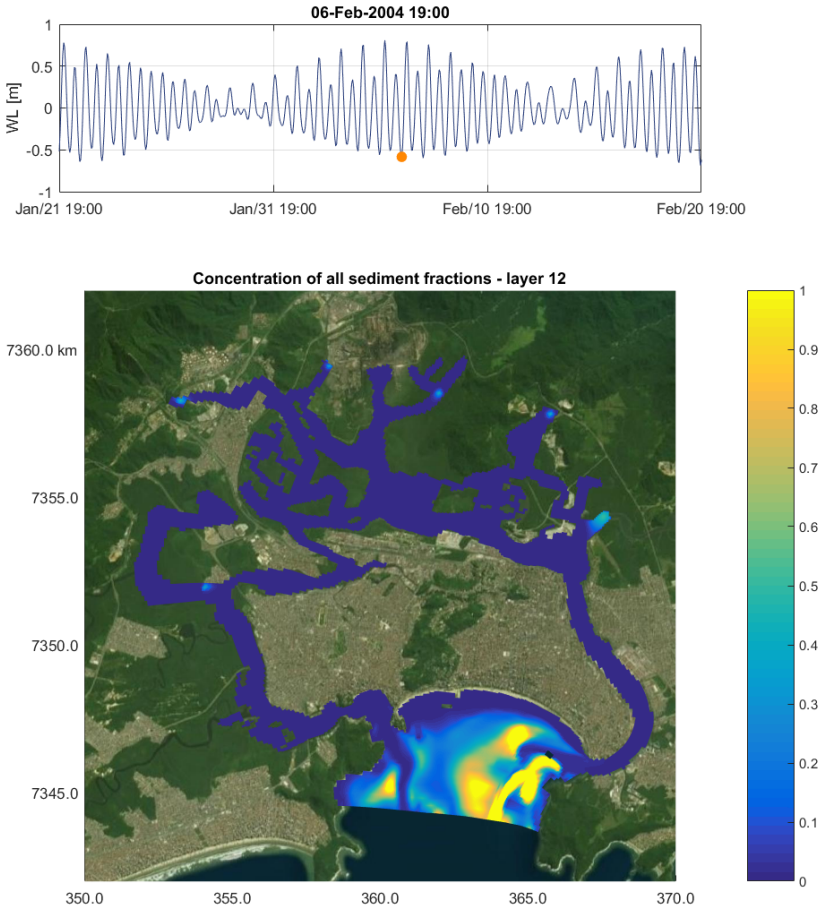

Figure D.28: Sediment concentration [g/l] in the first layer above the bed during summer, spring tide, low water. All fractions.

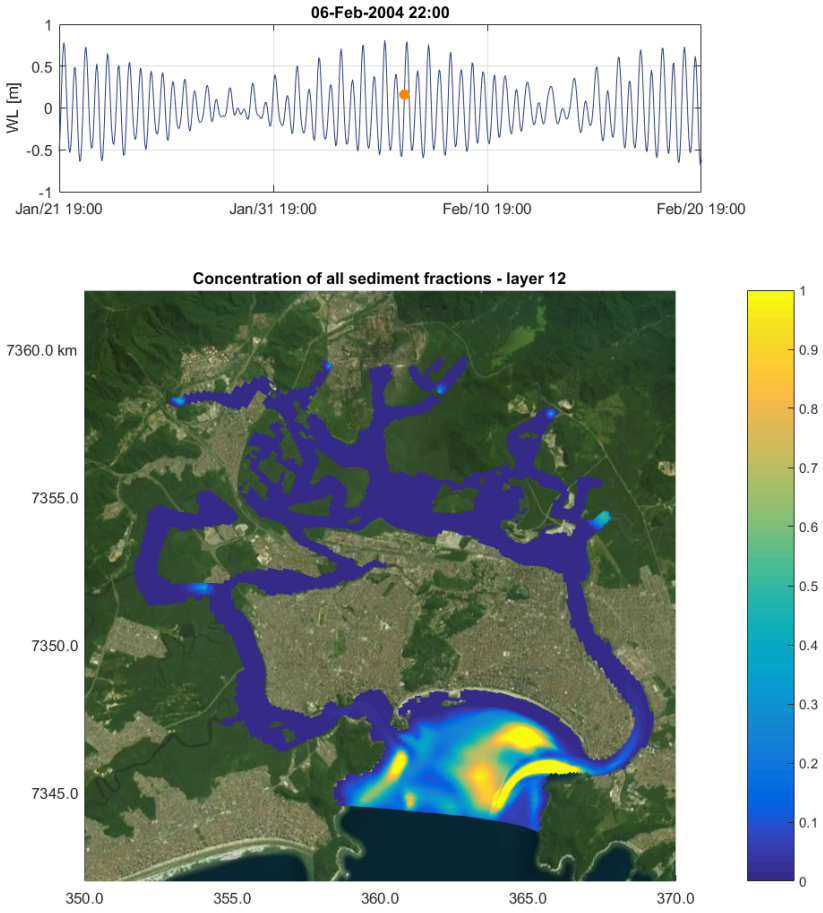

Figure D.29: Sediment concentration [g/l] in the first layer above the bed during summer, spring tide, mean water, flood. All fractions.

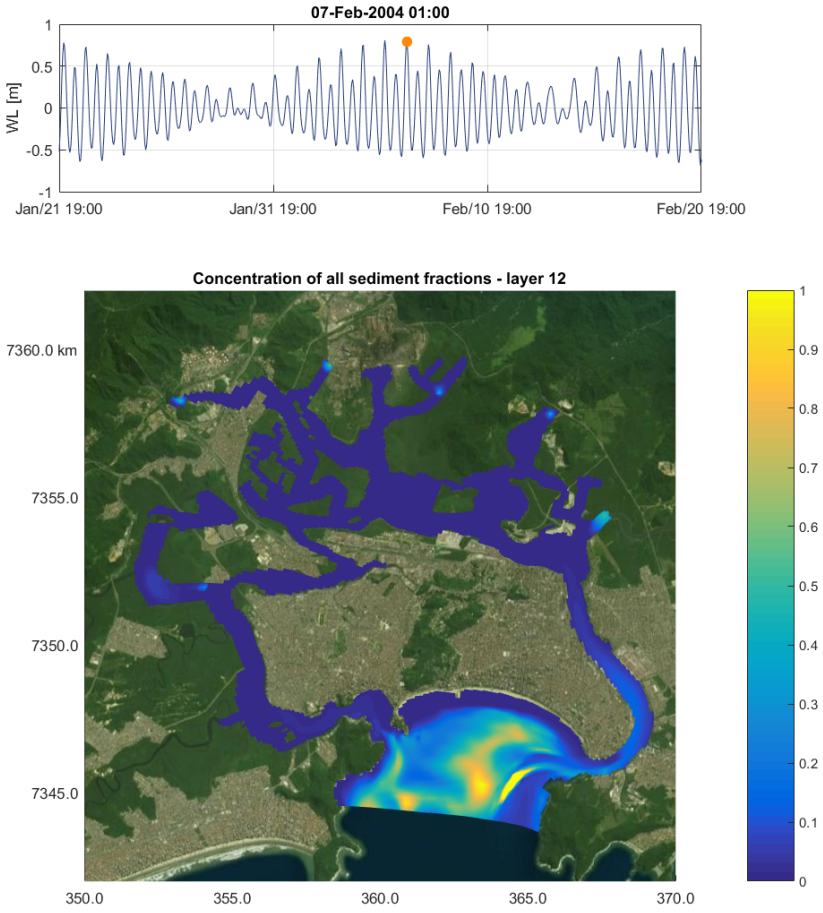

Figure D.30: Sediment concentration [g/l] in the first layer above the bed during summer, spring tide, high water. All fractions.

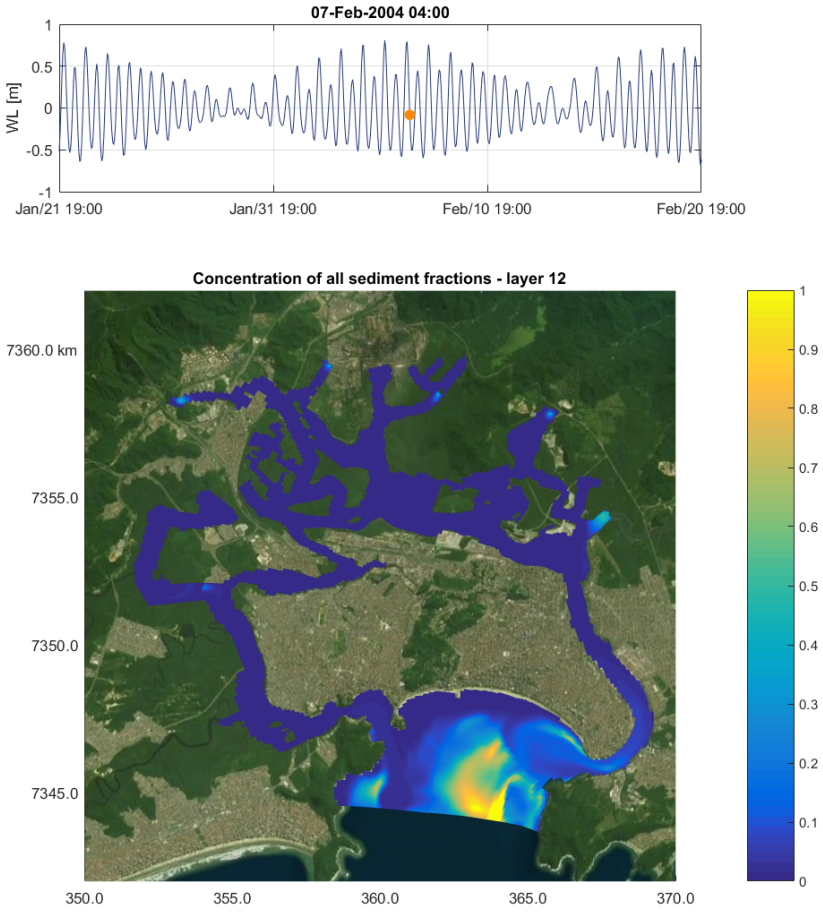

Figure D.31: Sediment concentration [g/l] in the first layer above the bed during summer, spring tide, mean water, ebb. All fractions.

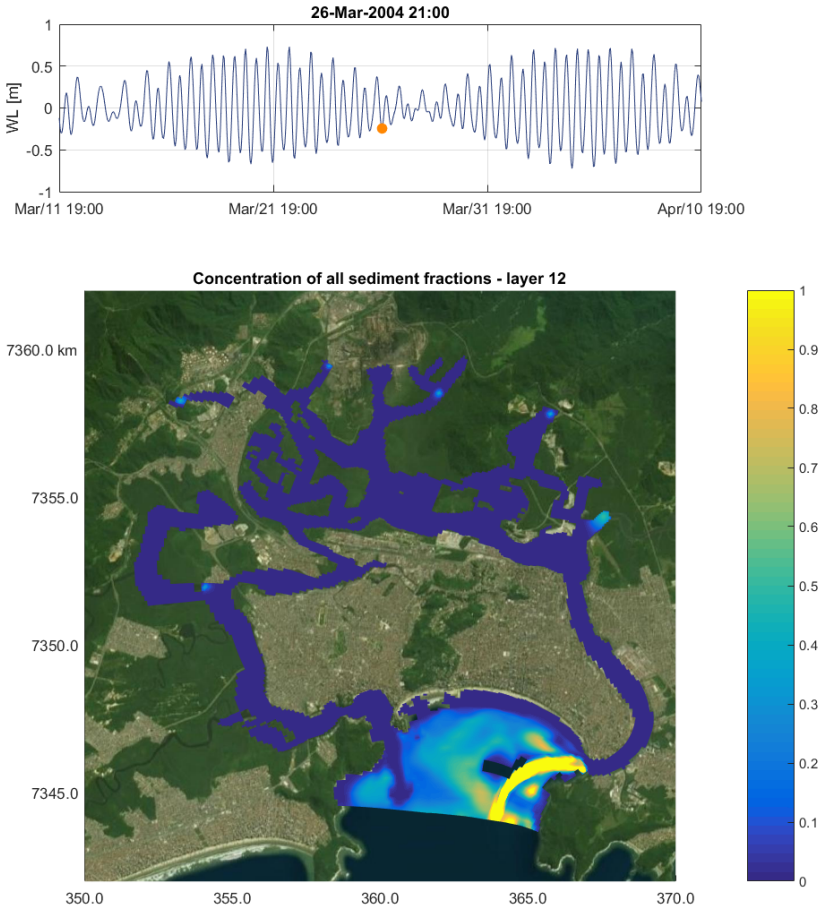

Figure D.32: Sediment concentration [g/l] in the first layer above the bed during summer, neap tide, low water. All fractions.

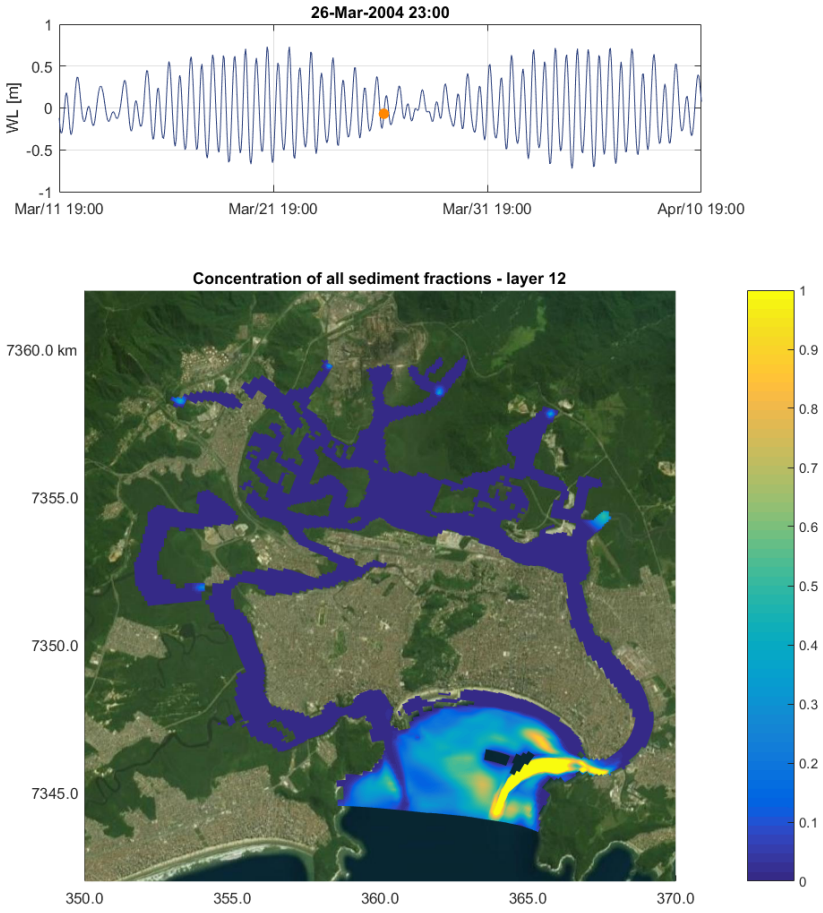

Figure D.33: Sediment concentration [g/l] in the first layer above the bed during summer, neap tide, mean water, flood. All fractions.

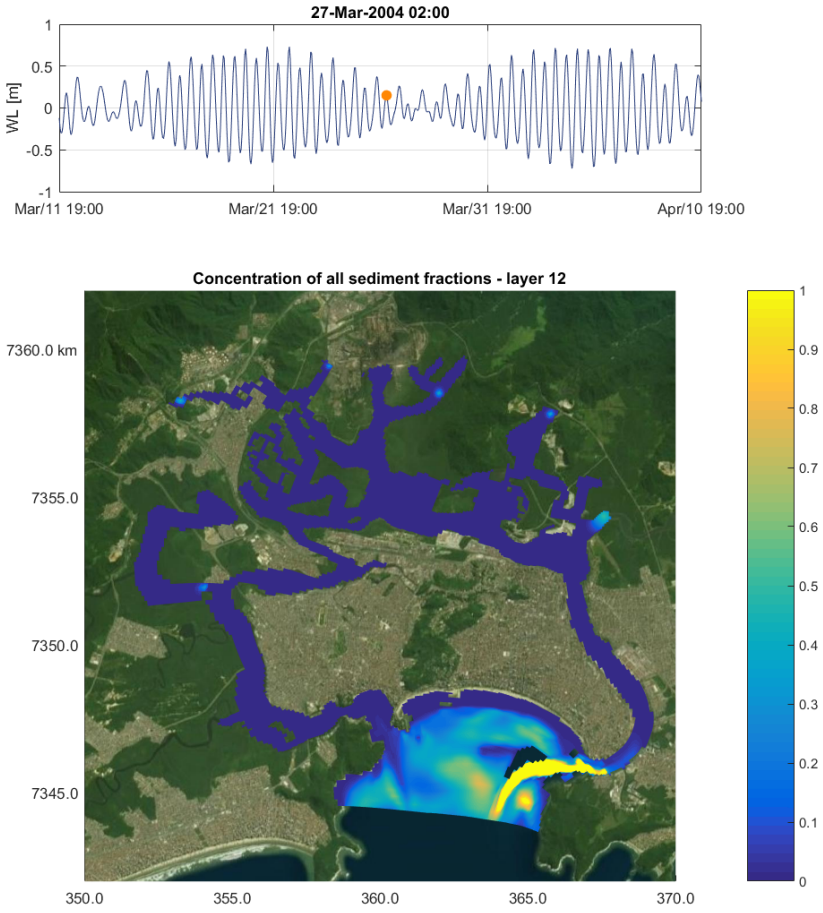

Figure D.34: Sediment concentration [g/l] in the first layer above the bed during summer, neap tide, high water. All fractions.

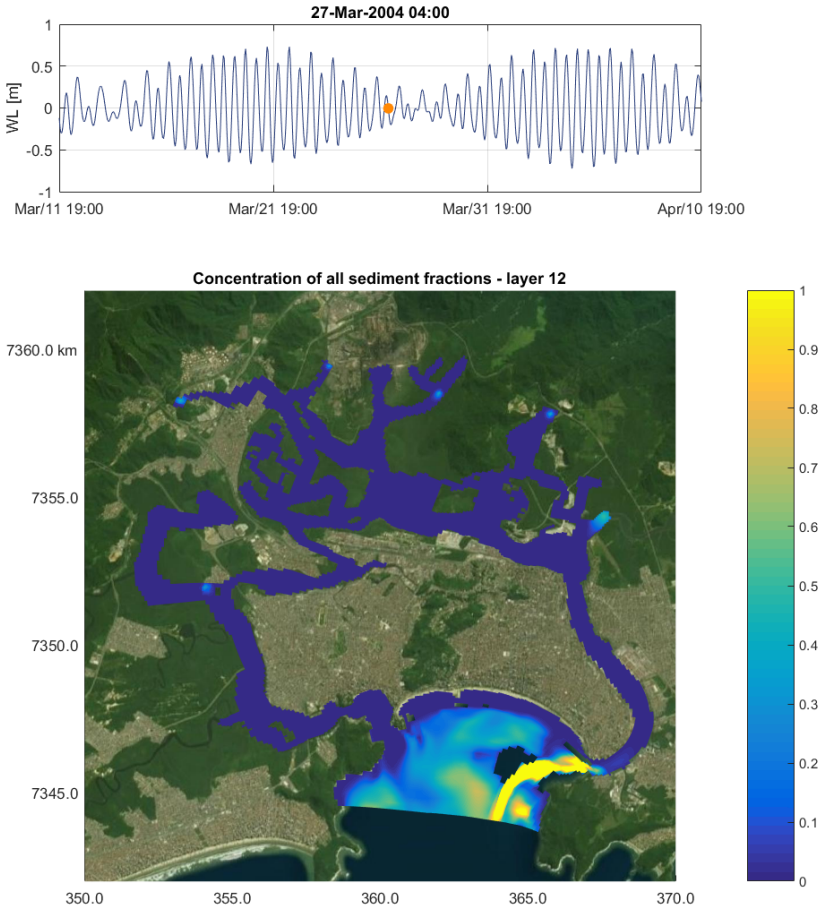

Figure D.35: Sediment concentration [g/l] in the first layer above the bed during summer, neap tide, mean water, ebb. All fractions.

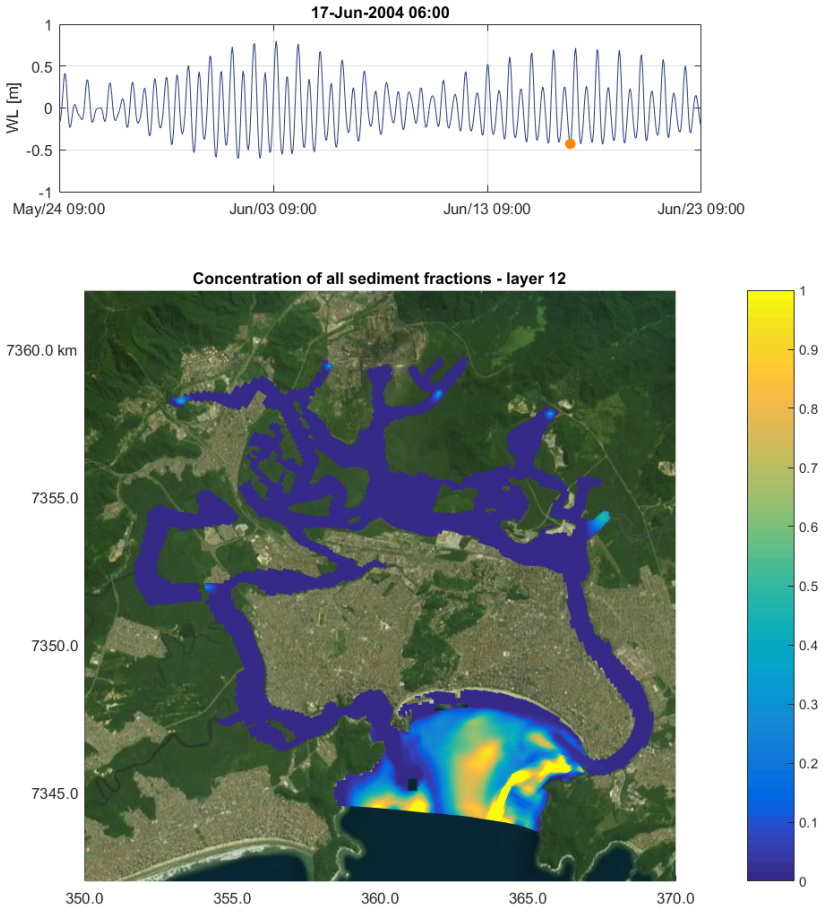

Figure D.36: Sediment concentration [g/l] in the first layer above the bed during winter, spring tide, low water. All fractions.

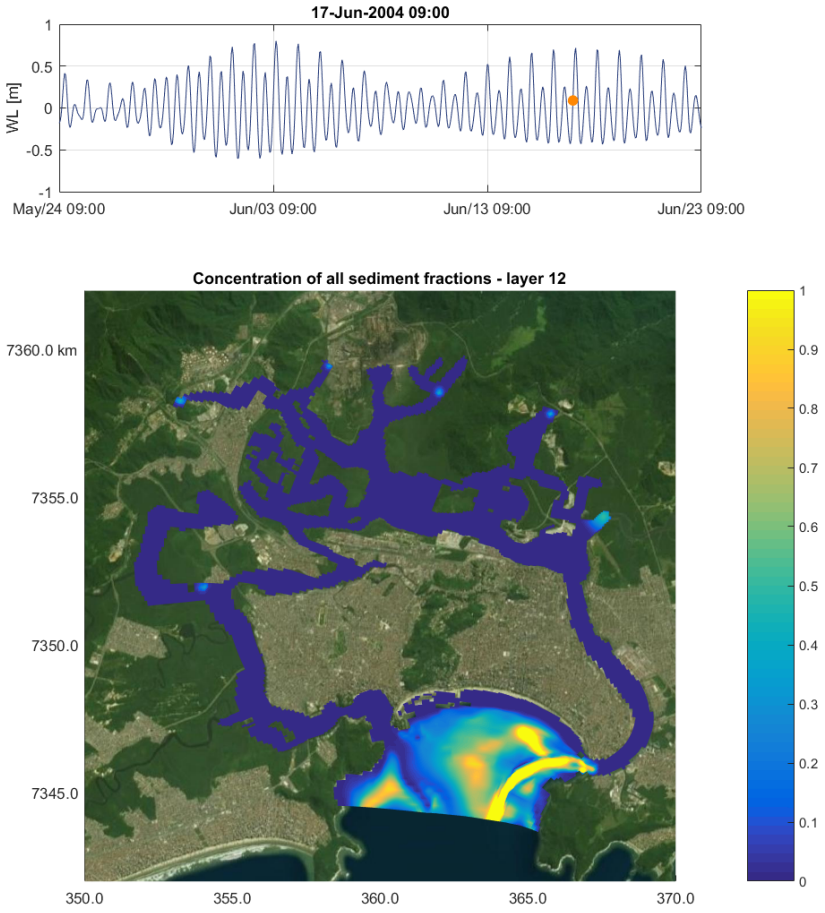

Figure D.37: Sediment concentration [g/l] in the first layer above the bed during winter, spring tide, mean water, flood. All fractions.

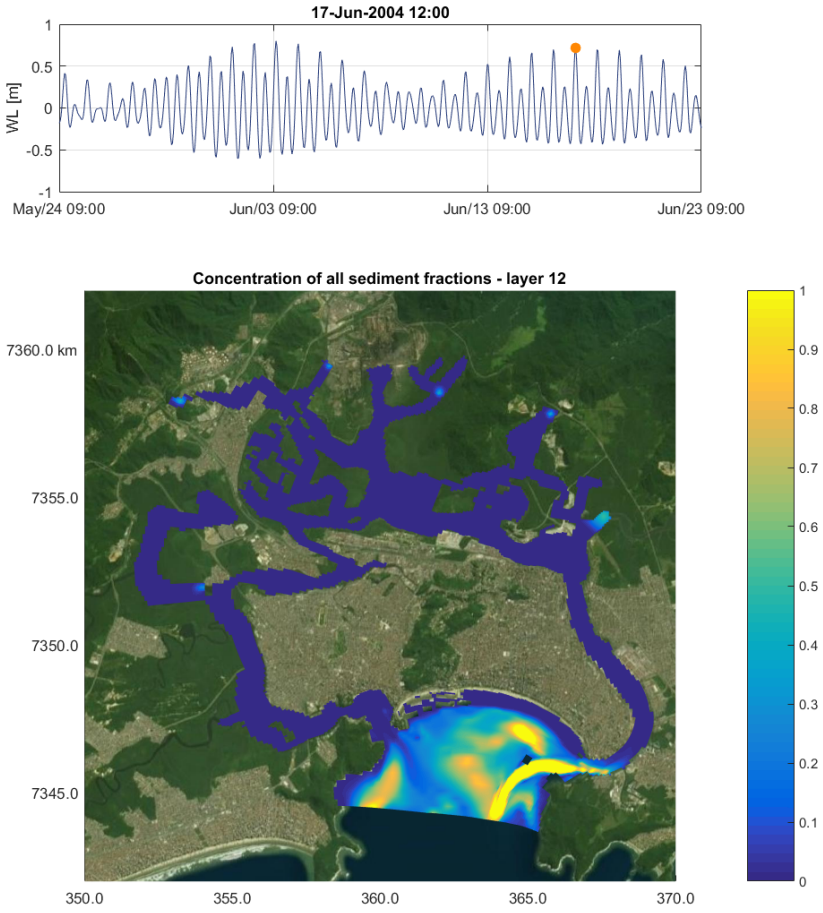

Figure D.38: Sediment concentration [g/l] in the first layer above the bed during winter, spring tide, high water. All fractions.

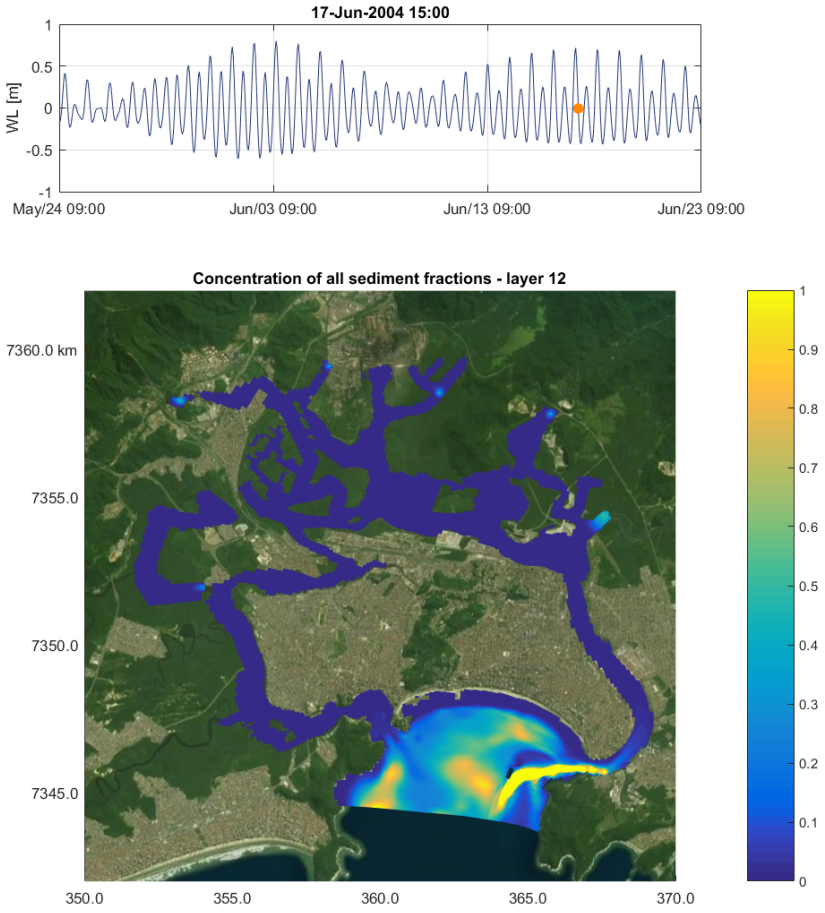

Figure D.39: Sediment concentration [g/l] in the first layer above the bed during winter, spring tide, mean water, ebb. All fractions.

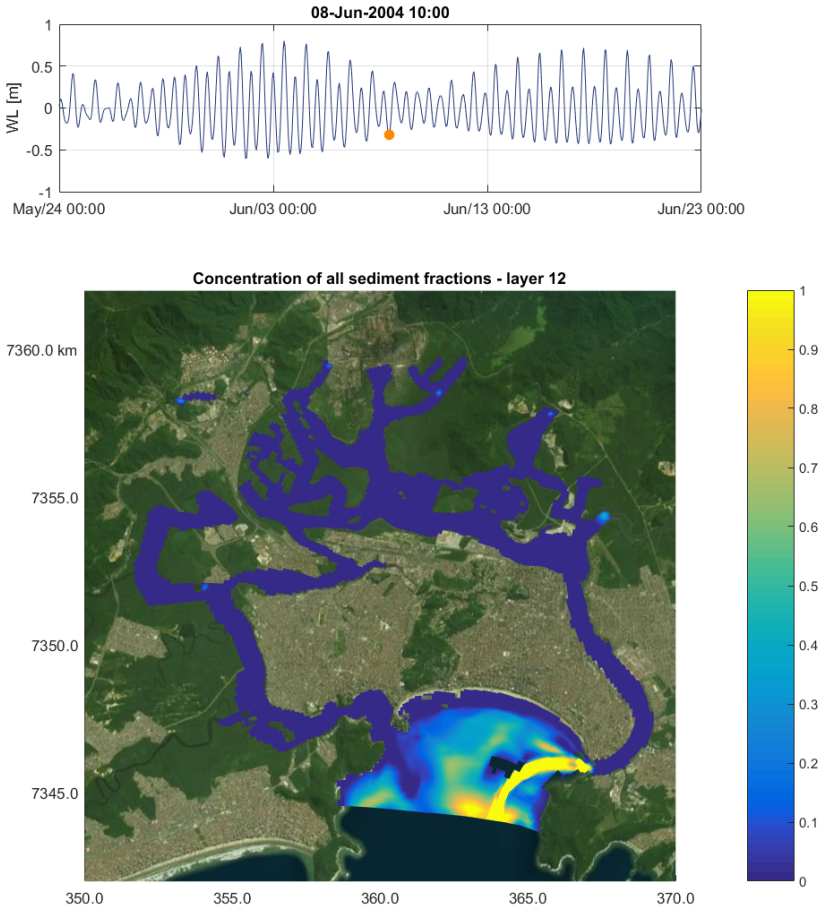

Figure D.40: Sediment concentration [g/l] in the first layer above the bed during winter, neap tide, low water. All fractions.

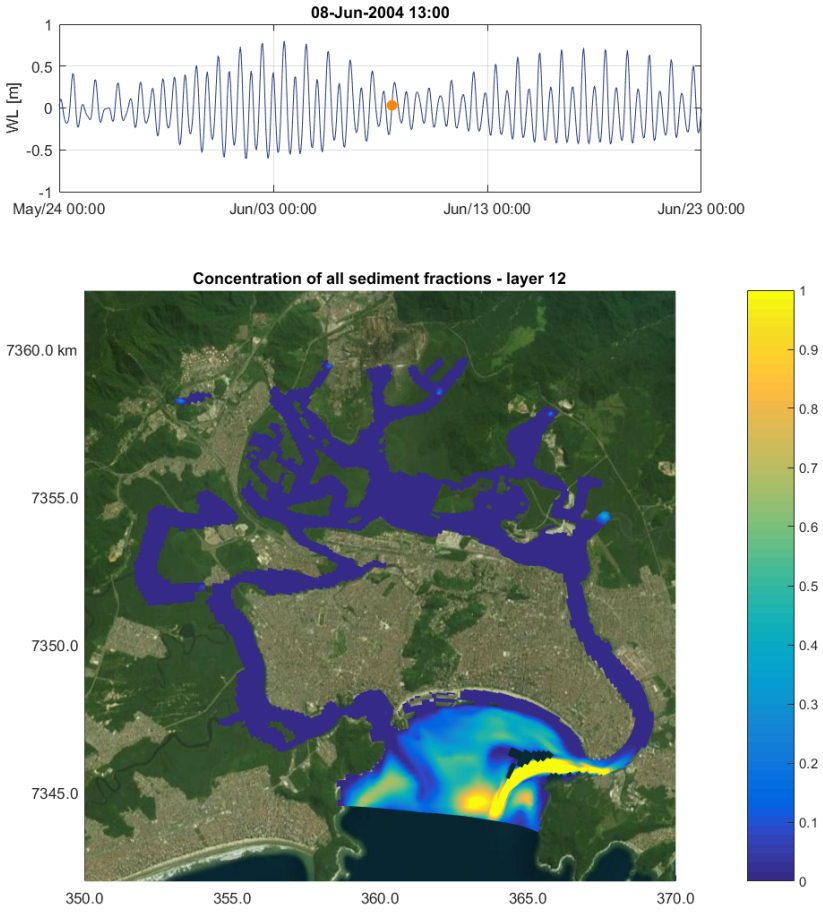

Figure D.41: Sediment concentration [g/l] in the first layer above the bed during winter, neap tide, mean water, flood. All fractions.

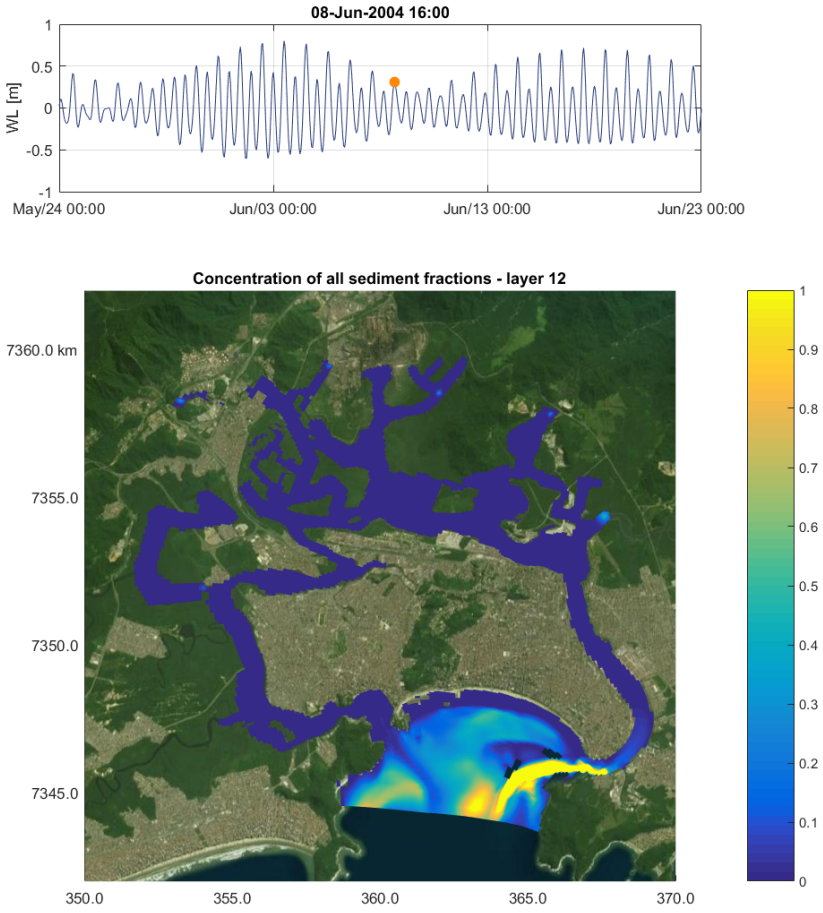

Figure D.42: Sediment concentration [g/l] in the first layer above the bed during winter, neap tide, high water. All fractions.

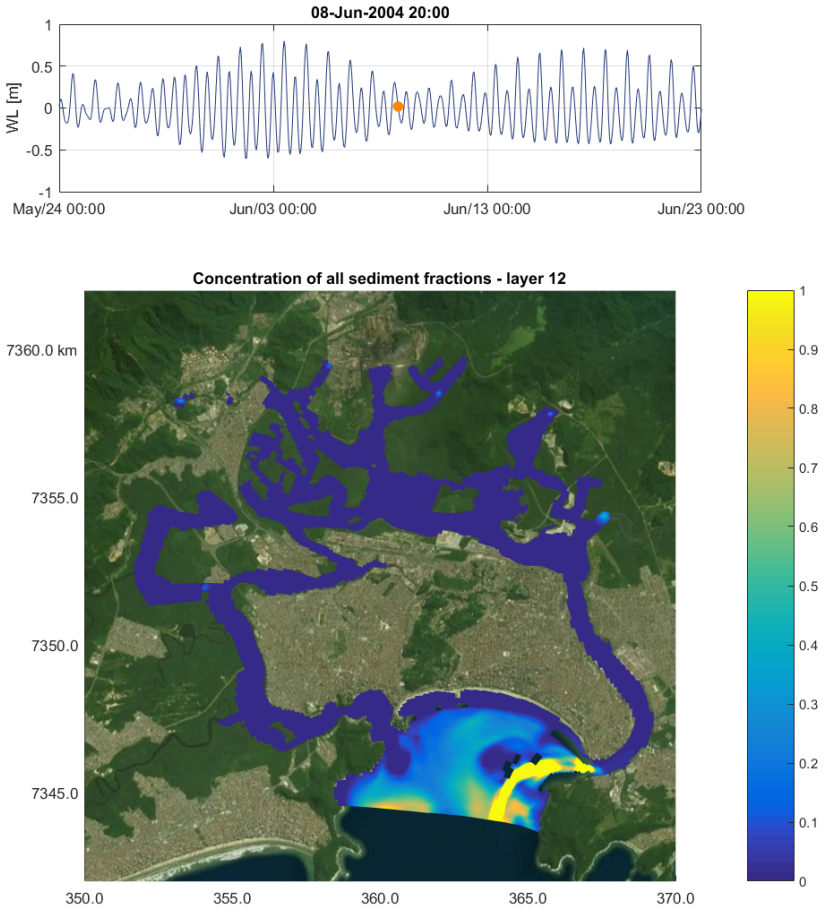

Figure D.43: Sediment concentration [g/l] in the first layer above the bed during winter, neap tide, mean water, ebb. All fractions.

D.5 Sedimentation - salinity on

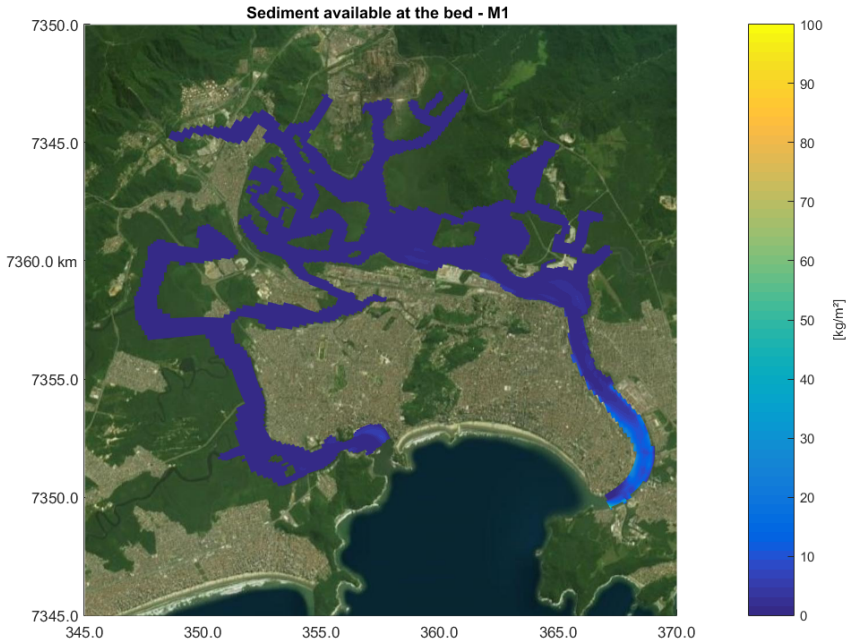

Figure D.44: Available sediment at the bed after six months. Sediment fraction M1.

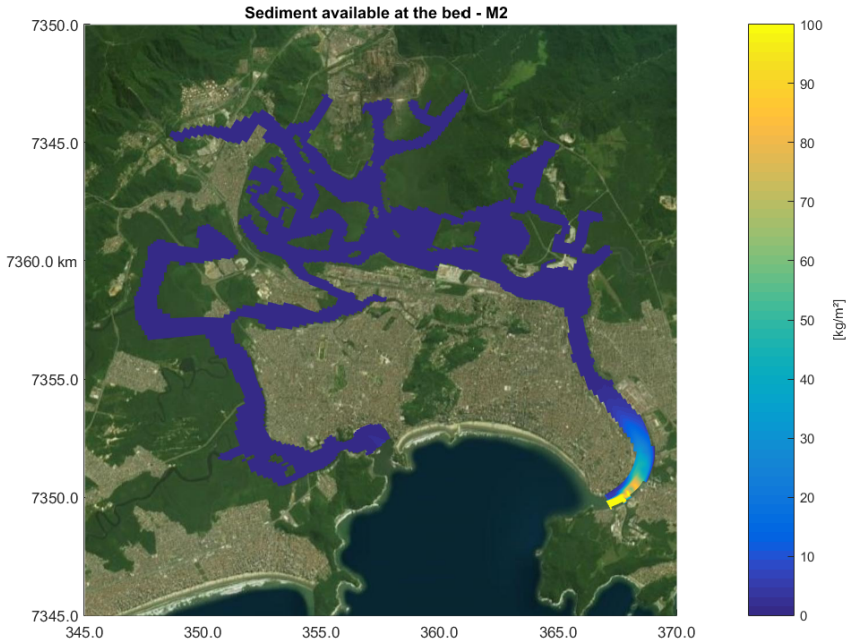

Figure D.45: Available sediment at the bed after six months. Sediment fraction M2.

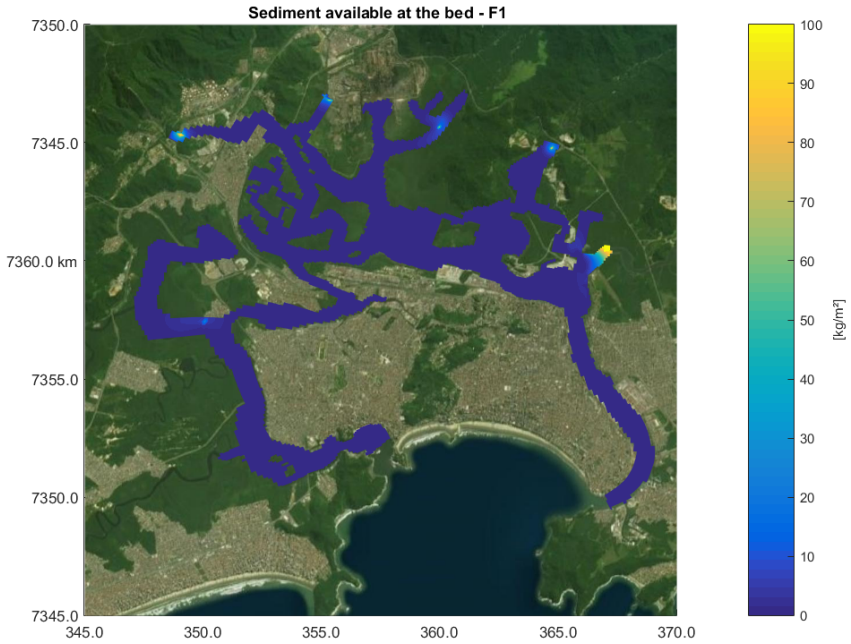

Figure D.46: Available sediment at the bed after six months. Sediment fraction F1.

D.6 Sedimentation - salinity off

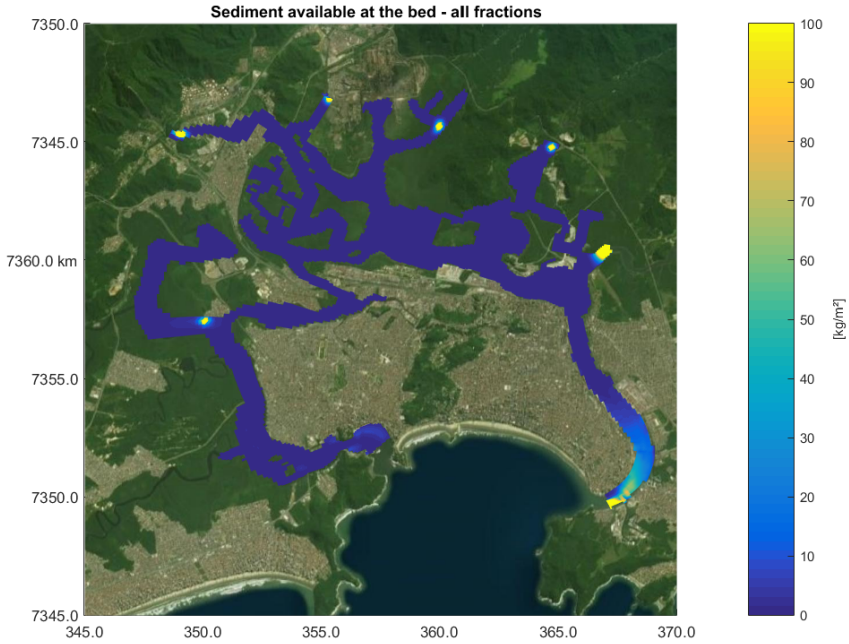

Figure D.47: Available sediment at the bed after six months. All sediment fractions.

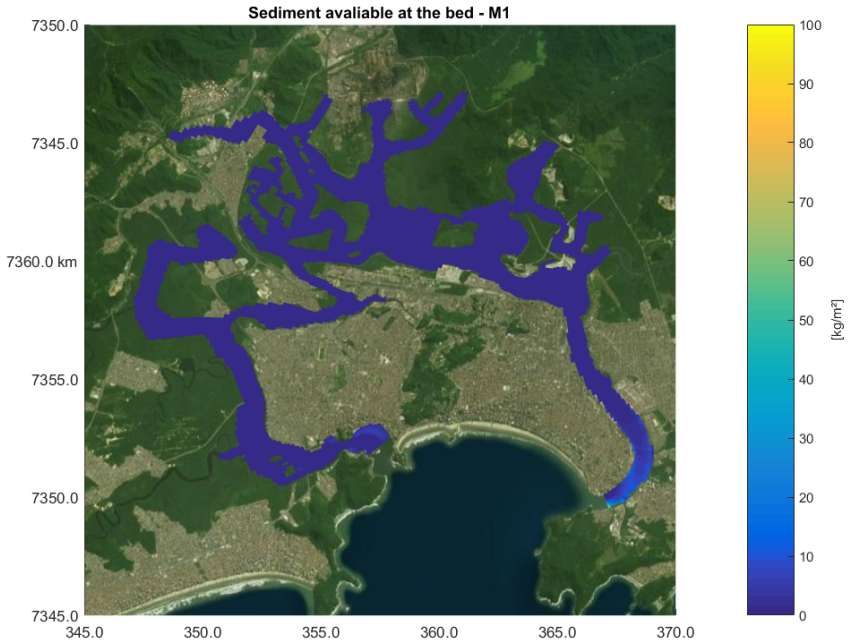

Figure D.48: Available sediment at the bed after six months. Sediment fraction M1.

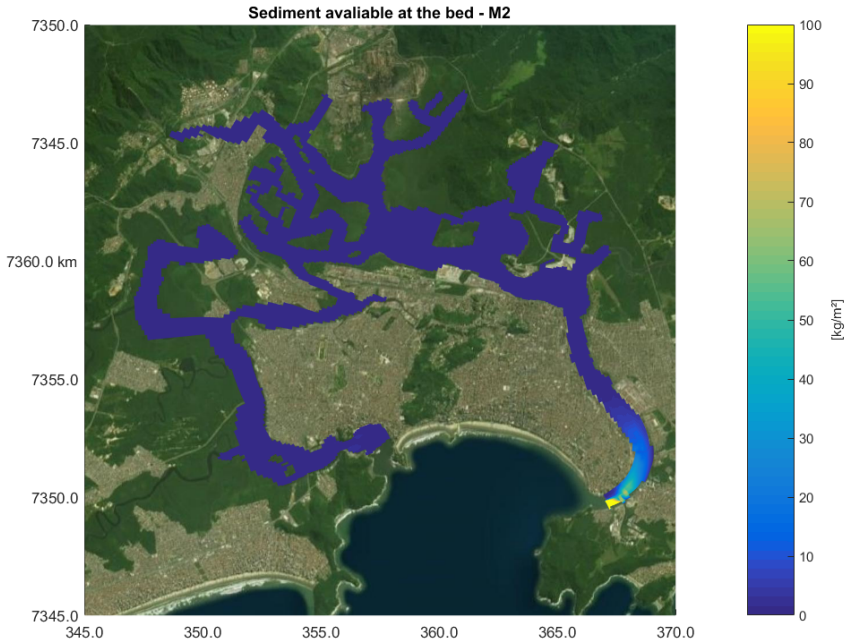

Figure D.49: Available sediment at the bed after six months. Sediment fraction M2.

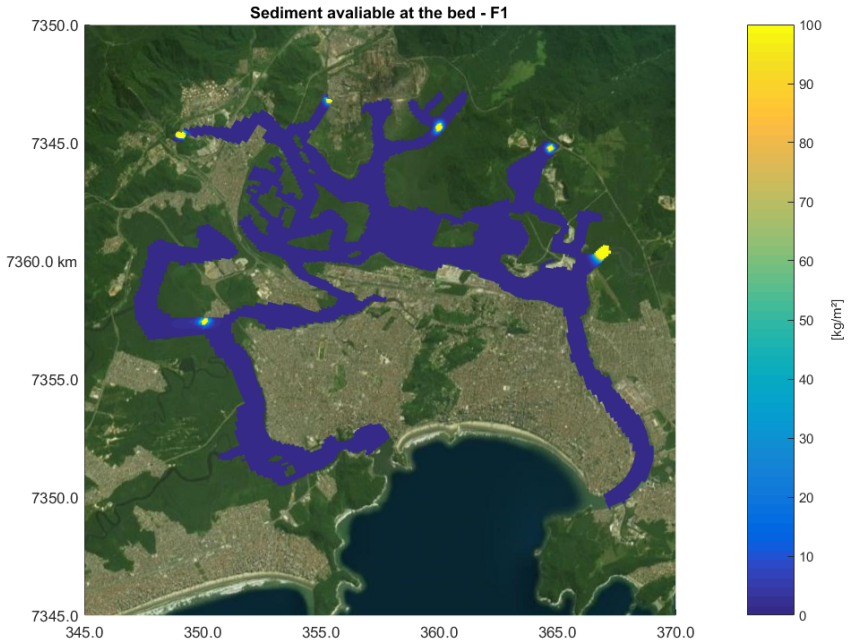

Figure D.50: Available sediment at the bed after six months. Sediment fraction F1.